Boundary-Bound Reactions:
Pattern Formation with and without Hydrodynamics

by

Aiden Huffman

A thesis
presented to the University of Waterloo
in fulfillment of the
thesis requirement for the degree of
Master of Mathematics
in
Applied Mathematics

Waterloo, Ontario, Canada, 2022

© Aiden Huffman 2022

Author's Declaration

I hereby declare that I am the sole author of this thesis. This is a true copy of the thesis, including any required final revisions, as accepted by my examiners.

I understand that my thesis may be made electronically available to the public.

Abstract

Pattern formation through chemical morphogenesis has received a significant amount of attention since Alan Turing's original analysis in a Chemical Basis for Morphogenesis. In that article, Turing showed the surprising result that pattern formation in bulk reaction-diffusion systems could be created through a diffusion-driven instability. More recently, researchers have studied active-membrane models; these models split the domain into two regions: a membrane where the reaction occurs and the bulk region where the reagents can diffuse and decay. Generally, the complexity of active-membrane models is far greater than boundary-bound reactions, where the primary source of reagents comes from boundary fluxes. These capture the behaviour of reaction systems where an enzyme or catalyst is necessary for the reaction to proceed, and we coat it along the boundary of the domain. We study these boundary-bound reactions, with specific applications to the control of pattern formation and fluid flow pattern formation.

Our investigation of boundary-bound reactions was originally motivated by the work of Balazs et al. (2020) in coupling chemical oscillations of boundary-bound reactions with the Boussinesq approximation of fluid flow. We begin by presenting a general overview of pattern formation without flow and obtain necessary conditions for pattern formation in terms of the reaction parameters and linear instability. To motivate our results, we consider the Schnakenberg system in two settings: the first demonstrates how boundary-bound reactions can be used to control pattern formation and chemical oscillations, and the second to study fluid flow pattern formation. In our analysis of fluid flow pattern formation, we begin by comparing and contrasting the behaviour of the boundary-bound model against the classical bulk reaction-diffusion problem without flow. Before, coupling it to the Boussinesq approximation for fluid flow. There we demonstrate how the diffusive instabilities change the behaviour of buoyancy-driven instabilities. Overall, these results provide possible mechanisms for controllable pattern formation, chemical signalling, and flows.

Acknowledgements

This thesis would not have been possible without the support of Dr. Henry Shum. Throughout the time that we have worked together, he has been patient, kind, shared his ideas and laughed at my jokes. Words alone cannot express how fortunate I am to have had a supportive supervisor. Hopefully, this thesis can demonstrate a fraction of its value. I would also like to thank my friends and colleagues all across Canada, whom I have had the pleasure to get to know since I began my journey in mathematics. While COVID-19 has made it difficult to join in the usual ways, if it were not for those hard days and joyful evenings, I do not believe I would be where I am today. And finally, my family, without whom I certainly would not exist. They have had the pleasure of seeing me through this, as well as hearing me try to explain it. I am grateful for their patience.

Dedication

To my partner, Sarah, for their love and support during our adventures; and for the pub they promised to purchase me at some point.

Table of Contents

List of Figures viii

List of Tables xii

1 Introduction 1

1.1 The Turing Instability . . . 5

1.1.1 The Two Reagent Case . . . 7

1.1.2 The Schnakenberg System . . . 9

1.1.3 Turing Parameter Space . . . 11

1.1.4 Summary . . . 16

1.2 Rayleigh-Bénard Instability . . . 19

1.2.1 Boussinesq Approximation . . . 19

1.2.2 Rayleigh-Bénard Instability . . . 20

1.2.3 Summary . . . 26

2 Boundary-Bound Reactions 28

2.1 General Framework for Boundary-Bound Reactions . . . 30

2.2 Boundary-Bound Reactions without Flow . . . 34

2.2.1 Reactions on a Shared Boundary . . . 37

2.2.2 Reactions on Opposing Boundaries . . . 39

2.2.3 Discussion . . . 40

2.2.4 An Example: Controlling Pattern Formation . . . 41
2.3 Boundary-Bound Reactions with Flow . . . 47
2.4 Summary . . . 51

3 Pattern Formation without Hydrodynamics 53
3.1 Non-Dimensionalization . . . 54
3.2 On Simulation Methods . . . 58
3.3 The Turing Instability . . . 60
3.3.1 Averaging Out Vertical Variation . . . 61
3.3.2 Amplitude Estimation . . . 65
3.4 Normal Mode Analysis . . . 74
3.4.1 Pattern Formation . . . 78
3.4.2 Chemical Oscillations . . . 83
3.4.3 On Simultaneous Instabilities . . . 90
3.5 Summary . . . 93

4 Pattern Formation with Hydrodynamics 95
4.1 Non-Zero Rayleigh Numbers . . . 97
4.1.1 R Driven Flows . . . 103
4.1.2 Flows on Patterns . . . 105
4.2 Summary . . . 107

5 Conclusion 111
5.1 Future Research . . . 113
5.1.1 Pattern Control at the Intersection . . . 113
5.1.2 Extending the Pattern Control Problem . . . 114
5.1.3 Large Rayleigh Numbers . . . 117

References 118

List of Figures

1.1 Schematic for the general boundary bound reaction problem between two infinite flat plates where reagents are generated at the boundary through enzyme coated plates. 2

1.2 A simplified sketch of the convective motion for the Rayleigh-Bénard instability. 5

1.3 A simulation at long time of a 1-dimensional Turing instability. In this figure, we plot the development of the pattern in time with $(a, b, \gamma, D) = (0.2, 2.0, 1, 50)$. 16

1.4 A simulation of the two dimensional the Turing Instability. As in Figure 1.3 the parameters chosen are $(a, b, \gamma, D) = (0.2, 2.0, 1, 50)$, with domain sizes selected to admit the unstable mode along both cardinal directions. 17

1.5 The critical diffusion ratio as a function of b for $c \in \{1/5,\ 1/7,\ 1/10\}$, $b = 2.0$ 18

1.6 We compare the behaviour of the critical wave number and critical diffusion through Equation 1.60 and Equation 1.61 as a function of $a/b = c$, with $b = \gamma = 1$. 18

1.7 (a) Critical Rayleigh numbers for various modes k calculated using a shooting method for Equation (1.99) with boundary conditions described in Equation (1.98) (b) Long time simulation of supercritical Rayleigh number . . . 26

2.1 We plot $\sigma_{s,\pm}$ from Equation (2.42) as a function of k with the value 1.5 marked. $(\lambda, \eta_1, \eta_2, D) = (0, 1, 5, 1/2)$ 38

2.2 A schematic for the system described in Equations (2.56) to (2.59) 42

2.3 (a) We plot the roots of Equation (2.68) as a function of k. (b) The critical diffusion for various k described by Equation (2.67). Both plots are for $(a, b, \eta_1) = (0.75, 1, 1)$ 44

2.4 Regions of stability predicted from the normal mode analysis for $\eta, \gamma = 1$ and various (a, b). Contours mark various critical diffusion values 45

3.1 A schematic for the model investigated in Chapter 3 and Chapter 4. Note that we assume the buoyancy forces are negligible in Chapter 3 55

3.2 Steady state concentrations for $Q(z)$ and $R(z)$ as determined in Equation (3.31) 61

3.3 (a) Critical diffusion estimate as a function of $\mu = \eta/\gamma$ for various c with $b = 2$. (b) Simulation of Q at supercritical diffusion after sometime $(a, b, \eta, \gamma, D) = (0.2, 2.0, 1, 1, 6)$. 66

3.4 Resting simulation amplitude for $\overline{Q}$ vs. estimate for various η and perturbations with $\gamma = 0.01$ 74

3.5 Resting simulation amplitude for $\overline{Q}$ vs. estimate for various η and perturbations with $\gamma = 0.1$ 75

3.6 Resting simulation amplitudes for $\overline{Q}$ from Figure 3.4 and Figure 3.5. 75

3.7 Emergence of Turing patterns as a function of time. 76

3.8 Bounding curves for the range of wavenumbers which have a positive critical diffusion given a particular γ. 80

3.9 (a) Surface of most critical mode as a function of (γ, η), $(a, b) = (0.2, 2.0)$ (b) Critical mode for varied η and $\gamma = 1$. (c) Critical mode for varied γ and $\eta = 1$. Both figures used the shared parameters $(a, b) = (0.2, 2.0)$. 81

3.10 (a) Normal mode estimate versus average estimate for critical diffusion for various η. (b) Normal mode estimate versus numerical estimate for critical diffusion for various η. Both figures used the shared parameters $(a, b, \gamma) = (0.2, 2.0, 1)$. 83

3.11 (a) Contour plot of critical η determined by solving Equation (3.155) as a function of (γ, D). (b) Contour plot of critical ω as a function of (γ, D). Values were calculated from (3.155) with shared parameters $(a, b) = (0.2, 2.0)$ 87

3.12 (a) Amplitude development over time for oscillating chemical patterns for various perturbations. (b) Resting amplitude of oscillations at long time as a function of perturbation. Both figures used the parameters $(a, b, D, \gamma) = (0.2, 2.0, 1.0, 1.0)$, and $\eta = (1 + \epsilon^2)\eta_c$, where η_c is calculated from Equation (3.155) for the parameters of interest. 88

3.13 The average concentration versus time. 89

3.14 (a) Critical curves for diffusion driven patterns and decay driven oscillations, $(a, b, \gamma) = (0.2, 2.0, 2.08)$. (b) Critical decay for various modes k with $(a, b, \gamma, D) \approx (0.2, 2.0, 2.08, 4.74)$. 90

3.15 Snapshots of a simulation of oscillating patterns. This is simulated with a warm up of 100s and captured for 40s. In this case, we have selected $\lambda_t = 0.001 = \lambda_o$ and $\gamma = 2.08$. 91

3.16 The top boundary of a simulation of oscillating patterns. This is simulated with a warm up of 100s and captured for 40s. In this case, we have selected $\lambda_t = 0.001 = \lambda_o$ and $\gamma = 2.08$. Horizontal marks indicate the snapshots plotted in Figure 3.15. 92

3.17 (a) A window of the observed transitory traveling waves along the boundary (b) A window of time capturing a transitory soliton along the boundary. Both figures were simulated with $\gamma = 2.08$, $\eta = 4.0$ and $D = 2.5$. 93

4.1 A simplified schematic for the behaviour at the onset of the instability where buoyancy driven flows are present. 97

4.2 (a) Critical Rayleigh number surface versus the diffusion ratio and wavenumber, $(\eta = 1,\ \gamma = 1)$. (b) Critical mode versus the diffusion ratio and decay, for $\gamma = 1$. Each Figure used $(a, b) = (0.2, 2.0)$ 102

4.3 (a) Comparison of shooting method estimate versus a bisection algorithm detecting the formation of patterns. (b) Derivative of the Critical Rayleigh number as a function of the diffusion coefficient D. Parameters for both Figures where $(a, b, \eta, \gamma) = (0.2, 2.0, 1, 1)$ 103

4.4 Comparison of critical Ra for Q and R driven flows as a function of the diffusion ratio, $(a, b, \eta, \gamma) = (0.2, 2.0, 1, 1)$ 105

4.5 (a) Critical Rayleigh number on the (δ^R, D) surface, $\delta^Q = 1$. (b) Close up of critical Rayleigh number for Q and R driven flows at the transition. Shared parameters for the two Figures were $(a, b, \eta, \gamma) = (0.2, 2.0, 1, 1)$ 106

4.6 Amplitude of $\overline{Q}$ versus the pertubations in the critical Rayleigh number, $(\eta, \gamma, D) = (1, 1, 1)$. 107

4.7 (a) Concentration of Q at the steady state for $D \approx 4.78$ and $\mathrm{Ra} = -1$ (b) Concentration of Q at the steady state for $D \approx 4.78$ and $\mathrm{Ra} = -1$ (c) Comparison of the width of the peak and trough relative to the domain size as a function of Ra. Shared parameters across the Figures were $(a, b, \eta, \gamma) = (0.2, 2.0, 1, 1)$ 108

4.8 (a) Effect of the Rayleigh number on oscillations near their critical values. We have marked Ra_c and simulated with $(\eta, \gamma, D) = (1.612, 1, 1)$ (b) Concentration of Q relative to steady state at upper boundary, $(\eta, \gamma, D, \mathrm{Ra}) = (3, 1.8, 3, -2250)$ demonstrating how oscillations can appear when we are far from the critical values. Snapshot was captured after 200 units of simulation time. 109

5.1 Pattern formation regions found in Section 2.2.4 with an elliptical path marked. 114

5.2 Q driven flow for the example in Chapter 2 with $(a, b, \eta, \gamma) = (0.2, 2.0, 1, 1)$. 116

5.3 Approximate peak and trough of stable oscillatory patterns with flow for Q after 200 units of simulation time, $(\eta, \gamma, D, \mathrm{Ra}) = (3, 1.8, 3, -2250)$. 117

List of Tables

3.1 Comparison of normal mode and bisection algorithm critical diffusion estimates. Values are rounded to third decimal place. 84

3.2 Critical decays and tested values for a fixed $D = 1$ and various γ. 87

4.1 Numerical estimate of critical Rayleigh number against bisection algorithm. Results are rounded to the third decimal place. 104

Chapter 1

Introduction

This thesis is organized into two main parts respectively treating boundary-bound reactions with and without fluid flow. The term boundary-bound reactions is used to refer to a chemical reaction which takes place at the boundary, as opposed to the bulk of the fluid domain. Since many biochemical reactions require enzymes to meaningfully occur by controlling the presence of enzymes we are able to influence where the reaction can meaningfully take place. If the location of these enzymes are limited to the boundary then the generation and removal of the various chemical species is limited to the boundary and can be modeled as fluxes. If the boundary is a selectively permeable membranes allowing material to transition between the domain and a reservoir, then the flux along the membrane can also be modeled as a boundary-bound reaction.

Since boundary-bound reactions can occur over a wide variety of complicated domain geometries, we focus our analysis on a single simple geometry. In particular, this work focus on boundary-bound reactions occurring on the surface of two flat plates. We will assume that these plates are separated by a small vertical length, and that the horizontal lengths are much larger then the vertical distance between them. As a consequence, we can effectively model the scenario with a horizontal domain that is infinite. A simple schematic for the general problem is provided in Figure 1.1. Furthermore, since we are interested in steady pattern formation with applications to biology or similar length scales, and since the density changes caused by concentration gradients are generally small, we can make use of the Boussinesq approximation for the Navier-Stokes equations which we introduce in this Chapter. Additionally, this will allow us to study how the formation of convective cells and Turing patterns along the boundary influence each other and how the chemical instabilities might be used to influence the buoyancy ones.

We begin by studying pattern formation in general in Chapter 2. Here we will obtain analytical results which help to explain some of the observations of Balazs et al. [1] as well as determine necessary conditions for the existence of pattern-forming instabilities. These conditions are expressed as a function of the reaction parameters and linear instability. We explore these results through two applications of the Schnakenberg reaction [2, 3], which is introduced in Section 1.1. The first application of the Schnakenberg reaction system is presented in Chapter 2 and considers a mechanism for the control of pattern formation by varying constant fluxes along one boundary; the second is presented in Chapter 3 and is primarily concerned with Turing pattern formation occurring at the boundary without flow. Afterwards, we use the results from Chapter 3 to to inform our study in Chapter 4 on pattern formation at the boundary with flow.

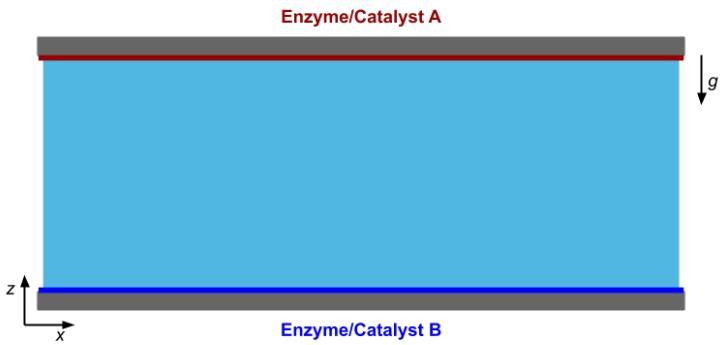


Figure 1.1: Schematic for the general boundary bound reaction problem between two infinite flat plates where reagents are generated at the boundary through enzyme coated plates.

In our first example studied in Chapter 2, will identify three regions as a function of fluxes at the bottom boundary: one which produces chemical oscillations, a spatial pattern forming one, and a stable region. We will also discuss how one can transition between these regions by changing fluxes along one side of the boundary. This model is particularly interesting since it allows us to design paths through the various regions, turning different instabilities on and off according to some schedule, or resetting the system after some transitory behaviour has decayed. This gives us a glimpse into how we might influence the buoyancy driven instability through the chemical one.

Since one of the primary motivations of this thesis is to study the relationship between the Turing instability and the onset of convection in buoyancy driven flows. We spend

out time in Chapter 3 studying the second example. Here, we consider the Schnakenberg system taking place on the upper boundary between two flat plates. During our analysis, we identify several differences between the classical Turing pattern formation problem and pattern formation for boundary-bound reactions. We also use this as an opportunity to study the chemical oscillations observed by Balazs et al. [1] and mentioned in Chapter 2. This is concluded by studying the behaviour near the intersection of the pattern forming instability and oscillatory instability. Here, we observe a slow manifold of oscillating patterns that eventually converges to a steady pattern. In addition, we are able to present more exotic transitory behaviour such as travelling waves and solitons along the boundary. These behaviours occur when both instabilities are unstable. We conclude with a discussion of how these results can be paired with the example in Chapter 2 on controlling pattern formation.

Once we have fully understood pattern formation without flow, we introduce buoyancy driven flows into the model by assuming that advection takes place according to the Boussinesq approximation of the Navier-Stokes equations in Chapter 4. As we will see, the coupling of Turing instabilities at the boundary and the formation of convective cells is very natural, and the underlying normal mode analysis can be seen as viewing the diffusion-driven pattern formation as a subcase of the buoyancy-driven one. Consequently, we find that the critical Rayleigh number is zero at the critical diffusion and as we transition from subcritical to supercritical diffusion ratios, the behaviour of the other non-dimensionalized parameters changes. This chapter is concluded with an investigation of how the buoyancy-driven flows influence pattern formation, as well as an example where stable chemical oscillations exist for supercritical Rayleigh numbers. Combined with the model in Chapter 2, it gives us an avenue for controlling the formation of convective cells as well as the resulting pattern as a function of the boundary fluxes. In the future, it may be possible to combine these results with high-precision programmable pattern formation that appears possible through Scalise and Schulman, [4] in combination with this work, it could be used to design intricate patterns of flow.

In order to begin our investigation, we start by introducing the two primary instabilities that are at the centre of this thesis. The first instability is the diffusion-driven Turing instability, while the second is the buoyancy-driven Rayleigh-Bénard instability. This chapter is primarily a review of well-known literature, and the majority of the material is adapted from Murray [5], Kundu [6] and Chandrasekhar [7]. We will begin by introducing the Turing instability for general two reagent systems before explicitly exploring the Schnakenberg system [2] used throughout this thesis. Afterwards, we will explore the temperature-driven Rayleigh-Bénard instability.

Introduced in 1952 [8], the Turing Instability has become one of the most well-studied mechanisms for pattern formation in mathematical biology. In his original analysis, Turing showed that pattern formation can come about in reaction-diffusion systems through asymmetric diffusion rates between two different reagents. This is surprising since diffusion generally reduces spatial fluctuations in systems. Moreover, should the patterning reagents be biological chemicals which control development then the resulting patterns could explain the occurrence of various patterns in nature. Murray [5] provides several examples of biological pattern formation which could be explained through Turing instabilities. These examples include felines' tails, cattle spots and the patterning on butterfly wings. For other biological applications outside of those provided by Murray, Kondo et al. [9] provide a recent review of the biological applications to zebrafish. We also recommend the paper by Krause et al. [10] for a review of current research in Turing-style instabilities.

In our review, we focus on the two reagent case like Murray [5] and Turing [8]. In the two reagent case the stability of the system with respect to changes in the diffusion ratio reduces to the analysis of a quadratic equation. From here, it is possible to derive sufficient conditions for the system to be linearly unstable to short-wavelength non-oscillatory patterns. The sufficient conditions for the formation of Turing patterns are called Turing conditions. As part of our introduction, we will determine the Turing conditions for the two reactant Schnakenberg [2] system, the information we gain to inform decisions such as parameter selection throughout this Thesis. The Schnakenberg reaction is a modification of Selkov [3] who had originally proposed it as a model for self-generated oscillations in glycolysis. The only change is the addition of a bulk source to one of the reaction terms. It is particularly popular due to its simple structure while exhibiting limit cycle behaviour and Turing instabilities. Our introduction will allow us to obtain closed formulas for the critical diffusion and the critical mode in the case of the Schnakenberg model. While these equations are not seen in Murray [5], Liu et al. [11] obtain equivalent equations for the critical diffusion and mode using an alternative methodology. For completeness, we conclude with some long-time simulations for super-critical values of diffusion ratio.

Having introduced the Turing instability, we can then turn our attention to the onset of convection through the Rayleigh-Bénard instability. The Rayleigh-Bénard instability describes the transition of a layer of fluid heated from below from a stable state without flow to a pattern of convection cells as the temperature difference between the top and bottom of the layer increases. Generally, water decreases in density as the temperature increases so heating the fluid from below results in denser fluid at the top than at the bottom. For small temperature differences, convection does not take place. Instead, small perturbations decay due to the thermal diffusivity and viscosity. As the temperature gradient increases, the differences in density grow and perturbations from the steady behaviour no longer decay

quickly enough, causing the fluid to turn over. This occurs when the Rayleigh number, which characterizes the ratio of buoyancy effects to viscous effects, exceeds a critical value. We provide a simplified drawing of the resulting behaviour in Figure 1.2. This figure also helps to motivate the interplay between Turing pattern formation and the formation of convective cells. If chemical concentration gradients influence the density profile, then a similar instability is possible. As we will see the onset of convection not only causes fluid motion, but the flows lead to peaks and valleys in the horizontal temperature profile that are very similar to Turing patterns in chemical concentration fields.

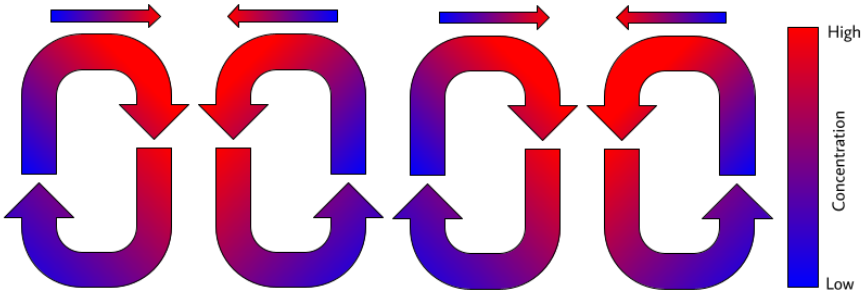


Figure 1.2: A simplified sketch of the convective motion for the Rayleigh-Bénard instability.

In our introduction to Rayleigh-Bénard convection we will introduce the Boussinesq approximation and perform a simple numerical study of the instability instead. Our introduction is adapted from Kundu [6] and Chandrasekhar [7]. From this introduction, we will be albe to introduce the fluid model and numerical techniques we will use later in this thesis; and sas a result, we are also able to provide both the critical curve as well as a simulation at long time of the system at a supercritical Rayleigh number.

1.1 The Turing Instability

While the Turing instability can exist for any number of interacting chemical reagents with asymmetric diffusion rates, we will stick to the original analysis performed by Turing [8], and by Murray [5]. As a result, we consider a system of two interacting chemical reactions able to diffuse freely in some periodic domain. Periodic domains are often a good approximation for large domains and will simplify some of our analysis.

If there are no other dynamics occurring in the bulk, then an approximate model for the behaviour of the two reagents, $\mathbf{u} = \begin{bmatrix} u & v \end{bmatrix}^T$, is given by

$$\frac{\partial \mathbf{u}}{\partial t} = \mathbf{F}(\mathbf{u}) + \mathcal{D}\nabla^2 \mathbf{u}. \tag{1.1}$$

Where $F(\mathbf{u})$ is a potentially non-linear reaction term and $\mathcal{D}$ is a constant diagonal diffusion matrix with all positive entries along the diagonal. If the reaction equations have some sort of equilibrium defined by $\mathbf{u}_0$ which satisfies $\mathbf{F}(\mathbf{u}_0) = 0$, we can consider the linear stability around that point. In fact, if $\mathbf{F}(\mathbf{u})$ is continuously differentiable then we can conclude that

$$\mathbf{F}(\mathbf{u}) = \mathbf{F}(\mathbf{u}_0) + \left.\frac{\partial \mathbf{F}}{\partial \mathbf{u}}\right|_{\mathbf{u}=\mathbf{u}_0} (\mathbf{u} - \mathbf{u}_0) + O(||\mathbf{u} - \mathbf{u}_0||^2) \tag{1.2}$$

$$\approx \left.\frac{\partial \mathbf{F}}{\partial \mathbf{u}}\right|_{\mathbf{u}=\mathbf{u}_0} (\mathbf{u} - \mathbf{u}_0). \tag{1.3}$$

If $\mathbf{u}$ is sufficiently close to the equilibrium then the $O(||\mathbf{u} - \mathbf{u}_0||^2)$ can be neglected. Consequently, we make the substitution $\mathbf{F}(\mathbf{u}) = \left.\frac{\partial \mathbf{F}}{\partial \mathbf{u}}\right|_{\mathbf{u}=\mathbf{u}_0} \mathbf{w}$, with $\mathbf{w} = \mathbf{u} - \mathbf{u}_0$. As a result, we can conclude that near the equilibrium the system is approximately governed by a linearized system,

$$\frac{\partial \mathbf{w}}{\partial t} = \left.\frac{\partial \mathbf{F}}{\partial \mathbf{u}}\right|_{\mathbf{u}=\mathbf{u}_0} \mathbf{w} + \mathcal{D}\nabla^2 \mathbf{w}. \tag{1.4}$$

As previously discussed, we have assumed that the domain is periodic in all dimensions. Therefore, we will perform a normal mode analysis assuming that solutions to the system take the form

$$\mathbf{w}(x, t) = \sum_{\mathbf{k}} \hat{\mathbf{w}}(\mathbf{k}) e^{\lambda t + i\mathbf{k}\cdot\mathbf{x}}, \tag{1.5}$$

where λ is the temporal growth or decay of the mode $\mathbf{k}$, and $\mathbf{k}$ is a vector of wavenumbers. The wavenumber for a particular coordinate is given by $k_i = 2\pi n / L_i$ where L_i is the length of the ith coordinate and $n \in \mathbb{Z}$.

Substituting Equation (1.5) into Equation (1.4) we obtain

$$\sum_{\mathbf{k}} \left(\lambda I - \left.\frac{\partial \mathbf{F}}{\partial \mathbf{u}}\right|_{\mathbf{u}=\mathbf{u}_0} + ||\mathbf{k}||^2 \mathcal{D} \right) \hat{\mathbf{w}}(\mathbf{k}) e^{\lambda t + i\mathbf{k}\cdot\mathbf{x}} = 0. \tag{1.6}$$

Noting that Fourier modes are linearly independent, this holds if and only if for each wavenumber $\mathbf{k}$

$$\left(\lambda I - \left.\frac{\partial \mathbf{F}}{\partial \mathbf{u}}\right|_{\mathbf{u}=\mathbf{u}_0} + ||\mathbf{k}||^2 \mathcal{D}\right) \hat{\mathbf{w}}(k) = 0. \tag{1.7}$$

As a consequence, the linear stability of a particular wavenumber is determined by eigenvalues of the matrix A,

$$A = \left.\frac{\partial \mathbf{F}}{\partial \mathbf{u}}\right|_{\mathbf{u}=\mathbf{u}_0} - ||\mathbf{k}||^2 \mathcal{D}. \tag{1.8}$$

If $\mathrm{Re}(\lambda) > 0$ then we expect the mode to be linearly unstable and random perturbations around the equilibrium should grow in magnitude. Conversely, if $\mathrm{Re}(\lambda) < 0$, then we expect the mode to be asymptotically stable and those small perturbations should decay near the equilibrium.

Similar to Turing [8], we will show in the following Section that if the two species have sufficiently different diffusion coefficients, then it is possible to make non-zero modes $||\mathbf{k}||^2$ unstable. As these unstable wavelengths grow in amplitude, we expect the non-linearities to also grow in magnitude. This eventually violates the assumption that $||u - u_0||^2$ is small. Turing argued that as a result, the system should reach an equilibrium where the non-linearities cause the perturbations to stop growing in size. This has been confirmed in various experiments since, and a review of some of them can be found in Konow et al. [12] Certainly, since the reaction equations describe a physical system, the exponential growth from the linear system could never be accurate indefinitely. In addition, as the reaction diverges from the steady state, the normal mode analysis suggests that the non-linear terms in the reaction should send energy into higher modes until they are effectively dampened by the diffusion term after having left the range of unstable modes predicted by the linear stability analysis.

1.1.1 The Two Reagent Case

In the case of two reagents Equation (1.1) can be expressed as

$$\frac{\partial}{\partial t}\begin{bmatrix} u \\ v \end{bmatrix} = \gamma \begin{bmatrix} f(u,v) \\ g(u,v) \end{bmatrix} + \nabla^2 \begin{bmatrix} d_u & 0 \\ 0 & d_v \end{bmatrix} \begin{bmatrix} u \\ v \end{bmatrix}, \tag{1.9}$$

where γ is a global reaction rate. As noted in Murray [5] such systems can always be non-dimensionalized so that the diffusion matrix reduces to,

$$\mathcal{D} = \begin{bmatrix} 1 & 0 \\ 0 & D \end{bmatrix}, \tag{1.10}$$

where $D = d_v/d_u$. Assuming such a non-dimensionalization has be chosen, then the Jacobian evaluated at some chemical equilibrium can be expressed as,

$$\left.\frac{\partial \mathbf{F}}{\partial \mathbf{u}}\right|_{\mathbf{u}=\mathbf{u}_0} = \gamma \begin{bmatrix} f_u & f_v \\ g_u & g_v \end{bmatrix}, \tag{1.11}$$

so that through Equation (1.8) the matrix for the eigenvalue problem is given by

$$A = \gamma \begin{bmatrix} f_u & f_v \\ g_u & g_v \end{bmatrix} - ||\mathbf{k}||^2 \begin{bmatrix} 1 & 0 \\ 0 & D \end{bmatrix}, \tag{1.12}$$

$$= \begin{bmatrix} \gamma f_u - q^2 & \gamma f_v \\ \gamma g_u & \gamma g_v - Dq^2 \end{bmatrix}, \tag{1.13}$$

where we have substituted $q^2 = ||\mathbf{k}||^2$ for compactness. In addition, we can immediately conclude that,

$$\begin{aligned} \mathrm{Tr}(A) &= \gamma(f_u + g_v) - q^2(1+D), \\ \det(A) &= Dq^4 - \gamma(g_v + Df_u)q^2 + \gamma^2(f_u g_v - f_v g_u), \end{aligned} \tag{1.14}$$

so that the eigenvalues for each mode are neatly calculated by,

$$\lambda_\pm = \frac{\mathrm{Tr}(A) \pm \sqrt{\mathrm{Tr}(A)^2 - 4\det(A)}}{2}. \tag{1.15}$$

Let us take a moment to consider what these equations tell us. For each mode, $\mathbf{k}$, the real part of $\lambda_\pm$ determines its stability. Noting that $||\mathbf{k}||^2 = q^2 = 0$ describes the stability of the steady state, we first determine conditions so that it is stable. In particular, since we are interested in how the normally stabilizing diffusion term can cause the formation of chemical patterns, we are particularly interested in when non-zero modes are unstable.

Setting $q^2 = 0$, the equation for $\lambda_\pm$ is given by,

$$\lambda_\pm = \gamma \frac{f_u + g_v \pm \sqrt{(f_u + g_v)^2 - 4(f_u g_v - f_v g_u)}}{2}. \tag{1.16}$$

Turing originally proposed the following sufficient conditions to ensure $\mathrm{Re}(\lambda) < 0$,

$$\begin{aligned} f_u + g_v &< 0 \\ f_u g_v - f_v g_u &> 0 \end{aligned} \tag{1.17}$$

However, these conditions also imply that $\mathrm{Tr}(A) = f_u + g_v - q^2(1+D) < 0$ for all non-zero q. Consequently, through Equation (1.15), we conclude that it is impossible to make any non-zero mode unstable without also requiring,

$$\det(A) = Dq^4 - \gamma(g_v + Df_u)q^2 + \gamma^2(f_u g_v - f_v g_u) < 0. \tag{1.18}$$

Viewing this as an equation in q^2, we solve for its minimum,

$$\frac{d}{d(q^2)}\det(A) = 2Dq^2 - \gamma(g_v + Df_u) = 0 \iff q^2 = \gamma\frac{Df_u + g_v}{2D}. \tag{1.19}$$

Since $q^2 > 0$, and $f_u + g_v < 0$ we conclude that f_u, g_v must have opposite signs and $D \neq 1$. Substituting this into (1.18), the resulting value must be negative, and implies, after eliminating a common γ term, that

$$\frac{(Df_u + g_v)^2}{4D} - \frac{(Df_u + g_v)^2}{2D} + (f_u g_v - f_v g_u) < 0. \tag{1.20}$$

Noting that $\gamma \neq 0$ is necessary for reaction dynamics to occur, we obtain sufficient conditions for a mode to be unstable,

$$f_u g_v - f_v g_u < \frac{(Df_u + g_v)^2}{4D}. \tag{1.21}$$

This can be expanded as a quadratic in D, and the roots define a critical value where we predict the instability occurs. Whether the root must be larger than or less than 1 depends on the signs of f_u and g_v. Further, our analysis allows us to say something much more general. Since f_u, f_v, g_u and g_v are just the elements of the Jacobian evaluated at a fixed point, we never made any assumptions about the general form of the reaction. As a result of our efforts, the inequalities we have discovered the general sufficient conditions for chemical pattern formation in a two-reactant system. We summarize them below:

$$f_u + g_v < 0, \qquad f_u g_v - g_u f_v > 0, \tag{1.22}$$

$$Df_u + g_v > 0, \qquad f_u g_v - f_v g_u < \frac{(Df_u + g_v)^2}{4D}, \tag{1.23}$$

$$D \neq 1. \tag{1.24}$$

1.1.2 The Schnakenberg System

Now that we have introduced the Turing conditions let us consider the example of the Schnakenberg system [2], which is known to give rise to Turing pattern formation and has been studied extensively [5, 13, 11] Due to its tractability and the wealth of information about it, we have chosen it to be the primary reaction system studied in this thesis. The remainder of this section will be spent reviewing the Turing pattern formation results discussed above and providing our own method for determining the space of parameters which satisfy the general Turing conditions.

One way to derive the Schnakenberg reaction system as described by Murray [5] is given by the following reaction kinetics,

$$A \underset{k_{-1}}{\overset{k_1}{\rightleftharpoons}} U, \quad B \xrightarrow{k_2} V, \quad 2U + V \xrightarrow{k_3} 3U, \tag{1.25}$$

where the k_i's are reaction rates. If the concentration of A and B are held constant or are so large that the limiting factor is the reaction step, such as the presence of enzymes, then there will be a constant generation of U and V through these reaction paths. As a result, the reaction-diffusion equations for the Schnakenberg system, taking place over a periodic domain $[0, L]^n$ for $1 \leq n \leq 3$ can be expressed as

$$\frac{\partial u}{\partial t} = \alpha - k_{-1}u + k_3 u^2 v + d_u \nabla^2 u, \tag{1.26}$$

$$\frac{\partial v}{\partial t} = \beta - k_3 u^2 v + d_v \nabla^2 v, \tag{1.27}$$

where α and β represent the constant generation of U and V. In addition d_u and d_v are positive constants representing the diffusion rates for u and v. For completeness, we begin in the usual fashion by non-dimensionalizing the system. Suppose that

$$\mathbf{x} = L\hat{\mathbf{x}}, \quad t = t_s \hat{t}, \quad u = u_s \hat{u}, \quad v = v_s \hat{v}, \quad D = \frac{d_u}{d_v}. \tag{1.28}$$

Making the necessary substitutions in Equation (1.26) and dropping the decorations we have

$$\frac{\partial u}{\partial t} = \frac{t_s \alpha}{u_s} - t_s k_{-1} u + t_s u_s v_s k_3 u^2 v + \frac{t_s d_u}{L^2} \nabla^2 u. \tag{1.29}$$

Choosing the diffusive time scale $t_s = L^2/d_u$, this reduces to,

$$\frac{\partial u}{\partial t} = \frac{L^2 \alpha}{d_u u_s} - \frac{L^2 k_{-1}}{d_u} u + \frac{L^2 u_s v_s k_3}{d_u} u^2 v + \nabla^2 u \tag{1.30}$$

and if we let $u_s = v_s = \sqrt{k_{-1}/k_3}$, we can make the further simplification,

$$\frac{\partial u}{\partial t} = \frac{L^2}{d_u} \left(\sqrt{\frac{k_3}{k_{-1}}} \alpha - k_{-1} u + k_{-1} u^2 v \right) + \nabla^2 u. \tag{1.31}$$

Upon factoring out the k_{-1} term, we can define a new non-dimensionalized reaction rate $\gamma = L^2 k_{-1}/d_u$ and $a = \sqrt{k_3/k_{-1}^3}\alpha$. Also performing similar steps with Equation (1.27)

yields the full system

$$\frac{\partial u}{\partial t} = \gamma\left(a - u + u^2 v\right) + \nabla^2 u, \tag{1.32}$$

$$\frac{\partial v}{\partial t} = \gamma\left(b - u^2 v\right) + D\nabla^2 v, \tag{1.33}$$

where the non-dimensionalized parameters are defined by

$$a = \sqrt{\frac{k_3}{k_{-1}^3}} \cdot \alpha, \qquad b = \sqrt{\frac{k_3}{k_{-1}^3}} \cdot \beta, \qquad t_s = \frac{L^2}{d_u},$$

$$u_s = \sqrt{\frac{k_{-1}}{k_3}}, \qquad v_s = \sqrt{\frac{k_{-1}}{k_3}}, \qquad D = \frac{d_u}{d_v}.$$

1.1.3 Turing Parameter Space

With a non-dimensionalization chosen, we can now investigate pattern formation. First determining the steady state chemical concentrations. In this state, we would expect there to be no spatial or temporal variation and therefore we can eliminate both the derivatives. Consequently, we obtain the following system of equations,

$$\begin{bmatrix} 0 \\ 0 \end{bmatrix} = \gamma \begin{bmatrix} a - u_0 + u_0^2 v_0 \\ b - u_0^2 v_0 \end{bmatrix} \tag{1.34}$$

which can be solved with,

$$\begin{bmatrix} u_0 \\ v_0 \end{bmatrix} = \begin{bmatrix} a + b \\ b/(a+b)^2 \end{bmatrix}. \tag{1.35}$$

Suppose that $a = cb$ for some $c \in \mathbb{R}^+$. If we substitute this into Equation (1.35), this reduces neatly too

$$\begin{bmatrix} u_0 \\ v_0 \end{bmatrix} = \begin{bmatrix} (1+c)b \\ \frac{1}{b(1+c)^2} \end{bmatrix}. \tag{1.36}$$

In this form we will be able to determine the conditions on (b, c) which make pattern formation possible. Moreover, we will also be able to recover analytical expressions for the critical diffusion and critical mode as a function of c.

The next step in determining the conditions for pattern formation is calculating the Jacobian of the non-linear reaction at the steady state,

$$\left.\frac{\partial \mathbf{F}}{\partial \mathbf{u}}\right|_{\mathbf{u}=\mathbf{u}_0} = \gamma \begin{bmatrix} \frac{1-c}{1+c} & (1+c)^2 b^2 \\ -\frac{2}{(1+c)} & -(1+c)^2 b^2 \end{bmatrix}. \tag{1.37}$$

From here we apply the various conditions from Equation (1.22) to determine sufficient conditions for the existence of Turing style instabilities.

Recalling that the diagonal terms must have opposite signs, we turn our attention to f_u and g_v. Regardless of the value of c, we know that $g_v < 0$ and that the critical diffusion ratio must be greater than one. As a result, we can also infer that $f_u > 0$, implying

$$f_u = \frac{1-c}{1+c} > 0. \tag{1.38}$$

Since we have assumed that (b, c) are both positive, this forces $c \in (0, 1)$.

Now, let's turn our attention to the other requirements. We will start with the conditions for the long-wavelength mode $q = 0$ to be stable. From Equation (1.22), these are

$$f_u + g_v < 0, \tag{1.39}$$
$$f_u g_v - g_u f_v > 0. \tag{1.40}$$

The trace condition given by Equation (1.39) is relatively easy to resolve and after some manipulation we have

$$\begin{aligned} f_u + g_v &< 0, \\ \frac{1-c}{1+c} - (1+c)^2 b^2 &< 0, \\ \sqrt{\frac{1-c}{(1+c)^3}} &< b. \end{aligned} \tag{1.41}$$

Further, Equation (1.40) is satisfied immediately with

$$\begin{aligned} f_u g_v - f_v g_u &= -(1-c)(1+c)b^2 + 2(1+c)b^2 \\ &= (1+c)^2 b^2 > 0, \end{aligned} \tag{1.42}$$

since we have already assumed b is positive and $c \in (0, 1)$.

Moving on to the conditions for there to be a short-wavelength instability, we must satisfy

$$D f_u + g_v > 0, \tag{1.43}$$
$$f_u g_v - f_v g_u < \frac{(D f_u + g_v)^2}{4D}. \tag{1.44}$$

Equation (1.43) implies that

$$\begin{aligned} Df_u + g_v &> 0, \\ D\frac{1-c}{1+c} - (1+c)^2 b^2 &> 0, \\ \sqrt{D\frac{1-c}{(1+c)^3}} &> b. \end{aligned} \tag{1.45}$$

Then by combining Equation (1.41) together with Equation (1.45) we obtain simple lower and upper bounds for b, in particular

$$\sqrt{\frac{1-c}{(1+c)^3}} < b < \sqrt{D\frac{1-c}{(1+c)^3}}. \tag{1.46}$$

We can now move onto the final condition given in Equation (1.44)

$$\begin{aligned} (1+c)^2 b^2 &< \frac{\left(D\frac{1-c}{1+c} - (1+c)^2 b^2\right)^2}{4D} \\ 4D(1+c)^4 b^2 &< \left(D(1-c) - (1+c)^3 b^2\right)^2. \end{aligned} \tag{1.47}$$

Expanding Equation (1.47) as a quadratic in b^2 gives

$$(1+c)^6 b^4 - 2(D(1-c)(1+c)^3 - 4D(1+c)^4) b^2 + D^2(1-c)^2 > 0. \tag{1.48}$$

We can determine when the inequality is satisfied by studying the roots of the equation in b^2 on the left hand side. The roots of Equation (1.48) are given by

$$b_{\pm}^2 = D\frac{c+3 \pm 2\sqrt{2c+2}}{(1+c)^3}. \tag{1.49}$$

By studying the numerator of Equation (1.49), we note that $c+3-2\sqrt{2c+2}$ is minimized at $c=1$ with a value of zero. As a result, we know that $b_{\pm}^2$ is non-negative for all $c \in (0,1)$, and therefore the solutions for b are real. Consequently, since we are restricting ourselves to positive values for b, we can omit the negative roots and conclude that

$$b < \sqrt{D\frac{3+c-2\sqrt{2c+2}}{(1+c)^3}}, \quad \text{or} \quad b > \sqrt{D\frac{c+3+2\sqrt{2c+2}}{(1+c)^3}}. \tag{1.50}$$

We note that the first condition in Equation (1.50) can always be satisfied for any given $b > 0$ and $c \in (0, 1)$, as there exists a D sufficiently large so that the condition holds. As a result, the only bound which restricts pattern formation is,

$$\sqrt{\frac{1-c}{(1+c)^3}} < b. \tag{1.51}$$

In all other cases there exists a D which implies the existence of an unstable mode. For instance, if $c = 1/10$, then we conclude the system allows for the formation of Turing patterns so long as b satisfies the lower bound in Equation (1.46),

$$\sqrt{\frac{1-c}{(1+c)^3}} = \frac{30}{\sqrt{11^3}} \approx 0.822 < b. \tag{1.52}$$

However, since we are generally unable to select the diffusion, we may be interested to know when given a fixed D what are the range of values for b which admit an unstable mode. It can be shown that the upper bound in Equation (1.46) is strictly larger than the optional lower bound in Equation (1.50). This implies that it cannot be satisfied without violating Equation (1.46). As a consequence, the optimal bounds are given by combining the upper bound in Equation (1.50) with the upper bound in Equation (1.46). To determine which bound is the strictest, we compare them to obtain the following string of inequalities

$$\sqrt{D\frac{3+c-2\sqrt{2c+2}}{(1+c)^3}} \leq \sqrt{D\frac{1-c}{(1+c)^3}}, \tag{1.53}$$

$$D\frac{3+c-2\sqrt{2c+2}}{(1+c)^3} \leq D\frac{1-c}{(1+c)^3}, \tag{1.54}$$

$$3+c-2\sqrt{2c+2} \leq 1-c, \tag{1.55}$$

$$4+2c \leq 2\sqrt{2c+2}, \tag{1.56}$$

$$1+c \leq \sqrt{2}\sqrt{c+1}, \tag{1.57}$$

$$\sqrt{1+c} \leq \sqrt{2}. \tag{1.58}$$

Noting that Equation (1.58) holds for all $c \in [0, 1)$. We can replace the upper bound in Equation (1.46) with the stricter upper bound in Equation (1.50) so that the range of b which admit an unstable mode is given by,

$$\sqrt{\frac{1-c}{(1+c)^3}} < b < \sqrt{D\frac{3+c-2\sqrt{2c+2}}{(1+c)^3}}. \tag{1.59}$$

This has the benefit of providing a method for determining the critical diffusion in the case of the Schnakenberg model. In particular we can consider the value of D which causes the transition from b having no unstable modes, to having unstable modes, which implies that,

$$D_c = \frac{(1+c)^3}{3+c-2\sqrt{2c+2}}b^2. \tag{1.60}$$

As a result, we can also conclude by substituting Equation (1.60) into Equation (1.19) that

$$q_c^2 = \gamma\frac{\sqrt{2c+2}-(1+c)}{c+1}. \tag{1.61}$$

Consequently, we can get an idea of the shape of the critical diffusion and critical mode as a function of the ratio between the reaction terms and capture this in Figure 1.6. We note in particular that as $a \to b$ and $c \to 1$, the critical mode becomes smaller and the critical diffusion blows up. In Figure 1.5 we look at the behaviour with respect to b for fixed ratios $a/b = c \in \{1/10, 1/7, 1/5\}$. Fixing $a = 0.2$ and $b = 2.0$ gives $c = 1/10$ and we can calculate the critical diffusion by substituting this into Equation (1.60) gives,

$$D_c = \frac{4(1.1)^3}{3.1-2\sqrt{2.2}} \approx 38.7. \tag{1.62}$$

Later in the thesis we will expand our model to contain several additional non-dimensionalized parameters. Since we are primarily concerned with the interactions between Turing instabilities and buoyancy driven ones, we will reduce the number of free parameters by fixing $a = 0.2$ and $b = 2.0$. We already know these parameters admit Turing instabilities, and therefore serve as a reasonable starting point to study how boundary-bound reactions may differ from the bulk model.

Using these parameters and the simulation techniques discussed later in Section 3.2, we simulate supercritical diffusion ratios for the 1-dimensional and 2-dimensional Turing instabilities. The results for the one dimensional patterns can be found in Figure 1.3. Here we plot the concentration of u as a function of time while the pattern is developing. This allows us to see the formation of the pattern from random noise. As we might expect, the patterns form around the steady state $a + b = 2.2$ before eventually stabilizing when the amplitude is sufficiently large. In Figure 1.4 we provide a snapshot of the two-dimensional Turing instability after 100 units of time while the pattern is still growing. As we will see in Chapter 3 the time for the patterns to stabilize can be quite long and is not capture here. Instead we would like to highlight how the patterns in u compare to v. A quick comparison of u and v shows that the peaks and troughs of u correspond with the troughs and peaks

of v. When we consider pattern formation along the boundary with flow, the pattern will impact how the reagents interaction through the density variations they produce.

Finally, while we did not investigate it in our short introduction, the pattern formation process is sensitive to the domain shape and can produce a much wider array of patterns than presented in our Figures. This is because the wavenumber q^2 is a function of k_x and k_y, so if there are multiple admissible wavenumbers $q^2 = k_x^2 + k_y^2$, these modes compete and the long time behaviour will depend on the initial conditions. In addition to this, since the normal modes are determined by the domain geometry, this will also play an important role in the final resting pattern. Murray [5] spends sometime discussing the impacts of domain geometry on Turing pattern formation in their text.

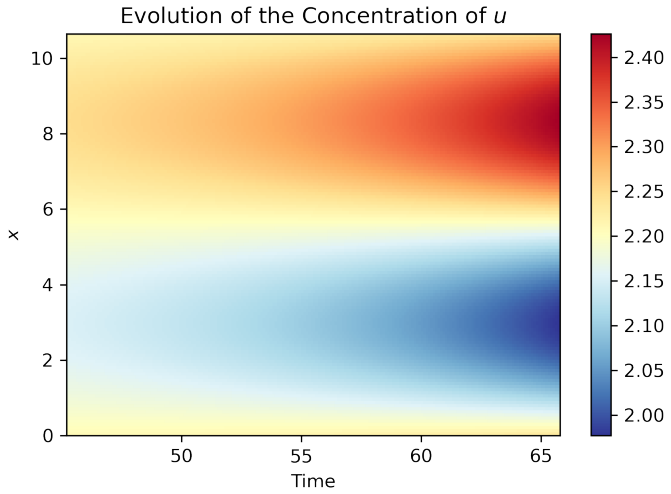


Figure 1.3: A simulation at long time of a 1-dimensional Turing instability. In this figure, we plot the development of the pattern in time with $(a, b, \gamma, D) = (0.2, 2.0, 1, 50)$.

1.1.4 Summary

In this section, we have quickly introduced the Turing instability as well as performed an analytical investigation for the two reagent Schnakenberg model. As a result, we have determined sufficient conditions for the existence of Turing patterns described in Equation

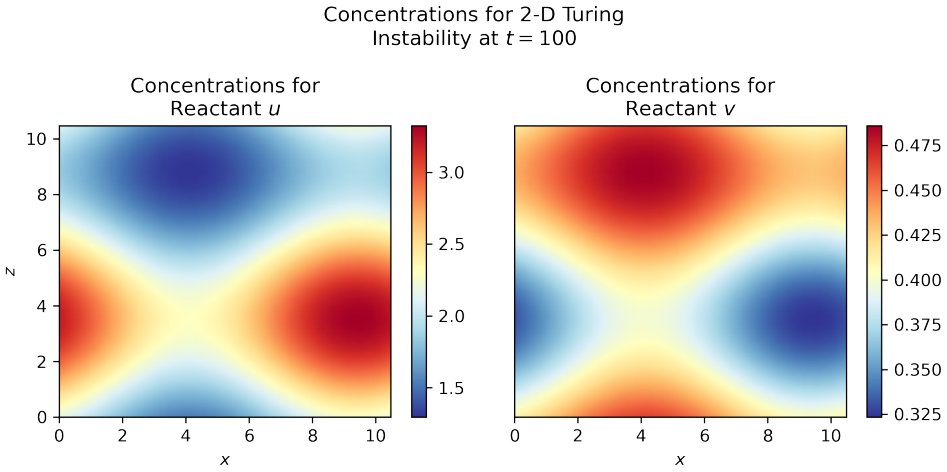


Figure 1.4: A simulation of the two dimensional the Turing Instability. As in Figure 1.3 the parameters chosen are $(a, b, \gamma, D) = (0.2, 2.0, 1, 50)$, with domain sizes selected to admit the unstable mode along both cardinal directions.

(1.22) and originally introduced by Turing [8],

$$\begin{aligned} f_u + g_v < 0, \qquad & f_u g_v - g_u f_v > 0, \\ D f_u + g_v > 0, \qquad & f_u g_v - f_v g_u < \frac{(D f_u + g_v)^2}{4D}, \\ D \neq 1. & \end{aligned}$$

We have also determined a closed form for the critical diffusion and critical mode of the Schnakenberg model in Equation (1.60) and Equation (1.19),

$$D_c = \frac{(1+c)^3}{3 + c - 2\sqrt{2c+2}} b^2, \qquad q_c^2 = \gamma \frac{\sqrt{2c+2} - (1+c)}{c+1}. \tag{1.63}$$

These equations were obtained by considering the space of parameters which admit unstable Turing patterns. In particular, we determined for our system if $a = cb$, then $0 < c < 1$ and the system is unstable only if,

$$\sqrt{\frac{1-c}{(1+c)^3}} < b < \sqrt{D \frac{3 + c - 2\sqrt{2c+2}}{(1+c)^3}}. \tag{1.64}$$

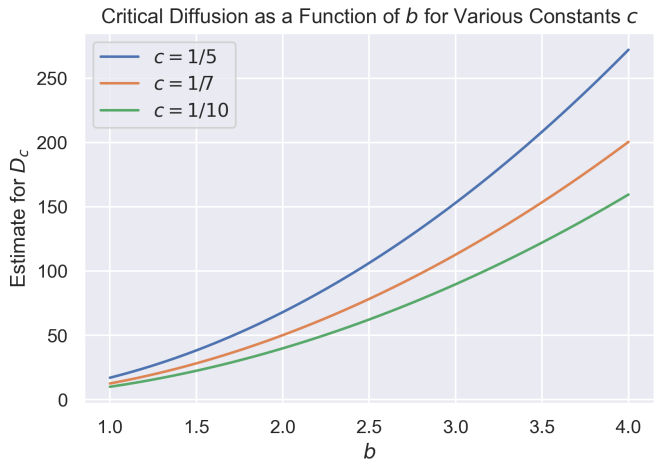


Figure 1.5: The critical diffusion ratio as a function of b for $c \in \{1/5,\ 1/7,\ 1/10\}$, $b = 2.0$

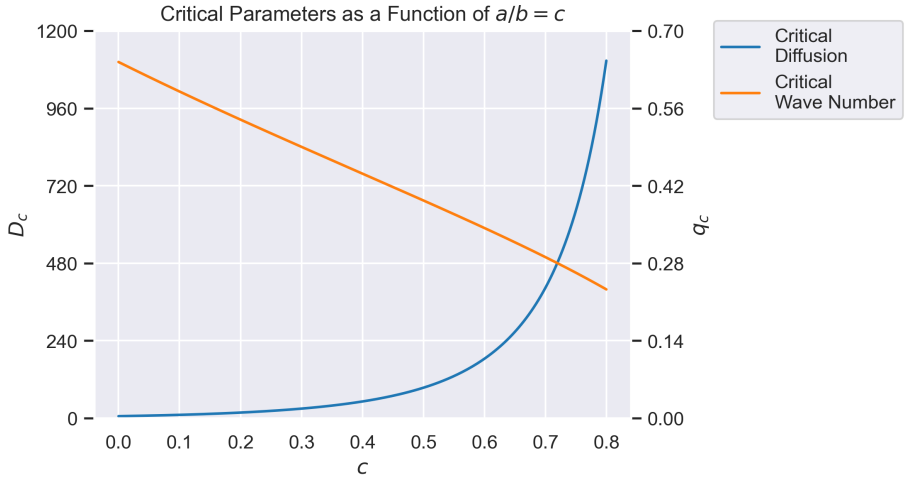


Figure 1.6: We compare the behaviour of the critical wave number and critical diffusion through Equation 1.60 and Equation 1.61 as a function of $a/b = c$, with $b = \gamma = 1$.

While there is much more to say about Turing patterns and the Turing instability for the Schnakenberg model, we will conclude our introduction of the Turing instability here. As we will see in Chapter 3, one of our models of interest can be reduced to a perturbation of the classic Schnakenberg reaction system in a special case and we will expand on some of this discussion there.

1.2 Rayleigh-Bénard Instability

As previously discussed, the Rayleigh-Bénard instability [14, 15] in its classical form describes the onset of convection in a fluid heated from below. One of the key components is the density variations created by the temperature gradient across the fluid. Consequently, many processes can generate Rayleigh-Bénard style instabilities. An example studied later in this thesis is generated from density variations through chemical concentration gradients. However, in this section, we focus on the classical temperature-driven instability. This gives us an opportunity to introduce the necessary assumptions for the Boussinesq approximation of the Navier-Stokes equations, to obtain an idea of the important characteristics that make Rayleigh-Bénard style instabilities possible and demonstrate some the mathematical techniques we will use to study it and similar instabilities throughout this thesis.

1.2.1 Boussinesq Approximation

The Boussinesq approximation for the Navier-Stokes equations assumes that density changes in the fluid are negligible in the continuity and momentum equations except for in the buoyancy term. Under this assumption we replace the continuity equations,

$$\frac{1}{\rho}\frac{D\rho}{Dt} + \nabla \cdot \mathbf{u} = 0,$$

with the incompressible form, $\nabla \cdot \mathbf{u} = 0$. However, as noted in Kundu [6], there are some situations where this approximation does not hold, such as when the Mach number of the fluid is large, the vertical scale is sufficiently large that hydrostatic pressure produces meaningful density changes, or when shock waves must be considered. The work in this thesis is primarily concerned with small reaction chambers or microfluidic devices at the onset of flow due to various instabilities where small density variations are caused by chemical reactions in water, so that we can assume the flow speeds are slow and utilise the approximation.

For the momentum equation, supposing that the only force acting on the fluid is the buoyancy force, the incompressible Navier-Stokes equations imply that the material derivative of the flow field is governed by

$$\rho \frac{D\mathbf{u}}{Dt} = -\nabla p + g\rho \mathbf{e}_z + \mu \nabla^2 \mathbf{u}. \tag{1.65}$$

Here, ρ is the fluid density, p is the pressure, g is the acceleration due to gravity, and μ is the fluid dynamic viscosity. Now, let us assume that we have a fluid of constant uniform density, ρ_0, which generates no flow. As a consequence, the viscous term and advective term vanish, and we conclude that $\nabla p_0(z) = g\rho_0 \mathbf{e}_z$. Solving for $p_0(z)$ we obtain a constant of integration which corresponds to the pressure at $z = 0$. Since the momentum equations depend only on ∇p_0, without loss of generality we can assume that this constant is zero so that,

$$p_0(z) = g\rho_0 z. \tag{1.66}$$

Assuming that there is a small perturbation in the density, so that $\rho = \rho_0 + \rho_1$ with $|\rho_1| \ll \rho_0$, we obtain a perturbation of the pressure $p = p_0 + p_1$. Substituting this into Equation (1.65), we find

$$(\rho_0 + \rho_1)\frac{D\mathbf{u}}{Dt} = -\nabla p_1 + g\rho_1 \mathbf{e}_z + \mu \nabla^2 \mathbf{u}, \tag{1.67}$$

$$\left(1 + \frac{\rho_1}{\rho_0}\right)\frac{D\mathbf{u}}{Dt} = -\frac{1}{\rho_0}\nabla p_1 + g\frac{\rho_1}{\rho_0}\mathbf{e}_z + \frac{\mu}{\rho_0}\nabla^2 \mathbf{u}. \tag{1.68}$$

Recalling that we have assumed density variations are small, i.e., that $|\rho_1/\rho_0| \ll 1$, we can omit this term from the material derivative. However, we must keep the buoyancy term due to its importance in driving the flow field. This gives us the momentum equation under the Boussinesq approximation obtained by Kundu et al. [6]

$$\frac{D\mathbf{u}}{Dt} = -\frac{1}{\rho_0}\nabla p_1 + g\frac{\rho_1}{\rho_0}\mathbf{e}_z + \nu \nabla^2 \mathbf{u}, \tag{1.69}$$

where $\nu = \mu/\rho_0$.

1.2.2 Rayleigh-Bénard Instability

Having discussed the form and underlying assumptions of the Boussinesq approximation for the Navier-Stokes equations we can move on to the Rayleigh-Bénard instability. The

analysis uses the Boussinesq approximation where the changes in buoyancy are due to the temperature changes in the fluid. Therefore, in order to begin we need to relate the changes in buoyancy caused by temperature to the Boussinesq approximation. Since the temperature variations in the fluid produce changes in density, we may be inclined to assume the Boussinesq approximation is no longer valid, however, we will assume that the changes in density due to changes in temperature are small, and since the original experiments by Bénard [14] were conducted with a thin film of liquid, that the thermal diffusivity reduces the variations in temperature are sufficiently small for the Boussinesq approximation to continue to hold. When we consider density variations due to the concentration of chemical reagents later in the thesis, similar assumptions are also necessary. As a consequence of these small temperature changes throughout the fluid, we can approximate the density changes due to temperature through a first order linear approximation,

$$\rho = \rho_0(1 - \alpha(T - T_0)), \tag{1.70}$$

where α is the thermal expansion coefficient for the fluid. Solving for ρ/ρ_0 in Equation (1.70), the buoyancy force is now a function of the variation in temperature and we obtain,

$$\begin{aligned} \frac{\partial T}{\partial t} &= -(\mathbf{u}\cdot\nabla)T + \kappa\nabla^2 T, \\ \frac{\partial \mathbf{u}}{\partial t} &= -(\mathbf{u}\cdot\nabla)\mathbf{u} - \frac{1}{\rho_0}\nabla p + \nu\nabla^2\mathbf{u} + g(1 - \alpha(T - T_0))\mathbf{e}_z, \\ \nabla\cdot\mathbf{u} &= 0. \end{aligned} \tag{1.71}$$

This is where we can begin our investigation of the Rayleigh-Bénard instability. However, boundary conditions are necessary to obtain unique solutions. To make the solution as simple as possible, we will choose boundary conditions which force a linear temperature gradient. Specifically, we will assume that the system takes place between two infinitely large flat plates with a distance H between them. We will also assume that the fluid velocity is zero along the boundary, known as the no slip condition. Finally, we will assume that the temperature at each boundary is held constant, so that $T(z = 0) = T_0$ and $T(z = H) = T_0 - \Gamma$. It follows that, at the equilibrium without flow, we have

$$\begin{aligned} 0 &= \kappa\nabla^2 T, \\ \mathbf{0} &= -\frac{1}{\rho_0}\nabla p + g(1 - \alpha(T - T_0))\mathbf{e}_z. \end{aligned} \tag{1.72}$$

Since the only symmetry breaking takes place along the vertical direction, we can safely assume that at the steady state T and p are functions of z and are constant in the horizontal

directions. Consequently, the equation for temperature reduces to

$$\frac{d^2T}{dz^2} = 0. \tag{1.73}$$

When subject to the boundary conditions, this is solved by $T(z) = T_0 - \Gamma z/H$ and implies that

$$\frac{dp}{dz}(z) = g\rho_0 \left(1 + \frac{\alpha\Gamma}{H} z\right), \tag{1.74}$$

which determines the pressure field up to an arbitrary constant of integration. Since the evolution equations depend only on the gradient of p, we can assume without loss of generality that $p(0) = 0$, so that the integral of Equation (1.74) is given by

$$p(z) = \rho_0 z \left(1 + \frac{\alpha\Gamma}{2H} z\right).$$

Now that we have determined equilibrium equations, we can now consider the behaviour of a small perturbation,

$$\begin{aligned} \mathbf{u} &= \mathbf{0} + \mathbf{u}_1, \\ T &= T_0 - \frac{\Gamma}{H} z + T_1, \\ p &= \rho_0 z \left(1 + \frac{\alpha\Gamma}{2H} z\right) + p_1. \end{aligned} \tag{1.75}$$

As is the case with most perturbation methods, this relies on the assumption that the functions are suitably well-behaved around the equilibrium. In particular, that the dynamics are well approximated by their linearizations since we will throw out the products of the perturbations. Assuming that this is the case, then upon substituting Equation (1.75) into Equation (1.71) we obtain

$$\begin{aligned} \frac{\partial \mathbf{u}_1}{\partial t} &= -\frac{1}{\rho_0}\nabla p_1 + \nu\nabla^2 \mathbf{u}_1 + g\alpha T_1 \mathbf{e}_z, \\ \frac{\partial T_1}{\partial t} &= \Gamma u_{1,z} + \kappa\nabla^2 T_1, \\ \nabla \cdot \mathbf{u}_1 &= 0, \end{aligned} \tag{1.76}$$

with

$$\mathbf{u}_1\Big|_{z=0,H} = 0, \qquad T_1\Big|_{z=0,H} = 0. \tag{1.77}$$

The only energy into the horizontal flow components is through the incompressibility condition and viscous terms. As a result, their stability is dependent on the stability of the reduced system containing only the vertical velocity component. If this reduced system is unstable, then the global system will be as well. Therefore, by omitting the horizontal flow components we obtain,

$$\begin{aligned} \frac{\partial u_{1,z}}{\partial t} &= -\frac{1}{\rho_0}\frac{\partial p_1}{\partial z} + \nu\nabla^2 u_{1,z} + g\alpha T_1, \\ \frac{\partial T_1}{\partial t} &= \Gamma u_{1,z} + \kappa\nabla^2 T_1, \end{aligned} \tag{1.78}$$

with

$$u_{1,z}\Big|_{z=0,H} = 0, \qquad T_1\Big|_{z=0,H} = 0. \tag{1.79}$$

In order for this system to solve the system, we will eliminate the pressure term. To do this we will consider the divergence of the flow term in Equation (1.71). By applying the incompressibility condition we obtain

$$\frac{\partial}{\partial t}(\nabla\cdot\mathbf{u}_1) = -\frac{1}{\rho_0}\nabla\cdot(\nabla p_1) + \nu\nabla^2(\nabla\cdot\mathbf{u}_1) + \alpha g\nabla(T_1\mathbf{e_z}), \tag{1.80}$$

$$\frac{1}{\rho_0}\nabla^2 p_1 = \alpha g\frac{\partial T_1}{\partial z}. \tag{1.81}$$

As a result, after differentiating with respect to z, we obtain

$$\frac{1}{\rho_0}\nabla^2\frac{\partial p_1}{\partial z} = \alpha g\frac{\partial^2 T_1}{\partial z^2}. \tag{1.82}$$

This gives us an equation for the Laplacian of $\frac{\partial p_1}{\partial z}$ and we can use this to eliminate the pressure term. In particular, by taking the Laplacian of the vertical velocity component in Equation (1.78), we obtain

$$\frac{\partial}{\partial t}(\nabla^2 u_{1,z}) = -\frac{1}{\rho_0}\nabla^2\frac{\partial p_1}{\partial z} + \nu\nabla^4 u_{1,z} + g\alpha\nabla^2 T_1 \tag{1.83}$$

which, after substituting Equation (1.82) and simplifying, gives

$$\frac{\partial}{\partial t}(\nabla^2 u_{1,z}) = \nu\nabla^4 u_{1,z} + g\alpha\nabla_H^2 T_1, \tag{1.84}$$

$$\frac{\partial T_1}{\partial t} = \Gamma u_{1,z} + \kappa\nabla^2 T_1, \tag{1.85}$$

where $\nabla_H^2 = \frac{\partial^2}{\partial x^2} + \frac{\partial^2}{\partial y^2}$ is the horizontal diffusion.

To non-dimensionalize the system we will fix the length scale to be H and suppose that

$$t = t_s \hat{t}, \quad T_1 = T_s \hat{T}_1, \quad u_{1,z} = u_s \hat{u}_{1,z}. \tag{1.86}$$

If $t_s = H^2/\kappa$, as in Kundu [6], then after substituting the non-dimensional variables into Equation (1.84) and Equation (1.85), we obtain

$$\frac{\kappa u_s}{H^4} \frac{\partial}{\partial t}(\nabla^2 u_{1,z}) = \frac{\nu u_s}{H^4} \nabla^4 u_{1,z} + g \frac{\alpha T_s}{H^2} \nabla_H^2 T_1, \tag{1.87}$$

$$\frac{\kappa T_s}{H^2} \frac{\partial T_1}{\partial t} = \Gamma u_s u_{1,z} + \frac{\kappa T_s}{H^2} \nabla^2 T_1. \tag{1.88}$$

We note that we have dropped the $\hat{}$ to reduce congestion. Simplifying the above gives

$$\frac{\kappa}{\nu} \frac{\partial}{\partial t}(\nabla^2 u_{1,z}) = \nabla^4 u_{1,z} + g \frac{\alpha H^2 T_s}{\nu u_s} \nabla_H^2 T_1, \tag{1.89}$$

$$\frac{\partial T_1}{\partial t} = \frac{H^2 \Gamma u_s}{\kappa T_s} u_{1,z} + \nabla^2 T_1. \tag{1.90}$$

This makes the choice for the non-dimensionalization of $u_{1,z}$ clear. In this case, we will choose $u_s = \kappa T_s/(\Gamma H^2)$, so that Equation (1.89) and Equation (1.90) become,

$$\frac{\kappa}{\nu} \frac{\partial}{\partial t}(\nabla^2 u_{1,z}) = \nabla^4 u_{1,z} + g \frac{\alpha \Gamma H^4}{\kappa \nu} \nabla_H^2 T_1, \tag{1.91}$$

$$\frac{\partial T_1}{\partial t} = u_{1,z} + \nabla^2 T_1. \tag{1.92}$$

$$\tag{1.93}$$

Recognizing some dimensionless parameters we have

$$\mathrm{Pr} = \nu/\kappa, \qquad \mathrm{Ra} = g\alpha\Gamma H^4/\kappa\nu,$$

for the Prandtl and Rayleigh numbers respectively. The final non-dimensionalized system is

$$\begin{aligned} \frac{1}{\mathrm{Pr}} \frac{\partial}{\partial t}(\nabla^2 u_{1,z}) &= \nabla^4 u_{1,z} + \mathrm{Ra} \nabla_H^2 T_1, \\ \frac{\partial T_1}{\partial t} &= u_{1,z} + \nabla^2 T_1. \end{aligned} \tag{1.94}$$

Noting that we have increased the order of our derivatives, it's necessary for us to also introduce additional boundary conditions. Since the horizontal flow components are identically zero at the boundary, these can be obtained through the incompressibility condition by assuming that the solutions are everywhere differentiable. This implies that the derivatives of the horizontal flow components are also zero at the boundary. Consequently, we can introduce

$$\left.\frac{\partial u_{1,z}}{\partial z}\right|_{z=0,1} = 0. \tag{1.95}$$

as an additional boundary condition in conjunction with the conditions described in Equation (1.79).

Our goal is to understand the stability of our system to these perturbations. Since we have reduced the system to a linear system of partial differential equations, we can perform a normal mode analysis much like we did while studying the Turing instability. In this case, we will assume that the solutions are separable and can be decomposed into modes of the following form,

$$\begin{aligned} u_{1,z} &= f(z)e^{\lambda t + i\mathbf{k}\cdot\mathbf{x}}, \\ T_1 &= w(z)e^{\lambda t + i\mathbf{k}\cdot\mathbf{x}}, \end{aligned} \tag{1.96}$$

where $\mathbf{k}, \mathbf{x} \in \mathbb{R}^2$. Substituting these modes into Equation (1.94) we find the governing equations for a fixed mode are given by,

$$\begin{aligned} \frac{\lambda}{\mathrm{Pr}}\left(\frac{d^2 f}{dz^2} - q^2 f\right) &= \left(\frac{d^4 f}{dz^4} - 2q^2\frac{d^2 f}{dz^2} + q^4 f\right) - q^2 \mathrm{Ra}\cdot w(z), \\ \lambda w(z) &= f(z) + \left(\frac{d^2 w}{dz^2} - q^2 w(z)\right), \end{aligned} \tag{1.97}$$

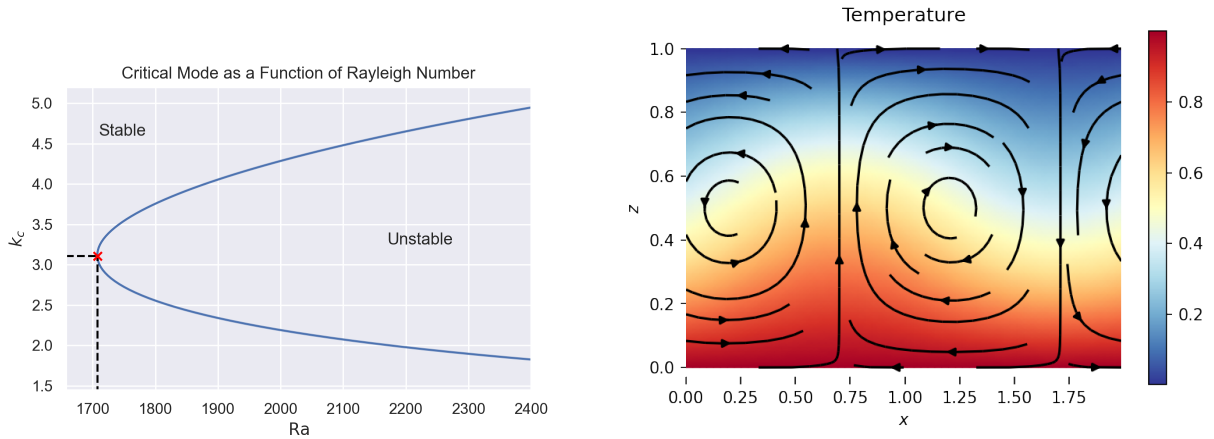
where we have again made the substitution $q^2 = ||\mathbf{k}||^2$. Finally, the system in Equation (1.97) inherits its boundary conditions from Equation (1.79) and Equation (1.95), implying that

$$\begin{aligned} f(0) = f(1) = 0 = \frac{df}{dz}(1) = \frac{df}{dz}(0), \\ w(0) = w(1) = 0. \end{aligned} \tag{1.98}$$

By fixing $\lambda = 0$, we are considering a marginally stable mode which satisfy the much simpler equations,

$$\begin{aligned} \left(\frac{d^4}{dz^4} - 2q^2\frac{d^2}{dz^2} + q^4\right) f(z) &= q^2 \mathrm{Ra}\; w(z), \\ \left(\frac{d^2}{dz^2} - q^2\right) w(z) &= -f(z). \end{aligned} \tag{1.99}$$

Stoer [16] refers to these as eigenvalue problems, where Ra is the eigenvalue. Kundu [6] and Chandrasekhar [7] both produce analytical estimates for the critical Rayleigh number using symmetry arguments. We highly recommend both of their texts. Instead of going in this direction, we will conclude by estimating the critical Rayleigh number numerically with a shooting method. We provide the results of this in Figure 1.7 along with a simulation of the instability. We have marked the critical Rayleigh number at $\mathrm{Ra}_c \approx 1707.3$ and the critical mode at $k_c \approx 3.1$. For an in-depth discussion of shooting methods and their applications to eigenvalue problems, we recommend Stoer [16]. For our particular problem, we will also discuss the method used in more detail in Chapter 4.



(a) (b)

Figure 1.7: (a) Critical Rayleigh numbers for various modes k calculated using a shooting method for Equation (1.99) with boundary conditions described in Equation (1.98) (b) Long time simulation of supercritical Rayleigh number

1.2.3 Summary

In this section, we have introduced the Boussinesq approximation and the classical Rayleigh-Bénard instability. While the majority of the material is adapted from Kundu [6] and Chandrasekhar [7], we have supplied some additional details to better understand how the final equations come about.

We solved the resulting eigenvalue problem using a shooting method. This allowed us to change the eigenvalue problem into a root-finding one, and as a consequence, we are able

to estimate the critical Rayleigh number ($\mathrm{Ra}_c \approx 1707.3$) and the critical mode ($k_c \approx 3.1$). These results coincide well with the analytical results that Kundu and Chandrasekhar present.

Finally, we concluded the discussion with Figure 1.7, which includes a simulation of the 2-dimensional Rayleigh-Bénard instability for a supercritical Rayleigh number. We direct the reader to pay special attention to the temperature profile. In particular, note how the temperature profile develops peaks and troughs in the bulk despite the boundaries being held at a fixed temperature. This results from the incompressible flow approaching the boundary and being forced to circle around. This kind of pattern is very similar to a one-dimensional Turing instability if it was diffusing from the boundary and provides some motivation for material in the following chapters.

Chapter 2

Boundary-Bound Reactions

Recently, active membrane models have become popular since their initial investigation by Levine et al. [17]. These active membrane models separate the domain into a reactive membrane region and bulk region. Material transitions from one region to the other through adsorption and desorption terms. Reagents in the membrane region are subject to a non-linear reaction whereas reagents in the bulk region undergo diffusive transport. Of particular interest, Levine et al. [17] were able to produce stable chemical patterns for a diffusion ratio of one. This showed that large diffusion ratios, which are seldom seen in natural reaction systems, are not necessary for patterns. As a consequence of their initial work, more complicated models of bulk-surface pattern formation have become recent objects of study, and a review of some of these results can be found in Gomez et al. [18]. Some examples include Madzvamuse et al. [19] who added diffusion to the membrane component, while Gomez et al. [20] demonstrated the existence of single spike solutions along the boundary in the case of the Gierer-Meinhardt reaction.

Boundary-bound reactions are simpler than active membrane models and function by assuming the reaction can be modeled as a boundary flux. As touched on in Chapter 1, there are at least two situations in which boundary fluxes can arise in an experimental setup. If a selectively permeable material is used for the walls of the reaction chamber, then certain chemical species can pass into and out of the chamber through the walls. A reservoir on the other side of the wall could be used to supply reagents through the permeable wall, for example. Another source of a boundary flux is if a reaction occurs at the wall. Many reactions, especially biochemical reactions, occur at negligible rates in the absence of an enzyme. By fixing the enzyme to a wall, we can restrict specific reactions to occur only at this surface. The generation and removal of species through reactions at the boundary is naturally described by boundary flux terms. Balazs et al. [1] studied a system of two

boundary-bound reactions taking place on opposing boundaries. Here, they were able to create an oscillatory instability which was enhanced or suppressed by the presence of a buoyancy-driven flow field. Taggart et al.[21], as well as Bdzil and Frisch [22] investigated the influence of a non-oscillatory reaction along a single boundary which can create density variations through the reaction pathway $A + A \rightarrow 2A$. However, we have not seen a general framework for pattern formation in boundary-bound reactions. Furthermore, the research studying the relationship between hydrodynamics to Turing patterns appears primarily concerned with bulk reaction-diffusion equations which we address in Chapter 4.

Therefore, in this Chapter, we will consider boundary-bound reactions occurring between two infinite flat plates. A schematic for the general problem was provided in Figure 1.1 back in Chapter 1. We use the separation distance between the plates as the length scale for non-dimensionalization of the system of equations. To keep the equations tractable, we assume there are only two reagents and that the non-constant reactions for the reagents either take place on the same boundary, or opposing boundaries.

By performing a normal mode analysis, we are able to reduce the analysis to the study of a quadratic polynomial and obtain analytical conditions for when pattern forming instabilities exist. Unlike the classical Turing and Rayleigh-Bénard instabilities, where arbitrary wavenumbers can be made unstable, we find that the existence of physical solutions to the boundary value problem depends on the wavenumber and linear growth rate. In addition, we are able to identify a handful of systems which reduce to a linear equation in the diffusion term and consequently obtain an analytical expression for the critical diffusion ratio for a fixed wavenumber.

We highlight these results by considering an example using the Schnakenberg reaction system [2]. Separating out the constant terms on one boundary and the reaction terms on the other. As a result, we are able to present a reaction network where we have control over the types of patterns formed by changing the rate of flux of reagents on one boundary. This is particularly interesting since we can imagine building time-varying paths between the various pattern-forming regions. As a result, we can turn on and off multiple behaviours according to some predefined schedule. This can make it possible to re-excite transitory behaviour, perform pattern selection and can produce programmable buoyancy-driven flows. After this investigation, we conclude with a short summary and look at the relationship between the instability and the reaction parameters. Here we find that in the case of boundary-bound reactions when the diffusion ratio is one, short-wavelength instabilities are always more stable than long-wavelength instabilities. As a consequence, we are able to provide an answer to why Balazs et al. only observe a long-wavelength oscillatory instability in their model when flows are negligible. Finally, we end the chapter

with a small piece on the problem with flow, obtaining necessary conditions for overstability when there is no bulk decay, as well as describing the general root-finding problem.

2.1 General Framework for Boundary-Bound Reactions

Let us begin by defining the general two-reagent boundary-bound reaction system with fluid flow governed by the Navier-Stokes equations with the Boussinesq approximation

$$\frac{\partial Q}{\partial t} = -\eta_1 Q + \nabla^2 Q - (\mathbf{u}\cdot\nabla)Q, \tag{2.1}$$

$$\frac{\partial R}{\partial t} = -\eta_2 R + D\nabla^2 R - (\mathbf{u}\cdot\nabla)R, \tag{2.2}$$

$$\frac{\partial \mathbf{u}}{\partial t} = -(\mathbf{u}\cdot\nabla)\mathbf{u} - \nabla p + \mathrm{Sc}\nabla^2\mathbf{u} + \mathrm{Gr}(\delta^Q Q + \delta^R R)\mathbf{e}_z, \tag{2.3}$$

$$\nabla\cdot\mathbf{u} = 0, \tag{2.4}$$

subject to the boundary conditions

$$\begin{aligned} \left.\frac{\partial Q}{\partial z}\right|_{z=0} &= \gamma f_0(Q,R), & \left.\frac{\partial Q}{\partial z}\right|_{z=1} &= \gamma f_1(Q,R), \\ D\left.\frac{\partial R}{\partial z}\right|_{z=0} &= \gamma g_0(Q,R), & D\left.\frac{\partial R}{\partial z}\right|_{z=1} &= \gamma g_1(Q,R), \\ \mathbf{u}\Big|_{z=0} &= 0, & \mathbf{u}\Big|_{z=1} &= 0. \end{aligned} \tag{2.5}$$

Here, $f_0(Q,R)$ and $g_0(Q,R)$ describe the potentially non-linear reactions that occur at the bottom boundary as a consequence of hypothetical enzyme B in Figure 1.1. Similarly $f_1(Q,R)$ and $g_1(Q,R)$ describe the resulting reaction at the upper boundary through hypothetical enzyme A. We allow for first-order decay of the two reagents in the interior of the domain with respective non-negative rate constants η_1 and η_2.

The remaining parameters can be described as follows: The diffusion ratio between reagents Q and R is given by D, the Schmidt coefficient, Sc, is the ratio between the viscosity and molecular diffusion, and Gr is the ratio of the buoyancy force to viscous force, called the Grashof number. Finally, γ defines a non-dimensionalized global rate of flux for the reagents, while δ^Q and δ^R describe how they change the density of the fluid.

We note that without loss of generality we may assume that $\gamma > 0$; if $\gamma = 0$, then the long time dynamics converge to zero, and if γ is negative, then we can absorb the sign into the reaction terms and consider the equivalent system.

In order to study the stability of this system, we consider an equilibrium without flow. Since the system is invariant to horizontal translations, the diffusion term should smooth our fluctuations and the only symmetry breaking property of our system are the fluxes along the vertical direction we search for a steady state that is constant in the horizontal directions. Under these assumptions, the original system reduces to the following system of PDEs:

$$\begin{aligned}
&\frac{\partial^2 Q}{\partial z^2} - \eta_1 Q = 0,\\
&\frac{\partial^2 R}{\partial z^2} - \eta_2 R = 0,\\
&\frac{\partial p}{\partial z} = \mathrm{Gr}(\delta^Q Q + \delta^R R),
\end{aligned}$$

with all partial derivatives with respect to x and y vanishing, subject to the boundary conditions in Equation (2.5). The general solutions are given by,

$$\begin{aligned}
Q_0(x,y,z,t) &= a_1 \cosh(\sqrt{\eta_1} z) + a_2 \sinh(\sqrt{\eta_1} z),\\
R_0(x,y,z,t) &= b_1 \cosh(\sqrt{\eta_2} z) + b_2 \sinh(\sqrt{\eta_2} z),\\
p_0(x,y,z,t) &= \mathrm{Gr} \int_0^z (\delta^Q Q_0 + \delta^R R_0) \mathrm{d}z.
\end{aligned} \tag{2.6}$$

When the functions f_0, g_0, f_1 and g_1 in the general formulation are given explicitly it is sometimes possible to solve the unknown coefficients for Q and R. We note however, that boundary values problems do not always admit solutions.

Supposing such a solution exists, in order to study the stability of this equilibrium, we consider a small perturbation:

$$\begin{aligned}
Q &= Q_0 + Q_1,\\
R &= R_0 + R_1,\\
\mathbf{u} &= \mathbf{u}_1,\\
p &= p_0 + p_1.
\end{aligned} \tag{2.7}$$

For boundary bound reactions we will study instabilities in the bulk decay η_1 and the diffusion ratio D. Substituting this in to the evolution equations and discarding any

products of perturbations we obtain a new system of partial differential equations which governs the evolution of these small perturbations,

$$\frac{\partial Q_1}{\partial t} = -\eta_1 Q_1 + \nabla^2 Q_1 - u_{1,z}\frac{\partial Q_0}{\partial z}, \tag{2.8}$$

$$\frac{\partial R_1}{\partial t} = -\eta_2 R_1 + D\nabla^2 R_1 - u_{1,z}\frac{\partial R_0}{\partial z}, \tag{2.9}$$

$$\frac{\partial \mathbf{u}_1}{\partial t} = -\nabla p_1 + \mathrm{Sc}\nabla^2 \mathbf{u}_1 + \mathrm{Gr}(\delta^Q Q_1 + \delta^R R_1)\mathbf{e}_z, \tag{2.10}$$

$$\nabla \cdot \mathbf{u}_1 = 0, \tag{2.11}$$

subject to boundary conditions obtained through our linearization of Equation (2.5) at the steady state,

$$\begin{aligned} \frac{\partial}{\partial z}\begin{bmatrix} Q_1 \\ DR_1 \end{bmatrix}\Bigg|_{z\in\{0,1\}} &= \begin{bmatrix} f_{z,Q} & f_{z,R} \\ g_{z,Q} & g_{z,R} \end{bmatrix}\begin{bmatrix} Q_1 \\ R_1 \end{bmatrix}\Bigg|_{z\in\{0,1\}}, \\ \mathbf{u}\Big|_{z\in\{0,1\}} &= 0. \end{aligned} \tag{2.12}$$

Following the same procedure to reduce the equation and eliminate the pressure term as demonstrated in Section 1.2, we obtain a reduced set of equations similar to Equation (1.94):

$$\frac{\partial Q_1}{\partial t} = -\eta_1 Q_1 + \nabla^2 Q_1 - u_{1,z}\frac{\partial Q_0}{\partial z}, \tag{2.13}$$

$$\frac{\partial R_1}{\partial t} = -\eta_1 R_1 + D\nabla^2 R_1 - u_{1,z}\frac{\partial R_0}{\partial z}, \tag{2.14}$$

$$\frac{\partial}{\partial t}\nabla^2 u_{1,z} = \mathrm{Sc}\nabla^4 u_{1,z} + \mathrm{Gr}\nabla_H^2(\delta^Q Q_1 + \delta^R R), \tag{2.15}$$

and the boundary conditions,

$$\begin{aligned} \frac{\partial}{\partial z}\begin{bmatrix} Q_1 \\ DR_1 \end{bmatrix}\Bigg|_{z\in\{0,1\}} &= \gamma\begin{bmatrix} f_{z,Q} & f_{z,R} \\ g_{z,Q} & g_{z,R} \end{bmatrix}\begin{bmatrix} Q_1 \\ R_1 \end{bmatrix}\Bigg|_{z\in\{0,1\}}, \\ u_{1,z}\Big|_{z\in\{0,1\}} &= 0, \\ \frac{\partial u_{1,z}}{\partial z}\Bigg|_{z\in\{0,1\}} &= 0, \end{aligned} \tag{2.16}$$

where $\nabla_H = \frac{\partial^2}{\partial x^2} + \frac{\partial^2}{\partial y^2}$.

Assuming that the solutions to our equations are separable, we consider perturbations of the form

$$\begin{bmatrix} q(z) \\ r(z) \\ w(z) \end{bmatrix} e^{\lambda t + i(k_x x + k_y y)}, \tag{2.17}$$

where $k = \sqrt{k_x^2 + k_y^2}$ is the wave number and λ determines the stability. It follows that the behaviour of a particular mode k near the equilibrium is governed by solutions to

$$\begin{aligned} &\left(\frac{d^2}{dz^2} - (\lambda + \eta_1 + k^2)\right) q = w\frac{dQ_0}{dz}, \\ &\left(\frac{d^2}{dz^2} - \left(\frac{\lambda + \eta_2}{D} + k^2\right)\right) r = w\frac{dR_0}{dz}, \\ &\left[\mathrm{Sc}\left(\frac{d^2}{dz^2} - k^2\right)^2 - \lambda\left(\frac{d^2}{dz^2} - k^2\right)\right] w = k^2 \mathrm{Gr}(\delta^Q q + \delta^R r), \end{aligned} \tag{2.18}$$

subject to the boundary conditions

$$\begin{aligned} \frac{d}{dz}\begin{bmatrix} q \\ Dr \end{bmatrix}\Bigg|_{z\in\{0,1\}} &= \gamma \begin{bmatrix} f_{z,Q} & f_{z,R} \\ g_{z,Q} & g_{z,R} \end{bmatrix} \begin{bmatrix} q \\ r \end{bmatrix}\Bigg|_{z\in\{0,1\}}, \\ w\Big|_{z\in\{0,1\}} &= 0, \\ \frac{dw}{dz}\Big|_{z\in\{0,1\}} &= 0. \end{aligned} \tag{2.19}$$

This system has the added benefit of being entirely linear in the functions q, r and w and can be reduced to a single eighth-order ordinary differential equation in many cases. Furthermore, if $\frac{dQ_0}{dz}$ and $\frac{dR_0}{dz}$ are constant, then the general solutions can be obtained analytically and are provided in Section 2.3. The resulting homogeneous solutions can then be fed into the boundary conditions to determine critical parameters. However, our analytical treatment will continue by considering the case without flow.

2.2 Boundary-Bound Reactions without Flow

Assuming that the Grashof number is small and density variations are negligible in (2.18), then we need only consider the reaction portion of our the system:

$$\begin{aligned} \frac{d^2q}{dz^2} - (\lambda + \eta_1 + k^2)q = 0, \\ \frac{d^2r}{dz^2} - \left(\frac{\lambda + \eta_2}{D} + k^2\right) r = 0. \end{aligned} \tag{2.20}$$

Under these conditions we have a system of homogeneous constant coefficient linear ordinary differential equations whose general solutions are known. Letting,

$$\Gamma_1 = \sqrt{\lambda + \eta_1 + k^2}, \qquad \Gamma_2 = \sqrt{\frac{\lambda + \eta_2}{D} + k^2}, \tag{2.21}$$

they can be expressed as:

$$q(z) = a_1 \cosh(\Gamma_1 z) + a_2 \sinh(\Gamma_1 z), \tag{2.22}$$

$$r(z) = b_1 \cosh(\Gamma_2 z) + b_2 \sinh(\Gamma_2 z). \tag{2.23}$$

In order to determine explicit solutions, we substitute Equations (2.22) and (2.23) into the boundary conditions defined in Equation (2.19) for the subsystem without flow. Consequently, we obtain a homogeneous linear system of equations,

$$M \begin{bmatrix} a_2 \\ b_2 \\ a_1 \\ b_1 \end{bmatrix} = \begin{bmatrix} 0 \\ 0 \\ 0 \\ 0 \end{bmatrix}. \tag{2.24}$$

With this ordering, M can be viewed as the block matrix,

$$M = \begin{bmatrix} \mathcal{A} & \mathcal{B} \\ \mathcal{C} & \mathcal{D} \end{bmatrix}, \tag{2.25}$$

whose entries are defined by,

$$\mathcal{A} = \begin{bmatrix} -\Gamma_1 & 0 \\ 0 & -D\Gamma_2 \end{bmatrix}, \tag{2.26}$$

$$\mathcal{B} = \gamma \begin{bmatrix} f_{0,Q} & f_{0,R} \\ g_{0,Q} & g_{0,R} \end{bmatrix}, \tag{2.27}$$

$$\mathcal{C} = \begin{bmatrix} -\Gamma_1 \cosh(\Gamma_1) + \gamma f_{1,Q} \sinh(\Gamma_1) & \gamma f_{1,R} \sinh(\Gamma_2) \\ \gamma g_{1,Q} \sinh(\Gamma_1) & -D\Gamma_2 \cosh(\Gamma_2) + \gamma g_{1,R} \sinh(\Gamma_2) \end{bmatrix}, \tag{2.28}$$

$$\mathcal{D} = \begin{bmatrix} -\Gamma_1 \sinh(\Gamma_1) + \gamma f_{1,Q} \cosh(\Gamma_1) & \gamma f_{1,R} \cosh(\Gamma_2) \\ \gamma g_{1,Q} \cosh(\Gamma_1) & -D\Gamma_2 \sinh(\Gamma_2) + \gamma g_{1,R} \cosh(\Gamma_2) \end{bmatrix}. \tag{2.29}$$

This system of equations has a non-trivial solution only if the determinant of M vanishes. Having expressed M as a 2×2 block matrix, the determinant of M can be computed as

$$\det(M) = \det(\mathcal{A}) \det(\mathcal{D} - \mathcal{C}\mathcal{A}^{-1}\mathcal{B}), \tag{2.30}$$

provided that $\mathcal{A}$ is invertible, see Shores [23]. We therefore assume that $\Gamma_1 \neq 0$ and $\Gamma_2 \neq 0$, which guarantees invertibility of $\mathcal{A}$ for $D > 0$. Since we are interested in pattern formation, we seek solutions to the problem where $k^2 \neq 0$ and $\lambda \in \mathbb{R}^+ \cup \{0\}$. In such cases, it will be true that $\Gamma_1 \neq 0$ and $\Gamma_2 \neq 0$. This allows us to reduce the problem to,

$$\det(\mathcal{D} - \mathcal{C}\mathcal{A}^{-1}\mathcal{B}) = 0. \tag{2.31}$$

In its most general form, after the resulting matrix products, the determinant is a quartic equation in γ. This can be seen by noting that the product $\mathcal{C}\mathcal{A}^{-1}\mathcal{B}$ results in a matrix with γ^2 along the diagonal so that the determinant results in a quartic. Unfortunately, the coefficients are not particularly tractable for analytical methods. Numerical methods are far more useful for studying this equation in general. Instead, we look at two simplified cases.

In the first case, we will assume the reaction occurs at the upper boundary so that f_1 and g_1 have non-trivial derivatives. Conversely, at the bottom boundary, we will assume that f_0 and g_0 are constant, implying that their partial derivatives vanish. In the second case we will assume that f_1 and g_0 have non-trivial first order partial derivatives, while f_0 and g_1 are constant. The first case is concerned with two reactions which interact through a shared boundary. To complement this, the second case deals with reactions that must propagate through the bulk fluid in order to interact.

In the first case $\mathcal{B} \equiv 0_{2\times 2}$, so that $\det(M)$ reduces to

$$\begin{aligned}\det(\mathcal{D}) = \gamma^2 \det(J_1)\cosh(\Gamma_1)\cosh(\Gamma_2) \\ - \gamma(D\Gamma_2\cosh(\Gamma_1)\sinh(\Gamma_2)f_{1,Q} + \Gamma_1\sinh(\Gamma_1)\cosh(\Gamma_2)g_{1,R}) \\ + D\Gamma_1\Gamma_2\sinh(\Gamma_1)\sinh(\Gamma_2)\end{aligned} \tag{2.32}$$

$$J_1 = \begin{bmatrix} f_{1,Q} & f_{1,R} \\ g_{1,Q} & g_{1,R}\end{bmatrix} \tag{2.33}$$

However, the second case is more complicated, since the blocks do not reduce as fully. Instead, we have

$$\begin{aligned}\mathcal{B} &= \gamma\begin{bmatrix} 0 & 0 \\ g_{0,Q} & g_{0,R}\end{bmatrix}, \\ \mathcal{C} &= \begin{bmatrix} -\Gamma_1\cosh(\Gamma_1) + \gamma f_{1,Q}\sinh(\Gamma_1) & \gamma f_{1,R}\sinh(\Gamma_2) \\ 0 & -D\Gamma_2\cosh(\Gamma_2)\end{bmatrix}, \\ \mathcal{D} &= \begin{bmatrix} -\Gamma_1\sinh(\Gamma_1) + \gamma f_{1,Q}\cosh(\Gamma_1) & \gamma f_{1,R}\cosh(\Gamma_2) \\ 0 & -D\Gamma_2\sinh(\Gamma_2)\end{bmatrix}.\end{aligned}$$

It follows therefore that

$$\mathcal{C}\mathcal{A}^{-1}\mathcal{B} = \begin{bmatrix} -\dfrac{f_{1,R}g_{0,Q}\gamma^2\sinh(\Gamma_2)}{D\Gamma_2} & -\dfrac{f_{1,R}g_{0,R}\gamma^2\sinh(\Gamma_2)}{D\Gamma_2} \\ g_{0,Q}\gamma\cosh(\Gamma_2) & g_{0,R}\gamma\cosh(\Gamma_2)\end{bmatrix}. \tag{2.34}$$

After substituting this into Equation (2.31), we can simplify our determinant equation to

$$\begin{aligned}\det(\mathcal{D} - \mathcal{C}\mathcal{A}^{-1}\mathcal{B}) = -\gamma^2\det(J_2) \\ + \gamma(D\Gamma_2\cosh(\Gamma_1)\sinh(\Gamma_2)f_{1,Q} - \Gamma_1\sinh(\Gamma_1)\cosh(\Gamma_2)g_{0,R}) \\ + D\Gamma_1\Gamma_2\sinh(\Gamma_1)\sinh(\Gamma_2),\end{aligned} \tag{2.35}$$

$$J_2 = \begin{bmatrix} f_{1,Q}\cosh(\Gamma_1) & f_{1,R} \\ g_{0,Q} & g_{0,R}\cosh(\Gamma_2)\end{bmatrix}. \tag{2.36}$$

Since we are interested in the roots of Equation (2.32) and Equation (2.35) as a function of γ, we rescale by $\operatorname{sech}(\Gamma_1)\operatorname{sech}(\Gamma_2)$ to obtain

$$\begin{aligned}0 = \gamma^2\det(J_1) - \gamma(D\Gamma_2\tanh(\Gamma_2)f_{1,Q} + \Gamma_1\tanh(\Gamma_1)g_{1,R}) \\ + D\Gamma_1\Gamma_2\tanh(\Gamma_1)\tanh(\Gamma_2),\end{aligned} \tag{2.37}$$

$$\begin{aligned}0 = -\gamma^2\det(\hat{J}_2) - \gamma(D\Gamma_2\tanh(\Gamma_2)f_{1,Q} - \Gamma_1\tanh(\Gamma_1)g_{0,R}) \\ + D\Gamma_1\Gamma_2\tanh(\Gamma_1)\tanh(\Gamma_2),\end{aligned} \tag{2.38}$$

where $\hat{J}_2$ is J_2 re-scaled by $\operatorname{sech}(\Gamma_1)\operatorname{sech}(\Gamma_2)$. Writing the equations in this way makes it easier to understand the short-wavelength behaviour. As the wavenumbers become large, so does Γ_i and therefore $\tanh(\Gamma_i)$ will tend to one, while $\operatorname{sech}(\Gamma_i)$ will tend to zero. This will be of importance to our investigations, since as the coefficients of each quadratic changes, so does the admissible solution set. In particular, we will demonstrate that for various ranges of wavenumbers the linear theory can or cannot predict instabilities in γ depending on the reaction parameters.

2.2.1 Reactions on a Shared Boundary

To begin our investigation, we consider Equation (2.37), which must vanish for some γ in order to solve the boundary value problem. We recall given the physical nature of the problem we have assumed that $\gamma \in \mathbb{R}$. This places conditions on the coefficients of the quadratic in Equation (2.37) that can be used to determine whether or not pattern forming instabilities exist. For instance, in order for the solutions of γ to be real, the discriminant must be positive. Calculating the discriminant for Equation (2.37) we obtain

$$\begin{aligned}\Delta &= (D\Gamma_2\tanh(\Gamma_2)f_{1,Q} + \Gamma_1\tanh(\Gamma_1)g_{1,R})^2 \\ &\quad - 4\det(J_1)D\Gamma_1\Gamma_2\tanh(\Gamma_1)\tanh(\Gamma_2), \end{aligned} \tag{2.39}$$

$$\begin{aligned}&= D^2\Gamma_2^2\tanh(\Gamma_2)f_{1,Q}^2 + 2D\Gamma_1\Gamma_2\tanh(\Gamma_1)\tanh(\Gamma_2)f_{1,Q}g_{1,R} \\ &\quad - 4D\Gamma_1\Gamma_2(f_{1,Q}g_{1,R} - f_{1,R}g_{1,Q})\tanh(\Gamma_1)\tanh(\Gamma_2) + \Gamma_1^2\tanh^2(\Gamma_1)g_{1,R}^2. \end{aligned} \tag{2.40}$$

We can view Equation (2.40) as a parabola in $f_{1,Q}$ whose leading coefficient is positive. It follows that the discriminant is negative if the value of $f_{1,Q}$ is between the two roots of Equation (2.40). Otherwise, the solutions to the boundary value problem would require γ to be complex valued, and violate our constraints. These roots are given by the equation,

$$\sigma_{s,\pm} = \frac{\Gamma_1 g_{1,R}\tanh(\Gamma_1)}{D\Gamma_2\tanh(\Gamma_2)} \pm 2\sqrt{\frac{-\Gamma_1\tanh(\Gamma_1)f_{1,R}g_{1,Q}}{D\Gamma_2\tanh(\Gamma_2)}}. \tag{2.41}$$

In the case where $\sigma_{s,\pm}$ is complex valued, then since the parabola in $f_{1,Q}$ opens upwards it must be above the line $\Delta = 0$. We conclude that the discriminant is positive for all $f_{1,Q}$ and real solutions in γ that solve Equation (2.37) will always exist. This is the case when $f_{1,R}$ and $g_{1,Q}$ have the same sign. Otherwise, we require $f_{1,Q} \notin (\sigma_{s,-},\ \sigma_{s,+})$ for solutions to be real. To get an idea of what this means, suppose that $g_{1,Q} = -1$ and $f_{1,R} = g_{1,R} = 1$

then Equation (2.41) becomes

$$\sigma_{s,\pm} = \frac{\Gamma_1 \tanh(\Gamma_1)}{D\Gamma_2 \tanh(\Gamma_2)} \pm 2\sqrt{\frac{\Gamma_1 \tanh(\Gamma_1)}{D\Gamma_2 \tanh(\Gamma_2)}}. \tag{2.42}$$

We plot the roots as a function of k for fixed parameters in Figure 2.1. For this parameter selection, $|\sigma_{s,\pm}| > 0.5$, it follows that if $f_{1,Q} \in (-0.5, 0.5)$ then Equation (2.40) is negative for all $k \neq 0$ and $\lambda \in \mathbb{R}^+ \cup \{0\}$. As a consequence, we conclude that the solutions for γ are always complex valued. We have also marked the line 1.5 in Figure 2.1. If $f_{1,Q} = 1.5$ then this serves as an example of how the solutions to Equation (2.37) in γ can transition from real to complex depending on the wavelengths considered.

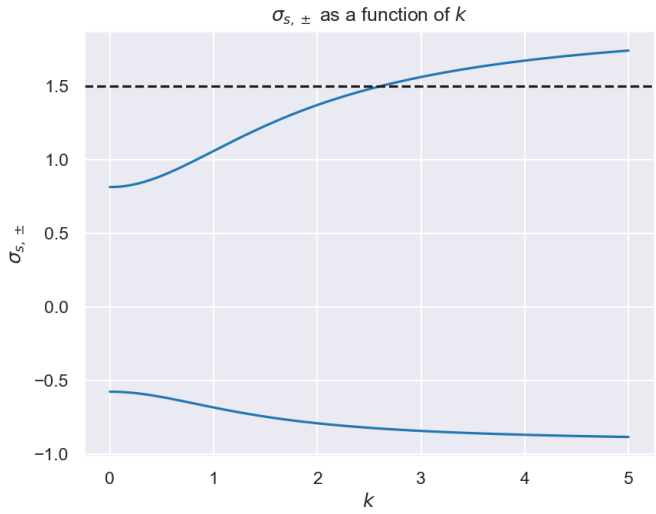


Figure 2.1: We plot $\sigma_{s,\pm}$ from Equation (2.42) as a function of k with the value 1.5 marked. $(\lambda, \eta_1, \eta_2, D) = (0, 1, 5, 1/2)$

With these conditions in mind, we can observe behaviour that is not present in the classical bulk reaction-diffusion problem. As we illustrated in Figure 2.1, Equation (2.41) depends on Γ_1 and Γ_2 and therefore the conditions change as the wavenumber k or growth rate λ is varied. Recalling Equation (2.21) we can study its behaviour for large k. This gives us insights into the behaviour of the constraints when we are interested in short-wavelength instabilities, as well ensures that the conditions are bounded when $g_{1,R}, \eta_i \neq 0$. In this case, we find that

$$\frac{\Gamma_1}{\Gamma_2} \xrightarrow{k\to\infty} 1. \tag{2.43}$$

Applying this limit to Equation (2.41) yields,

$$\sigma_{s,\pm} = \frac{g_{1,R}}{D} \pm 2\sqrt{-\frac{f_{1,R}g_{1,Q}}{D}}. \tag{2.44}$$

Finally, we note that if $\Gamma_2 \neq 0$ for all k then the conditions imposed on $f_{1,Q}$ are bounded. This makes it possible for explicit problems to define pattern forming regions, transitory regions and regions where no pattern formation is predicted. This is unlike the classical Turing problem or Rayleigh-Bénard problem, where any mode can be made linearly unstable for a sufficiently large diffusion ratio or Rayleigh number.

2.2.2 Reactions on Opposing Boundaries

We will analysis the opposing boundaries problem described by Equation (2.38) in a similar fashion. In this case, we are considering the situation where the non-constant portions of the reactions occur on opposing boundary. This much of the analysis is identical, we will not go into as much detail. In this case the discriminant for Equation (2.38) is given by

$$\begin{aligned}\Delta = {} & D^2\Gamma_2^2 \tanh^2(\Gamma_2) f_{1,Q}^2 \\ & + 2D\Gamma_1\Gamma_2 \tanh(\Gamma_1)\tanh(\Gamma_2) f_{1,Q} g_{0,R} \\ & - 4D\Gamma_1\Gamma_2 \tanh(\Gamma_1)\tanh(\Gamma_2)\operatorname{sech}(\Gamma_1)\operatorname{sech}(\Gamma_2) f_{1,R} g_{0,Q} \\ & + \Gamma_1^2 g_{0,R}^2 \tanh^2(\Gamma_1).\end{aligned} \tag{2.45}$$

As before, the leading coefficient for $f_{1,Q}$ is strictly positive, and we therefore need to be outside of the interval bounded by the roots of Equation (2.45), given below as,

$$\sigma_{op,\pm} = -\frac{\Gamma_1 \tanh(\Gamma_1) g_{0,R}}{D\Gamma_2 \tanh(\Gamma_2)} \pm 2\sqrt{\frac{\Gamma_1 \tanh(\Gamma_1) f_{1,R} g_{0,Q}}{D\Gamma_2 \cosh(\Gamma_1)\sinh(\Gamma_2)}}. \tag{2.46}$$

The asymptotic behaviour also changes slightly when compared with the results for Equation (2.37). In particular, $\sigma_{op,\pm}$ in the short-wavelength limit, converges to a single value

$$\sigma_{op,\pm} \xrightarrow{k\to\infty} -\frac{g_{0,R}}{D} \tag{2.47}$$

This allows us to conclude that the values of $f_{1,Q}$ which do not admit a real γ reduce to a single point.

2.2.3 Discussion

By considering the simplified problem of investigating boundary-bound reactions which take place only on shared or opposing boundaries we were able to find conditions for the existence of γ where pattern formation is possible. We summarise these conditions for pattern formation starting with the case of reactions on a shared boundary. For reactions on a shared boundary we reduced the analysis to Equation (2.37). We note that for solutions to be physical that the roots in γ had to be real, so that in order for such solutions to exist which solve Equation (2.32), the discriminant obtained in Equation (2.41) must be positive. We chose to view the discriminant as a quadratic in $f_{1,Q}$, and determined that real solutions for γ required that either, $f_{1,Q}$ and $g_{1,R}$ have the same signs, or

$$\left| f_{1,Q} - \frac{\Gamma_1 g_{1,R} \tanh(\Gamma_1)}{D\Gamma_2 \tanh(\Gamma_2)} \right| > 2\sqrt{\frac{-\Gamma_1 \tanh(\Gamma_1) f_{1,R} g_{1,Q}}{D\Gamma_2 \tanh(\Gamma_2)}}. \tag{2.48}$$

Similarly, for reactions taking place on opposing boundaries, in order for the solutions to Equation (2.35) in γ to be real, we considered the discriminant in Equation (2.45). This required that either $f_{1,Q}$ and $g_{0,R}$ have opposite signs, or

$$\left| f_{1,Q} + \frac{\Gamma_1 \tanh(\Gamma_1) g_{0,R}}{D\Gamma_2 \tanh(\Gamma_2)} \right| > 2\sqrt{\frac{\Gamma_1 \tanh(\Gamma_1) f_{1,R} g_{0,Q}}{D\Gamma_2 \cosh(\Gamma_1) \sinh(\Gamma_2)}} \tag{2.49}$$

In both cases we discussed how the specific instability being considered influenced the existence of solutions. This differed from the classical Turing and Rayleigh-Bénard problems. In these problems, we could always find a critical value for any wavenumber. This was demonstrated with a hypothetical system in Figure 2.1. There we saw how a particular system can transition from admitting real γ to only admitting complex solutions as the wavenumber changed.

We also investigated the short-wavelength limits for both problems. These limits have the benefit of ensuring that the conditions imposed on $f_{1,Q}$ are bounded when $\Gamma_2 \neq 0$ for all k. An example of when this might hold is given by $\eta_2 \neq 0$. Similar arguments can be made with respect to the linear growth rate λ to ensure the conditions are bounded with respect to this variable, but were not explicitly treated here. Finally we note that while these results are necessary for pattern formation, they are not sufficient. As we will see in the following section.

To conclude this summary, we turn our attention to an important algebraic simplification we made. In particular, to ease congestion, we defined Γ_i in Equation (2.21). However,

this has the benefit of making clear why pattern formation should not be expected when $D = 1$. In particular, suppose that a solution to Equation (2.37) or Equation (2.38) is known for a fixed set of parameters. Since $(\lambda,\ k)$ are shared across the two equations we have

$$\lambda + \eta_1 + k^2 = \Gamma_1^2, \tag{2.50}$$

$$\frac{\lambda + \eta_2}{D} + k^2 = \Gamma_2^2. \tag{2.51}$$

We can solve the system for the two free parameters, (λ, k). In the case where $D \neq 1$,

$$\lambda = \Gamma_1^2 - \eta_1 - \frac{\Gamma_2^2 - \Gamma_1^2 + \eta_1 - \eta_2}{D - 1}, \tag{2.52}$$

$$k^2 = \frac{\Gamma_2^2 - \Gamma_1^2 + \eta_1 - \eta_2}{D - 1}. \tag{2.53}$$

As a result, one real solution translates to a single real instability. However, when $D = 1$ this is no longer the case. Assuming that we have solved the system for some instability, $\lambda = \lambda_r + i\lambda_i$ and $k \neq 0$, it follows that

$$\Gamma_1 = \sqrt{\lambda_r + i\lambda_i + \eta_1 + k^2}, \qquad \Gamma_2 = \sqrt{\lambda_r + i\lambda_i + \eta_2 + k^2}. \tag{2.54}$$

However, γ_c depends only on the value of Γ_1 and Γ_2. Hence, this also solves the case $\lambda' = (\lambda_r + k^2) + i\lambda_i$, where instead we absorb the value of k^2 into the growth rate and assume the mode considered was the constant one. As a result, the original system also solves

$$\Gamma_1 = \sqrt{\lambda_r' + i\lambda_i' + \eta_2}, \qquad \Gamma_2 = \sqrt{\lambda_r' + i\lambda_i' + \eta_2}. \tag{2.55}$$

Since $\lambda_r' > \lambda_r$, we conclude that the long-wavelength mode is always more unstable. As a result, we obtain a similar result as the classical Turing analysis, concluding that $D \neq 1$ is necessary for pattern formation near the transition and that patterning is primarily a result of the asymmetric diffusion ratios.

With the two cases thoroughly studied, we turn our attention to an example where the critical diffusion can be solved for. In doing so, we will be able to relate the results of this Chapter back to the classical Turing analysis presented in Chapter 1.

2.2.4 An Example: Controlling Pattern Formation

In this section, we consider a simple model where the stability of the system can be controlled through fluxes along one boundary. As a result, this system can be used to encode

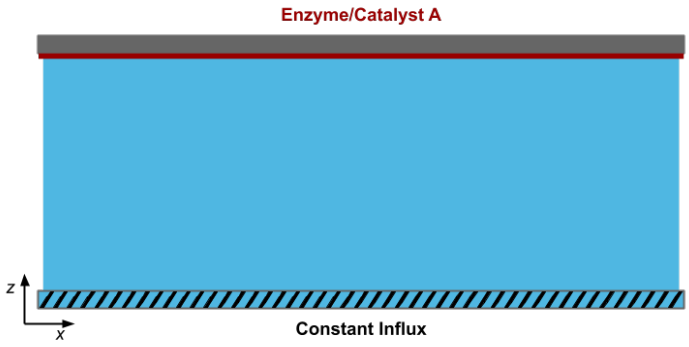


Figure 2.2: A schematic for the system described in Equations (2.56) to (2.59)

chemical signals which vary in space and time. These signals can be used for chemically driven control, or as we will discuss later, as a possible mechanism for influencing buoyancy-driven flows. To do this, we will break the Schnakenberg reaction network into two components. We will place the constant influxes ($a,\ b$) on the bottom boundary and place the reaction terms on the upper boundary. The resulting model coincides with the shared boundary case since the constant fluxes along the bottom boundary reduce to zero in the linearization. We provide a schematic for the model in Figure 2.2

We will also suppose that the bulk decay only acts on Q, so that $\eta_2 = 0$. As a result, we will be able to recover a linear equation in the diffusion ratio D when studying marginal stability. In addition, by studying the diffusion ratio, rather than γ, we are able to easily connect our results back to Chapter 1 and the original Turing analysis. Consequently, we suppose our system evolves according to the following

$$\frac{\partial Q}{\partial t} = -\eta_1 Q + \nabla^2 Q, \tag{2.56}$$

$$\frac{\partial R}{\partial t} = D\nabla^2 R, \tag{2.57}$$

and whose boundary satisfies

$$\frac{\partial Q}{\partial z}(0) = -a, \qquad \frac{\partial Q}{\partial z}(1) = \gamma(-Q + Q^2 R), \tag{2.58}$$

$$D\frac{\partial R}{\partial z}(0) = -b, \quad D\frac{\partial R}{\partial z}(1) = -\gamma Q^2 R. \tag{2.59}$$

As before, we assume that the steady state has no horizontal variation, so that we can

reduce the equations to

$$\frac{\partial^2 Q}{\partial z^2} - \eta_1 Q = 0, \tag{2.60}$$

$$\frac{\partial^2 R}{\partial z^2} = 0. \tag{2.61}$$

It follows that the general solutions are

$$Q_0(x, y, z) = a_1 \cosh(\Gamma z) + a_2 \sinh(\Gamma z), \qquad \Gamma = \sqrt{\eta_1} \tag{2.62}$$

$$R_0(x, y, z) = b_1 z + b_2. \tag{2.63}$$

Substituting these into the boundary conditions an exact solution is given by

$$Q_0(x, y, z) = \gamma \frac{a\Gamma \cosh(\Gamma(z-1)) + b\Gamma \cosh(\Gamma z) - a\gamma \sinh(\Gamma(z-1))}{\Gamma(\sinh(\Gamma) + \gamma \cosh(\Gamma))}, \tag{2.64}$$

$$R_0(x, y, z) = \frac{b}{\gamma} \left(\frac{\Gamma \sinh(\Gamma) + \gamma \cosh(\Gamma)}{a + b \cosh(\Gamma)} \right)^2 - \frac{b}{D}(z-1). \tag{2.65}$$

Expanding Equation (2.37) for this particular reaction system gives

$$\begin{aligned} 0 = {} & D\Gamma_1\Gamma_2 \tanh(\Gamma_1)\tanh(\Gamma_2) - 2\gamma D\Gamma_2 Q_0(1) R_0(1) \tanh(\Gamma_2) \\ & + \gamma D\Gamma_2 \tanh(\Gamma_2) + \gamma\Gamma_1 Q_0(1)^2 \tanh(\Gamma_1) + Q_0^2(1)\gamma^2 \end{aligned} \tag{2.66}$$

We will focus on the case of marginal stability and consequently since $\eta_2 = 0$, we conclude that $\Gamma_2 = k$. Expanding $R_0(1)$, we can solve the resulting linear equation for the critical diffusion ratio,

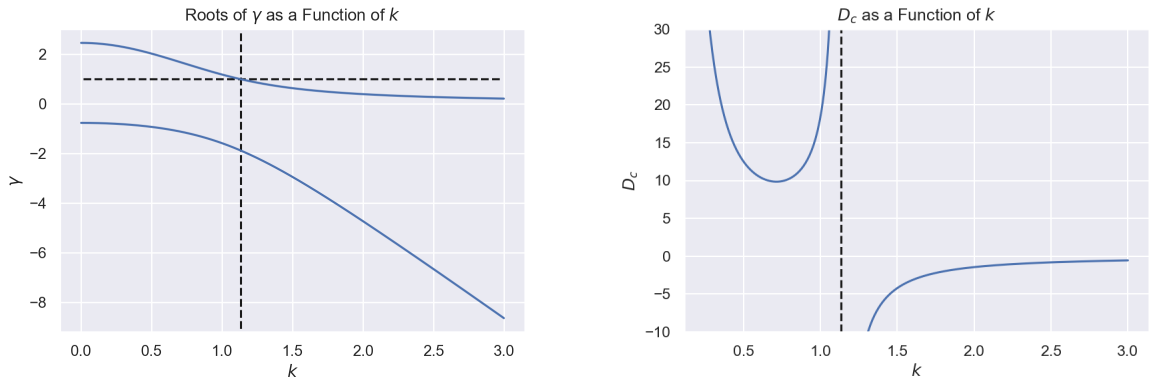
$$D_c = \frac{-Q_0(1)^2(\gamma L)^2(\Gamma_1 \tanh(\Gamma_1) + \gamma)}{k \tanh(k)(\Gamma_1 \gamma L^2 \tanh(\Gamma_1) - 2bQ_0(1)(\Gamma \sinh(\Gamma) + \gamma \cosh(\Gamma))^2 + (\gamma L)^2)}, \tag{2.67}$$

where we have defined $L = a + b\cosh(\Gamma)$ for compactness.

Since the diffusion ratio is a positive parameter and the numerator is strictly negative a critical diffusion exists if and only if the denominator in Equation (2.67) is negative. Since $k \tanh(k) \geq 0$, by $k = \sqrt{k_x^2 + k_y^2} > 0$, we can focus on the second term in the product,

$$p(\gamma) = \Gamma_1 \gamma L^2 \tanh(\Gamma_1) - 2bQ_0(1)(\Gamma \sinh(\Gamma) + \gamma \cosh(\Gamma))^2 + (\gamma L)^2 < 0. \tag{2.68}$$

Viewing this as a quadratic in γ, if the value of γ for our system is between the two roots of this polynomial then the solutions for D are always positive. Otherwise, there is no



(a) (b)

Figure 2.3: (a) We plot the roots of Equation (2.68) as a function of k. (b) The critical diffusion for various k described by Equation (2.67). Both plots are for $(a, b, \eta_1) = (0.75, 1, 1)$

physical value for the diffusion ratio which admits the linear instability being considered. In Figure 2.3a we plot the roots of Equation (2.68) as a function of k fixing the other parameters, $(a, b, \eta_1) = (0.75, 1, 1)$. Here, we have marked the value of $\gamma = 1$, as well as the value of k where the transition occurs. We see that a vertical asymptote occurs at $k \approx 1.13$, which corresponds to the transition where $\gamma = 1$ goes from between the roots of $p(\gamma)$ to outisde of them. Consequently, the vertical asymptote in Figure 2.3b, coincides exactly with the marked transition in Figure 2.3a.

Since we are interested in controlling pattern formation, we can investigate the regions where critical diffusion exists as a function of the constant fluxes (a, b). Motivated by Balazs et al. [1] who observed a long wavelength oscillatory instabilities as a function of the decay. We test both for pattern formation, and a long wavelength oscillatory instability. This requires extending the root finding problem originally posed in Equation (2.66) by replacing $\lambda \in \mathbb{R}$ with $\lambda_r, \lambda_i \in \mathbb{R}$, representing the growth rate and frequency of the linear instability. As a result, Γ_1 and Γ_2 become

$$\Omega_1 = \sqrt{\lambda_r + i\lambda_i + \eta_1 + k^2}, \qquad \Omega_2 = \sqrt{\frac{\lambda_r + i\lambda_i}{D} + k^2}. \tag{2.69}$$

The roots are then solved numerically with the assumption that λ_r and k are zero and optimized as functions of λ_i and η_1. We will return to the long-wavelength oscillatory mode in Chapter 3 to investigate its behaviour in more detail for a similar model.

In order to classify the regions, we perform our calculations in two steps. First, we calculate the critical diffusion using Equation (2.67) assuming (η_1, γ) are both unity and vary the fluxes (a, b). If the parameter set returns a positive critical diffusion, the pair (a, b) is possibly pattern forming. Next, we calculate the critical decay for the oscillatory instability with the recently obtained critical diffusion. If the critical decay is less than one, then we conclude that the decay is supercritical at the critical diffusion. It follows that pattern formation at the critical mode is only marginally stable, while the long wavelength oscillatory mode is supercritical. We conclude that the linear theory predicts that chemical oscillations will dominate there and we mark this point as oscillatory instead of pattern forming. The identified regions are provided in Figure 2.4 with the contours for fixed diffusion ratios marked.

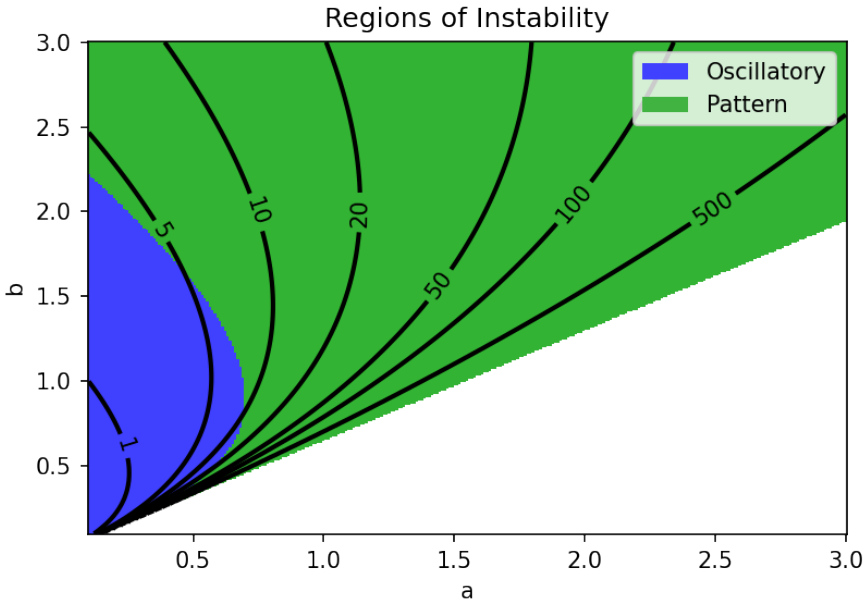


Figure 2.4: Regions of stability predicted from the normal mode analysis for $\eta, \gamma = 1$ and various (a, b). Contours mark various critical diffusion values

Given an appropriately fixed diffusion ratio, we can turn pattern formation on and off by varying (a, b) between the regions of stability and instability. As a result, through this boundary-bound reaction network, we have created a situation where the pattern formation properties of the system can be controlled through fluxes on the boundary. For instance, in Figure 2.4, if $D = 10$, then everything in the green region and to the left of the

relevant contour line has a short-wavelength linear instability, whereas in the blue region, the pattern formation and oscillatory modes compete.

Finally, we direct our attention to the contour corresponding to a critical diffusion of 1. This contour is contained entirely in the blue oscillatory region as we would expect from our discussion in Section 2.2.3. There we showed that while short-wavelength instabilities may exist for a diffusion ratio of 1 the long-wavelength instability will always be the most unstable.

We conclude by noting that linear equations in the diffusion are general phenomena that can be obtained when $\eta_2,\ \lambda$ are zero. In this case, $\Gamma_2 = k$ and since it no longer depends on D it is possible to find the critical diffusion for an arbitrary wavenumber $k \neq 0$. In particular, if the steady state reactions do not depend on the diffusion then,

$$D_{c,s} = \gamma \frac{\Gamma_1 g_{1,R} \sinh(\Gamma_1) + \gamma(f_{1,R}g_{1,Q} - f_{1,Q}g_{1,R})\cosh(\Gamma_1)}{k\tanh(k)(\Gamma_1 \sinh(\Gamma_1) - \gamma f_{1,Q}\cosh(\Gamma_1))}, \tag{2.70}$$

$$\begin{aligned} D_{c,op} = \gamma &\frac{\Gamma_1^2 g_{0,R}\sinh(\Gamma_1) - \gamma\Gamma_1 f_{1,Q}g_{0,R}\cosh(\Gamma_1)}{k\Gamma_1\tanh(k)(\Gamma_1\sinh(\Gamma_1) - \gamma f_{1,Q}\cosh(\Gamma_1))} \\ &+ \frac{\gamma\Gamma_1 f_{1,R}g_{0,Q}\cosh(\Gamma_1 - k) - \gamma^2 f_{1,Q}f_{1,R}g_{0,Q}\sinh(\Gamma_1 - k)}{k\Gamma_1\sinh(k)(\Gamma_1\sinh(\Gamma_1) - \gamma f_{1,Q}\cosh(\Gamma_1))}. \end{aligned} \tag{2.71}$$

As we did when considering the problem in γ, by examining when the ratio changes sign we can determine when positive diffusion ratios exist. For example, a positive critical diffusion in the shared boundary case exists only if

$$(\Gamma_1 g_{1,R}\sinh(\Gamma_1) - \gamma\det(J_1)\cosh(\Gamma_1))(\Gamma_1\sinh(\Gamma_1) - \gamma f_{1,Q}\cosh(\Gamma_1)) > 0. \tag{2.72}$$

Noting that the signs transitions at

$$f_{1,Q} = \frac{\Gamma_1\tanh(\Gamma_1)}{\gamma} + \frac{f_{1,R}g_{1,Q}}{g_{1,R}} \tag{2.73}$$

and

$$f_{1,Q} = \frac{\Gamma_1}{\gamma}\tanh(\Gamma_1). \tag{2.74}$$

We conclude that the value of $f_{1,Q}$ must either be bounded by these roots, or outside of them depending on the sign of $g_{1,R}$.

2.3 Boundary-Bound Reactions with Flow

We now turn our attention to a special case of the problem with fluid flow. Here we will extend some of the results of Kundu [6] and Chandrasekhar [7] to our model. If we recall Equation (2.20), but assume $\eta_i = 0$ then the steady state solutions for Q_0 and R_0 have a linear profile, when they exist. It follows that Equation (2.18) takes the form

$$\begin{aligned}
&\left(\frac{d^2}{dz^2} - (\lambda + k^2)\right) q = c_Q w \\
&\left(\frac{d^2}{dz^2} - \left(\frac{\lambda}{D} + k^2\right)\right) r = c_R w \\
&\left[\mathrm{Sc}\left(\frac{d^2}{dz^2} - k^2\right)^2 - \lambda\left(\frac{d^2}{dz^2} - k^2\right)\right] w \quad = k^2 \mathrm{Gr}(\delta^Q q + \delta^R r)
\end{aligned} \tag{2.75}$$

Due to general boundary conditions there is no vertical symmetry in our problem. As a result, it is not possible to use classical methods to estimate Ra, let alone verify the principle of exchange stabilities. However, we can provide sufficient conditions for when the system has this property, and it does provide some insight into the mechanism for overstability in boundary-bound reaction systems with hydrodynamics. In particular, we will assume that $f_{z,R} = g_{z,Q} = 0$, such as the case when the reactions are independent of each other. Multiplying each differential equation by the conjugate of the underlying function, we obtain

$$q^*\left(\frac{d^2}{dz^2} - (\lambda + k^2)\right) q = c_Q q^* w \tag{2.76}$$

$$r^*\left(\frac{d^2}{dz^2} - \left(\frac{\lambda}{D} + k^2\right)\right) r = c_R r^* w \tag{2.77}$$

$$w^*\left[\mathrm{Sc}\left(\frac{d^2}{dz^2} - k^2\right)^2 - \lambda\left(\frac{d^2}{dz^2} - k^2\right)\right] w = k^2 \mathrm{Gr}(\delta^Q w^* q + \delta^R w^* r) \tag{2.78}$$

Beginning with Equation (2.76), we integrate, giving

$$\int_0^1 q^*\left(\frac{d^2}{dz^2} - (\lambda + k^2)\right) q \mathrm{d}z = c_Q \int_0^1 q^* w \mathrm{d}z. \tag{2.79}$$

From here, we can then perform a series of manipulations,

$$\int_0^1 q^* \frac{d^2 q}{dz^2} - (\lambda + k^2)|q|^2 \mathrm{d}z = c_Q \int_0^1 q^* w \mathrm{d}z, \tag{2.80}$$

$$q^* \frac{dq}{dz}\Big|_0^1 - \int \left|\frac{dq}{dz}\right|^2 - (\lambda + k^2)|q|^2 \mathrm{d}z = c_Q \int_0^1 q^* w \mathrm{d}z, \tag{2.81}$$

$$\gamma(f_{1,Q}|q(1)|^2 - f_{0,Q}|q(0)|^2) - \int_0^1 \left|\frac{dq}{dz}\right|^2 - (\lambda + k^2)|q|^2 \mathrm{d}z = c_Q \int_0^1 q^* w \mathrm{d}z. \tag{2.82}$$

By letting

$$I_{1,Q} = \gamma(f_{1,Q}|q(1)|^2 - f_{0,Q}|q(0)|^2) - \int_0^1 \left|\frac{dq}{dz}\right|^2 - k^2|q|^2 \mathrm{d}z \tag{2.83}$$

$$I_{2,Q} = \int_0^1 |q|^2 \mathrm{d}z \tag{2.84}$$

Equation (2.82) can be re-expressed as,

$$I_{1,Q} + I_{2,Q}\lambda = c_Q \int_0^1 q^* w \mathrm{d}z. \tag{2.85}$$

We note that by construction, $I_{1,Q}, I_{2,Q} \in \mathbb{R}$ and $I_{2,Q} > 0$ if $q \not\equiv 0$. Similarly for $r(z)$ we have

$$\gamma(g_{1,R}|r(1)|^2 - g_{0,R}|r(0)|^2) - \int_0^1 \left|\frac{dr}{dz}\right|^2 - \left(\frac{\lambda}{D} + k^2\right)|r|^2 \mathrm{d}z = c_R \int_0^1 r^* w \mathrm{d}z \tag{2.86}$$

$$I_{1,R} + \lambda I_{2,R} = c_R \int_0^1 r^* w \mathrm{d}z \tag{2.87}$$

where we define $I_{1,R}$ and $I_{2,R}$ as,

$$I_{1,R} = \gamma(g_{1,R}|r(1)|^2 - g_{0,R}|r(0)|^2) - \int_0^1 \left|\frac{dr}{dz}\right|^2 - k^2|r|^2 \mathrm{d}z, \tag{2.88}$$

$$I_{2,R} = \int_0^1 \frac{|r|^2}{D}. \tag{2.89}$$

Similarly, $I_{1,R}, I_{2,R} \in \mathbb{R}$ with $I_{2,R} > 0$ if $r \not\equiv 0$ satisfying similar conditions as $I_{1,Q}$ and $I_{2,Q}$. Finally, for Equation (2.78) we perform the following series of reductions,

$$\int_0^1 w^* \left[\left(\frac{d^2}{dz^2} - k^2 \right)^2 - \frac{\lambda}{\mathrm{Sc}} \left(\frac{d^2}{dz^2} - k^2 \right) \right] w \mathrm{d}z = \int_0^1 k^2 \mathrm{Ra} (\delta^Q w^* q + \delta^R w^* r) \mathrm{d}z, \tag{2.90}$$

$$\int_0^1 w^* \left(\frac{d^2}{dz^2} - k^2 \right)^2 w + \frac{\lambda}{\mathrm{Sc}} \int_0^1 \left| \frac{dw}{dz} \right|^2 - k^2 |w|^2 \mathrm{d}z = \int_0^1 k^2 \mathrm{Ra} (\delta^Q w^* q + \delta^R w^* r) \mathrm{d}z, \tag{2.91}$$

$$\int_0^1 \left| \frac{d^2 w}{dz^2} \right|^2 - 2 \left| \frac{dw}{dz} \right|^2 + k^2 |w|^2 + \frac{\lambda}{\mathrm{Sc}} \int_0^1 \left| \frac{dw}{dz} \right|^2 - k^2 |w|^2 \mathrm{d}z = \int_0^1 k^2 \mathrm{Ra} (\delta^Q w^* q + \delta^R w^* r) \mathrm{d}z. \tag{2.92}$$

In this case we define

$$I_{1,W} = \int_0^1 \left| \frac{d^2 w}{dz^2} \right|^2 - 2 \left| \frac{dw}{dz} \right|^2 + k^2 |w|^2 - \int_0^1 k^2 |w|^2 \mathrm{d}z, \tag{2.93}$$

$$I_{2,W} = \frac{1}{\mathrm{Sc}} \int_0^1 \left| \frac{dw}{dz} \right|^2, \tag{2.94}$$

which again satisfy $I_{1,W}, I_{2,W} \in \mathbb{R}$ and $I_{2,W} > 0$ if $w \not\equiv 0$. Noting that the right hand side is in fact the complex conjugate of Equation (2.85) and Equation (2.87), upon substitution into Equation (2.92) we recover,

$$I_{1,W} + \lambda I_{2,W} = k^2 \mathrm{Ra} \left(\delta^Q \frac{I_{1,Q} + \lambda^* I_{2,Q}}{c_Q} + \delta^R \frac{I_{1,R} + \lambda^* I_{2,R}}{c_R} \right), \tag{2.95}$$

and by equating the imaginary components we have

$$\lambda_i \left[I_{2,W} + k^2 \mathrm{Ra} \left(\delta^Q \frac{I_{2,Q}}{c_Q} + \delta^R \frac{I_{2,R}}{c_R} \right) \right] = 0. \tag{2.96}$$

It follows that this is only possible if

$$\mathrm{Ra} = - \frac{I_{2,W}}{k^2 \left(\delta^Q \frac{I_{2,Q}}{c_Q} + \delta^R \frac{I_{2,R}}{c_R} \right)}. \tag{2.97}$$

Such a scenario can be made impossible depending on the direction of the buoyancy force and the signs of (δ^Q, δ^R, c_Q, c_R). For instance, if all these terms are positive, then when

the direction of the buoyancy results in positive Rayleigh numbers, Equation (2.97) can only be satisfied if $\lambda_i = 0$ and we observe a similar behaviour when everything is negative. Therefore, we expect that the principle of exchange stabilities holds in these specific cases. As a result, in these instances at least one of $f_{1,R}$ and $g_{1,Q}$ must be non-zero in order for more complicated behaviour to be possible.

For completeness, we can also calculate the general solutions at the onset of convection when $\lambda = 0$ of this case. Solving for w in terms of q in Equation (2.75) we have

$$w = \frac{1}{c_Q}\left(\frac{d^2}{dz^2} - k^2\right) q. \tag{2.98}$$

Upon substituting this back into Equation (2.75) implies that w is governed by

$$\left[\frac{\mathrm{Sc}}{c_Q}\left(\frac{d^2}{dz^2} - k^2\right)^3 - \delta^Q k^2 \mathrm{Gr}\right] q = \frac{\delta^R}{\delta^Q} k^2 \mathrm{Gr}\ r. \tag{2.99}$$

This reduces the whole system to

$$\left(\frac{d^2}{dz^2} - k^2\right)\left[\frac{\mathrm{Sc}}{c_Q}\left(\frac{d^2}{dz^2} - k^2\right)^3 - \delta^Q k^2 \mathrm{Gr}\right] q = \frac{\delta^R k^2 \mathrm{Gr} c_R}{c_Q}\left(\frac{d^2}{dz^2} - k^2\right) q. \tag{2.100}$$

Expanding and collecting the various terms we obtain a single eigth order linear ordinary differential equation in q,

$$\left(\frac{d^2}{dz^2} - k^2\right)\left[\left(\frac{d^2}{dz^2} - k^2\right)^3 - k^2\left(\delta^Q c_Q + \delta^R c_R\right)\mathrm{Ra}\right] q = 0. \tag{2.101}$$

The characteristic equation for which tells us immediately that $\pm k$ is a root and remaining roots are given by solving

$$\left(r^2 - k^2\right)^3 - k^2 \mathrm{Ra}\left(\delta^Q c_Q + \delta^R c_R\right) = 0. \tag{2.102}$$

This can be quickly solved to conclude that,

$$r^2 = k^2 + \sqrt[3]{k^2 \mathrm{Ra}(\delta^Q c_Q + \delta^R c_R)}. \tag{2.103}$$

where we have taken the principle cube root of -1. There are two other solutions given by

$$r^2 = k^2 - \frac{1}{2}(1 - \sqrt{3}i)\sqrt[3]{k^2 \mathrm{Ra}(\delta^Q c_Q + \delta^R c_R)},$$
$$r^2 = k^2 - \frac{1}{2}(1 + \sqrt{3}i)\sqrt[3]{k^2 \mathrm{Ra}(\delta^Q c_Q + \delta^R c_R)}.$$

Each of these solutions define two solutions for r. As we would expect, there are eight roots when we include $\pm k$ and we list them all here

$$\begin{aligned} r_{1,2} &= \pm k, \\ r_{3,4} &= \pm\sqrt{k^2 + \sqrt[3]{k^2\mathrm{Ra}(\delta^Q c_Q + \delta^R c_R)}}, \\ r_{5,6} &= \pm\sqrt{k^2 - \frac{1}{2}(1-\sqrt{3}i)\sqrt[3]{k^2\mathrm{Ra}(\delta^Q c_Q + \delta^R c_R)}}, \\ r_{7,8} &= \pm\sqrt{k^2 - \frac{1}{2}(1+\sqrt{3}i)\sqrt[3]{k^2\mathrm{Ra}(\delta^Q c_Q + \delta^R c_R)}}. \end{aligned} \tag{2.104}$$

It follows that the general solution can be expressed as

$$q(z) = \sum_{n=1}^{4} a_{2n-1}\cosh(r_{2n}z) + a_{2n}\sinh(r_{2n}z). \tag{2.105}$$

By substituting Equation (2.105) into Equation (2.98) and Equation (2.99) we likewise obtain the general solutions for $w(z)$ and $r(z)$. This will define eight systems of homogeneous linear equations whose solution exists only if the determinant of corresponding matrix vanishes, much like the previous section. The critical value for Ra can therefore be solved numerically with an appropriately implemented root finding algorithm.

2.4 Summary

In this chapter, we have looked at two-reagent boundary-bound reactions from a high level. We were able to determine several interesting properties in the case without flow. In particular, we obtained a quartic polynomial in γ, the global rate of flux, whose roots determine whether there exists a physical system with a fixed linear instability of interest. Focusing on the non-oscillatory case, we derived two quadratics from the higher-order polynomial. These quadratics described the case where reactions take place on a shared boundary, versus when they take place on an opposing boundary. By forcing the global rate of flux to be a positive quantity we obtained conditions on the existence of solutions in γ. Consequently, we determined that the existence of solutions depended on the instability considered and its growth rate. We were also able to some general families where pattern formation does and does not exist.

Afterwards, we noted that if one of the two reagents does not include a bulk decay term then the system can often be expressed as a linear equation in D. We provide the

solutions for the critical diffusion given a fixed wavenumber k, in both the shared boundary and opposing boundary cases. Since the diffusion ratio must be positive, it is possible to determine conditions on the existence of solutions by studying when the ratio changes sign. Recalling Equation (2.70) and Equation (2.71), we can also see see how the (λ, k)-surface influences the sign of these equations.

We showcased many of these behaviours by considering an example where we showed how one could control pattern formation through boundary fluxes. In this example, we split the Schnakenberg reaction into two parts, the constant terms were placed on one boundary and the reaction terms were placed on the opposing boundary. This coincided with the shared boundary case since the derivatives of the constant fluxes vanish after performing the perturbation analysis. Here, we were able to identify the regions of instability as a function of the two constant fluxes (a, b). There were three regions in total, corresponding to pattern formation, a long-wavelength oscillatory instability and no instability. As an application, we proposed programming paths in (a, b) through Figure 2.4, which travel through the various regions resulting in scheduled behaviours in space and time.

We also looked at the case when the diffusion ratio was one. Here, we found that the instability is not uniquely determined by the reaction parameters. As a result, we have a family of solutions which are made unstable for a particular γ. This degeneracy in the system of equations allowed us to conclude that the most unstable mode will always correspond to the constant one. This helps to explain observations made by Balazs et al. [1] where they were unable to produce instabilities of non-zero modes when the diffusion ratio was fixed as one.

Finally, we spent a small amount of time on the case with flow. Here we illustrated how the interactions between reagents at the boundary are often necessary to introduce more complex behaviour such as overstability. To do this, we assumed that the steady state profiles of the reactions were linear so that we could study a more general Rayleigh-Bénard style instability. As a result, we were also able to derive the general solution to the system of partial differential equations which can be substituted into the boundary equations to solve the eigenvalue problem in a specific case.

Chapter 3

Pattern Formation without Hydrodynamics

In this chapter we will expand on the results discussed in Chapter 2, studying the pattern formation process for the Schnakenberg system [2, 3] taking place on the top boundary. We will focus on the behaviour without flow, using it as an opportunity to understand the pattern formation behaviour before introducing buoyancy driven flows in Chapter 4. Since the reaction is restricted to the boundary, we find that the pattern formation properties become coupled to the bulk decay and as a result, we are able to reduce the critical diffusion ratio approximately eight times.

Furthermore, by working with two reactions on a shared boundary we are able to apply the results of Chapter 2 as well as obtain an equation for the critical diffusion ratio given a fixed wavenumber. Given that we are interested in the coupling Turing-style instabilities at the boundary to fluid flow, we study the pattern formation properties of the system from the aforementioned equation. In addition, since we have an analytical solution for the critical diffusion, we are able to easily investigate its behaviour as a function of the other non-dimensionalized parameters and similar to Chapter 2 we find that a real positive critical diffusion does not exist for all wavenumbers. Given the importance of the wavenumber, we spend some time investigating its behaviour as a function of the bulk decay and global rates of flux. Finally, when the vertical variation is small we are able to determine analytical amplitude estimates for the vertically averaged equations that coincide with our simulations.

We also investigate the oscillatory instability mentioned in Chapter 2, providing both an analytical justification for its existence in our model, as well as a numerical exploration

of its behaviour relative to the other reaction parameters. As a result, we extend some of the original investigations done by Balazs et al. [1] to a model with asymmetric diffusion rates. We conclude our study without flow by looking at combinations of the Turing instability with the oscillatory one. Here, we demonstrate the existence of a slow manifold of oscillatory patterns that eventually decays to a steady pattern, as well as transitory travelling waves and solitons.

3.1 Non-Dimensionalization

We recall the reaction kinetics for the Schnakenberg equations provided in Equation (1.25). For consistency with Chapter 2, and to avoid confusion with u for the flow field, we substitute Q and R for U and V in Equation (1.25). As mentioned above, we assume that these reactions occur along the upper boundary with a linear decay for Q in the bulk. This bulk decay can come about by assuming that Q is an unstable product of A in Equation (1.25). As before, if the quantities of A and B are sufficiently large so that the limiting step for the production of Q and R is the quantity of necessary enzymes at the boundary, the reaction pathways taking $A \to Q$ and $B \to R$ can be effectively modeled as constant fluxes.

To avoid an additional non-dimensionalization in Chapter 4, we will non-dimensionalize the entire system with flow governed by the Navier-Stokes equations with the Boussinesq approximation so that the evolution equations be expressed as,

$$\begin{aligned}
\frac{\partial Q}{\partial t} &= -k_{-2}Q + d_Q\nabla^2 Q - (\mathbf{u}\cdot\nabla)Q, \\
\frac{\partial R}{\partial t} &= d_R\nabla^2 Q - (\mathbf{u}\cdot\nabla)R, \\
\frac{\partial \mathbf{u}}{\partial t} &= -(\mathbf{u}\cdot\nabla)\mathbf{u} - \frac{1}{\rho_0}\nabla p + \nu\nabla^2\mathbf{u} + g(\beta^Q Q + \beta^R R)\mathbf{e}_z, \\
\nabla\cdot\mathbf{u} &= 0,
\end{aligned} \tag{3.1}$$

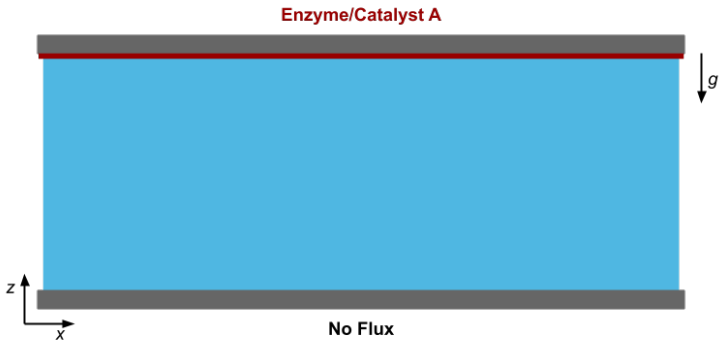


Figure 3.1: A schematic for the model investigated in Chapter 3 and Chapter 4. Note that we assume the buoyancy forces are negligible in Chapter 3

subject to the following boundary conditions

$$\left.\frac{\partial Q}{\partial z}\right|_{z=0} = 0, \qquad \left. d_Q \frac{\partial Q}{\partial z}\right|_{z=H} = \alpha - k_{-1}Q + k_3 Q^2 R, \tag{3.2}$$

$$\left.\frac{\partial R}{\partial z}\right|_{z=0} = 0, \qquad \left. d_R \frac{\partial R}{\partial z}\right|_{z=H} = \beta - k_3 Q^2 R, \tag{3.3}$$

$$\mathbf{u}\Big|_{z=0} = 0 = \mathbf{u}\Big|_{z=H}. \tag{3.4}$$

In this case k_i represent reaction rate constants, while d_Q and d_R are diffusion coefficients. We also have ν, β^Q and β^R which correspond to the fluid kinematic viscosity and solutal expansion coefficients of Q and R respectively. Finally, ρ_0 corresponds to the mean fluid density, g the acceleration due to gravity, while α and β are constant positive in-fluxes of reagents. A schematic of the model can be found in Figure 3.1. The selection of boundary value problem allows us to restrict the Schnakenberg reaction to the upper boundary. Given that we have already discussed its ability to produce Turing Patterns in Chapter 1, this is a natural choice if we are interested in understanding how the diffusion driven pattern formation along the boundary interacts with buoyancy driven instabilities.

Starting from Equation (3.1), let

$$\begin{aligned} Q = Q_s\hat{Q}, \quad R = R_s\hat{R}, \quad x{=}x_s\hat{x}, \quad y{=}y_s\hat{y}, \\ z = z_s\hat{z}, \quad \mathbf{u} = u_s\hat{\mathbf{u}}, \quad t{=}\ t_s\hat{t}, \quad p{=}p_s\hat{p}. \end{aligned} \tag{3.5}$$

Since we are working with periodic conditions in the horizontal direction, and our desire to study buoyancy driven instabilities caused by vertical concentration gradients, we will

set the characteristic length-scale $z_s = H$ the height of our chamber. Furthermore, by setting $x_s = y_s = z_s$ we avoid the introduction of the aspect ratio as an additional non-dimensionalized parameter. Upon substitution, we obtain

$$\frac{Q_s}{t_s}\frac{\partial Q}{\partial t} = -k_{-2}Q_sQ + \frac{d_Q Q_s}{H^2}\nabla^2 Q - \frac{u_s Q_s}{H}(\mathbf{u}\cdot\nabla)Q \tag{3.6}$$

$$\frac{R_s}{t_s}\frac{\partial R}{\partial t} = \frac{d_R R_s}{H^2}\nabla^2 R - \frac{u_s R_s}{H}(\mathbf{u}\cdot\nabla)R \tag{3.7}$$

$$\frac{u_s}{t_s}\frac{\partial \mathbf{u}}{\partial t} = -\frac{u_s^2}{H}(\mathbf{u}\cdot\nabla)\mathbf{u} - \frac{p_s}{H\rho_0}\nabla p + \frac{\nu u_s}{H^2}\nabla^2\mathbf{u} + g(\beta^Q Q_s Q + \beta^R R_s R)\mathbf{e}_z \tag{3.8}$$

where we have dropped the $\widehat{\ }$'s from our parameters to ease congestion. We'll look at each equation individually, and make decisions about our various parameters as we go. For instance, starting with Equation (3.6) we have

$$\frac{\partial Q}{\partial t} = -t_s k_{-2}Q + \frac{t_s d_Q}{H^2}\nabla^2 Q - \frac{u_s t_s}{H}(\mathbf{u}\cdot\nabla)Q. \tag{3.9}$$

Since one of our instabilities of interest is the Turing Instability, we will choose as our characteristic time $t_s = H^2/d_Q$. This is a diffusive timescale, based on the diffusion of Q over a length scale of H and reduces Equation (3.9) to

$$\frac{\partial Q}{\partial t} = -\frac{H^2 k_{-2}}{d_Q}Q + \nabla^2 Q - \frac{H u_s}{d_Q}(\mathbf{u}\cdot\nabla)Q. \tag{3.10}$$

By letting $u_s = d_Q/H$, and taking the non-dimensionalized parameter $\eta = H^2 k_{-2}/d_Q$. We obtain a simple dimensionless system,

$$\frac{\partial Q}{\partial t} = -\eta Q + \nabla^2 Q - (\mathbf{u}\cdot\nabla)Q. \tag{3.11}$$

Now, we turn our attention to the fluxes in Equation (3.2). Only the top boundary has any significance in our non-dimensionalization. Substituting our non-dimensionalized terms from Equation (3.5) into Equation (3.2) gives

$$\left.\frac{\partial Q}{\partial z}\right|_{z=1} = \frac{H}{d_Q Q_s}\left(\alpha - k_{-1}Q_sQ + k_3 Q_s^2 R_s Q^2 R\right). \tag{3.12}$$

We can obtain a global rate of flux by setting, $Q_s = R_s = \sqrt{k_{-1}/k_3}$. In particular, this implies that Equation (3.12) can be written as,

$$\left.\frac{\partial Q}{\partial z}\right|_{z=1} = \frac{H}{d_Q}\left(\sqrt{\frac{k_3}{k_{-1}}}\alpha - k_{-1}Q + k_{-1}Q^2 R\right), \tag{3.13}$$

so that it is possible to factor out k_{-1} and obtain a rate of flux defined by $\gamma = Hk_{-1}/d_Q$. Furthermore, by relabeling our non-dimensional term $a = \sqrt{k_3/k_{-1}} \cdot k_{-1}^{-1}\alpha$, we obtain a reduced equation similar to one of the reactants in Equation (1.32),

$$\left.\frac{\partial Q}{\partial z}\right|_{z=1} = \gamma(a - Q + Q^2 R). \tag{3.14}$$

If we perform the same steps for R, then for $\frac{\partial R}{\partial t}$, we will obtain

$$\frac{\partial R}{\partial t} = D\nabla^2 R - (\mathbf{u}\cdot\nabla)R, \tag{3.15}$$

with

$$\left.\frac{\partial R}{\partial z}\right|_{z=1} = \frac{\gamma}{D}\left(b - Q^2 R\right), \tag{3.16}$$

and where $D = d_R/d_Q$ is the ratio between the two diffusion terms.

Now we can turn our attention to the non-dimensionalization of the flow field in Equation (3.8). So that we can consider cases where Q or R dominate the behaviour of the flow, we define $\beta^{\max} = \max\{|\beta^Q|,\ |\beta^R|\}$, further by letting $p_s = u_s H\rho_0/t_s$ we can simplify Equation (3.8) further to,

$$\frac{\partial \mathbf{u}}{\partial t} = (\mathbf{u}\cdot\nabla)\mathbf{u} - \nabla p + \frac{\nu t_s}{H^2}\nabla^2\mathbf{u} + \frac{g t_s^2 \beta^W Q_s}{H}\left(\frac{\beta^Q}{\beta^{\max}}Q + \frac{\beta^R}{\beta^{\max}}R\right)\mathbf{e}_z. \tag{3.17}$$

From here it is possible to introduce several non-dimensional parameters of interest. In particular, we have the Schmidt coefficient, the Grashof number and δ^Q or δ^R are expansion coefficients relative to the largest absolute expansion, $\beta^{\max}$. We summarise the newly defined non-dimensional parameters below,

$$\begin{aligned} \mathrm{Sc} &= \frac{\nu t_s}{H^2} = \frac{\nu}{d_Q}, \quad \mathrm{Gr} = \frac{g t_s^2 \beta^{\max} Q_s}{H} = \sqrt{\frac{k_{-2}}{k_3}}\cdot\frac{H^3\beta^Q g}{d_Q^2}, \\ \delta^R &= \frac{\beta^R}{\beta^{\max}}, \qquad \delta^Q = \frac{\beta^Q}{\beta^{\max}}. \end{aligned} \tag{3.18}$$

All together the chosen non-dimensionalization allows us to write the system as

$$\begin{aligned} \frac{\partial Q}{\partial t} &= -\eta Q + \nabla^2 Q + (\mathbf{u}\cdot\nabla)Q, \\ \frac{\partial R}{\partial t} &= D\nabla^2 R + (\mathbf{u}\cdot\nabla)R, \\ \frac{\partial \mathbf{u}}{\partial t} &= (\mathbf{u}\cdot\nabla)\mathbf{u} - \nabla p + \mathrm{Sc}\nabla^2\mathbf{u} + \mathrm{Gr}(\delta^Q Q + \delta^R R)e_z, \\ \nabla\cdot\mathbf{u} &= 0, \end{aligned} \tag{3.19}$$

with non-dimensionalized boundary conditions

$$\left.\frac{\partial Q}{\partial z}\right|_{z=0} = 0, \qquad \left.\frac{\partial Q}{\partial z}\right|_{z=1} = \gamma(a - Q + Q^2 R), \tag{3.20}$$

$$\left.\frac{\partial R}{\partial z}\right|_{z=0} = 0, \qquad \left.\frac{\partial R}{\partial z}\right|_{z=1} = \gamma\frac{b - Q^2 R}{D}, \tag{3.21}$$

$$\mathbf{u}\Big|_{z=0} = 0 = \mathbf{u}\Big|_{z=1}. \tag{3.22}$$

We also collect the various transformed variables below

$$\begin{aligned} Q &= \sqrt{\frac{k_{-1}}{k_3}}\hat{Q}, \quad R = \sqrt{\frac{k_{-1}}{k_3}}\hat{R}, \quad x = H\hat{x}, \quad y = H\hat{y}, \\ z &= H\hat{z}, \qquad \mathbf{u} = \frac{d_Q}{H}\hat{\mathbf{u}}, \qquad t = \frac{H^2}{d_Q}\hat{t}, \quad p = \frac{d_Q^2\rho_0}{H^2}\hat{p}, \end{aligned} \tag{3.23}$$

as well as the dimensionless parameters which will serve as the central objects of our study

$$\begin{aligned} \gamma &= \frac{Hk_{-1}}{d_Q}, \qquad \eta = \frac{H^2 k_{-2}}{d_Q}, \qquad D = \frac{d_R}{d_Q}, \\ a &= \sqrt{\frac{k_3}{k_{-1}}}\alpha, \qquad b = \sqrt{\frac{k_3}{k_{-1}}}\beta, \quad \delta^Q = \frac{\beta^Q}{\beta^{\max}}, \\ \delta^R &= \frac{\beta^R}{\beta^{\max}}, \qquad \mathrm{Sc} = \frac{\nu}{d_Q}, \qquad \mathrm{Gr} = \sqrt{\frac{k_{-1}}{k_3}}\frac{H^3\beta^Q g}{d_Q^2}. \end{aligned} \tag{3.24}$$

3.2 On Simulation Methods

With the model of interest non-dimensionalized, we address the methods used in this thesis for numerical simulations. For our purposes, we have decided to use the spectral methods implemented in the Python package Dedalus [24]. Dedalus is a high-level implementation of pseudo-spectral methods, which makes prototyping and simulating various models quick and efficient. Details on pseudo-spectral methods can be found in Boyd [25]. One of the many problems that Dedalus is able to solve is initial value problems of the form

$$M\frac{\partial \mathbf{x}}{\partial t} + L\mathbf{x} = F(\mathbf{x}, t). \tag{3.25}$$

They define M and L as matrices of linear differential operators and F is a vector of general non-linear expressions. By expressing the problem in this form, and using a modified tau method [26, 27], Dedalus is able to solve the evolution equations, constraint equations and boundary conditions directly. Their modifications to the tau method allow them to produce sparse banded matrices for a variety of general problems and obtain performance improvements for their algorithms as a result. The details for their implementations can be found in [24].

To select a time-stepping algorithm, we note that many of the methods utilised by Dedalus were investigated by Ruuth [28, 29] for their ability to accurately simulate the Turing pattern formation process. In particular, the author recommends the semi-implicit backwards difference schemes (SBDF) due to their ability to reduce aliasing by numerically dampening the higher-order modes. Dedalus implements several variable step-size SBDF schemes originally described by Wang and Ruuth [30] and the conditions for consistency and zero-stability can also be found in Wang [31]. Given the available literature, we have opted to use the third order variable timestep SBDF3 scheme described in Wang [30] and implemented in Dedalus. We note that this does not align with Ruuth's original recommendation. In their work, they recommend the second order SBDF2 method, rather than SBDF3 due to the performance trade-off with the higher-order method. However, in testing, we did not find any significant performance loss when opting for the higher-order method.

Unless otherwise specified we simulate our domains with a horizontal length of $2\pi/k_c$ where k_c is the estimated critical wavenumber. In doing so, we can ensure that the critical mode is included in the simulation up to numerical precision. All simulations assume that the horizontal direction has periodic boundary conditions and are simulated with a Fourier basis. For the vertical direction, a Chebyshev basis is used in order to implement the non-linear fluxes as described in Dedalus [24]. Since we are interested in the stability of the steady state to random perturbations, the initial conditions are chosen to be the steady-state concentrations for the parameters, plus a small random perturbation.

Finally, in order to determine appropriate grid sizes for our study of steady pattern formation, we simulated the system without flow at an unstable diffusion ratio D at several grid sizes. We compare the results against a maximum grid size of 512×512 by interpolating the coarser grid onto the finer grid and define the error as the L_2-norm of the difference. We find that the estimates are very good for steady pattern formation. For the 16×16 grid the error is approximately 1.51×10^{-7}. For the 32×32 grid and higher resolutions, the error compared against the 512×512 grid is below 10^{-12}. Since we are interested in pattern formation near the critical values, we simulate at a resolution of 64×64, which

also has an error below 10^{-12} compared to the 512×512 grid. However, this grid size is sufficiently coarse that the difference between the values for various grid points are perceptible when plotting with matplotlib's pcolormesh function. This is because it uses a linear interpolation method or nearest neighbour style shading algorithm and as a result produces visual effects in plots when the number of grid points is small. To resolve this we use a finer grid in the simulations used for plotting figures. Grid sizes were either 128×128 or 256×256.

3.3 The Turing Instability

We now turn our attention to the formation of Turing style instabilities. We begin as always, by searching for steady states in the same fashion as Chapter 2. Returning to Equation (3.19) and dropping the hydrodynamics, we assume that the horizontal variation is zero when the system is at its steady state. As a result, we recover the following equations:

$$0 = -\eta Q + \frac{\partial^2 Q}{\partial z^2}, \tag{3.26}$$

$$0 = D\frac{\partial^2 R}{\partial z^2}, \tag{3.27}$$

and

$$\left.\frac{\partial Q}{\partial z}\right|_{z=0} = 0, \qquad \left.\frac{\partial Q}{\partial z}\right|_{z=1} = \gamma(a - Q + Q^2 R), \tag{3.28}$$

$$\left.\frac{\partial R}{\partial z}\right|_{z=0} = 0, \qquad \left.\frac{\partial R}{\partial z}\right|_{z=1} = \gamma\frac{b - Q^2 R}{D}. \tag{3.29}$$

$$\tag{3.30}$$

Which is given by,

$$\begin{aligned} Q(z) &= \gamma\frac{(a+b)}{\Gamma\sinh(\Gamma) + \gamma\cosh(\Gamma)}\cosh(\Gamma z), \\ R(z) &= \frac{b}{Q(1)^2}. \end{aligned} \tag{3.31}$$

where $\Gamma = \sqrt{\eta}$. We provide an example of the chemical concentrations in Figure 3.2. Now we can begin to study the formation of Turing Patterns.

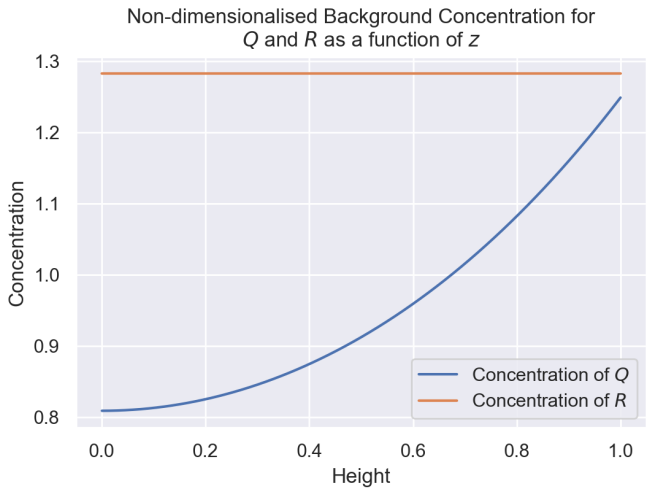


Figure 3.2: Steady state concentrations for $Q(z)$ and $R(z)$ as determined in Equation (3.31)

3.3.1 Averaging Out Vertical Variation

In the case where the distance between the two plates is small and the wavelengths of the expected patterns are much longer than the height of the chamber then we can expect that the vertical variations in concentration fields are negligible. This can occur in the case of a microfluidic device with a chamber that has large horizontal dimensions relative to its height. Working from this assumption, it is possible to replace Q and R in Equation (3.19) with their vertically averaged quantities. However, this will certainly not hold in general and we note that vertical averaging should not be applied to the flow field, since convection cycles cannot be described without vertical variations in velocity. Despite these considerations, by averaging out concentration fields in the vertical direction, we will be able to reduce the dimensionality of the model and obtain an initial estimate for the critical diffusion, make predictions about the final resting patterns, and provide analytical justification for the occurrence of chemical oscillations. All of this is important for our understanding of pattern formation with boundary-bound reactions without hydrodynamics. In fact, the dynamics will reduce to a perturbation of the original Schnakenberg equations. However, in order to continue our analysis with flow, and to obtain more general estimates, we will need to perform the normal mode analysis seen in Chapter 2.

Therefore, suppose that

$$Q(x,y,z,t) \approx \overline{Q}(x,y,t) = \int_0^1 Q(x,y,z)\mathrm{d}z \tag{3.32}$$

$$R(x,y,z,t) \approx \overline{R}(x,y,t) = \int_0^1 R(x,y,z)\mathrm{d}z. \tag{3.33}$$

Focusing our attention to $Q(x,y,z,t)$ in Equation (3.19), we consider the total amount of reagent in a rectangular volume V which spans the vertical direction and has horizontal lengths of Δx and Δy. We know that the volume satisfies a mass balance equation. In particular, the change in the quantity of reactant in our volume is given by the bulk reaction plus any flux, $\mathbf{J}_Q$, out of the boundary

$$\int_V \frac{\partial Q}{\partial t}\mathrm{d}V = \int_V -\eta Q \ \mathrm{d}V + \int_{\partial V} \mathbf{J}_Q \cdot \mathbf{n} \ \mathrm{d}A. \tag{3.34}$$

In our chosen non-dimensionalization Fick's First Law [6] states $\mathbf{J}_Q = -\nabla Q$. If we divide the boundary into the six faces of the rectangular region then the normal will extract a single component of the gradient along each face. This way we can replace the second integral on the right-hand side of Equation (3.34) with the sum of the following six integrals:

$$-\int_y^{y+\Delta y}\int_0^1 \frac{\partial Q}{\partial x}(x,y,z) \ \mathrm{d}z\mathrm{d}y, \tag{3.35}$$

$$\int_y^{y+\Delta y}\int_0^1 \frac{\partial Q}{\partial x}(x+\Delta x,y,z) \ \mathrm{d}z\mathrm{d}y, \tag{3.36}$$

$$-\int_x^{x+\Delta x}\int_0^1 \frac{\partial Q}{\partial y}(x,y,z) \ \mathrm{d}z\mathrm{d}x, \tag{3.37}$$

$$\int_x^{x+\Delta x}\int_0^1 \frac{\partial Q}{\partial y}(x,y+\Delta y,z) \ \mathrm{d}z\mathrm{d}x, \tag{3.38}$$

$$-\int_y^{y+\Delta y}\int_x^{x+\Delta x} \frac{\partial Q}{\partial z}(x,y,0) \ \mathrm{d}x\mathrm{d}y, \tag{3.39}$$

$$\int_y^{y+\Delta y}\int_x^{x+\Delta x} \frac{\partial Q}{\partial z}(x,y,1) \ \mathrm{d}x\mathrm{d}y. \tag{3.40}$$

From the boundary conditions we know that $\frac{\partial Q}{\partial z}(x,y,0) = 0$ and at the top boundary we have

$$\frac{\partial Q}{\partial z}(x,y,1) = \gamma(a - Q + Q^2 R). \tag{3.41}$$

Therefore, since we know that $\int_0^1 Q(x,y,z)\ dz = \overline{Q}(x,y) \approx Q(x,y)$, we can make a substitution. Eliminating several integrals, and reducing the flux terms to

$$-\int_y^{y+\Delta y} \frac{\partial \overline{Q}}{\partial x}(x,y)\ \mathrm{d}y, \tag{3.42}$$

$$\int_y^{y+\Delta y} \frac{\partial \overline{Q}}{\partial x}(x+\Delta x,y)\ \mathrm{d}y, \tag{3.43}$$

$$-\int_x^{x+\Delta x} \frac{\partial \overline{Q}}{\partial y}(x,y)\ \mathrm{d}x, \tag{3.44}$$

$$\int_x^{x+\Delta x} \frac{\partial \overline{Q}}{\partial y}(x,y+\Delta y)\ \mathrm{d}x, \tag{3.45}$$

$$\int_y^{y+\Delta y}\int_x^{x+\Delta x} \gamma(a-\overline{Q}+\overline{Q}^2\overline{R})\mathrm{d}x\mathrm{d}y. \tag{3.46}$$

Finally, by applying the same substitution to the left hand side of the governing equation for Q in Equation (3.19), we obtain,

$$\begin{aligned}\int_y^{y+\Delta y}\int_x^{x+\Delta x} \frac{\partial \overline{Q}}{\partial t}(x,y)\mathrm{d}x\mathrm{d}y = -\eta \int_y^{y+\Delta y}\int_x^{x+\Delta x} \overline{Q}(x,y)\mathrm{d}x\mathrm{d}y \\ -\int_y^{y+\Delta y} \frac{\partial \overline{Q}}{\partial x}(x,y)\ \mathrm{d}y + \int_y^{y+\Delta y} \frac{\partial \overline{Q}}{\partial x}(x+\Delta x,y)\ \mathrm{d}y \\ -\int_x^{x+\Delta x} \frac{\partial \overline{Q}}{\partial y}(x,y)\ \mathrm{d}x + \int_x^{x+\Delta x} \frac{\partial \overline{Q}}{\partial y}(x,y+\Delta y)\ \mathrm{d}x \\ +\int_y^{y+\Delta y}\int_x^{x+\Delta x} \gamma(a-\overline{Q}+\overline{Q}^2\overline{R})\mathrm{d}x\mathrm{d}y.\end{aligned} \tag{3.47}$$

From here we can multiply through on both sides by $(\Delta x \Delta y)^{-1}$ and taking the limit as $\Delta x,\ \Delta y \to 0$ gives evolution equations for the mean concentration

$$\frac{\partial \overline{Q}}{\partial t} = -\eta\overline{Q} + \left(\frac{\partial^2}{\partial x^2} + \frac{\partial^2}{\partial y^2}\right)\overline{Q} + \gamma(a-\overline{Q}+\overline{Q}^2\overline{R}). \tag{3.48}$$

We obtain a nearly identical result for $\overline{R}$, in this case $\mathbf{J}_R = -D\nabla R$ and as a consequence we obtain,

$$\frac{\partial \overline{R}}{\partial t} = D\left(\frac{\partial^2}{\partial x^2} + \frac{\partial^2}{\partial y^2}\right)\overline{R} + \gamma(b-\overline{Q}^2\overline{R}). \tag{3.49}$$

This provides us with an approximation of reduced dimensionality and removed the separation of bulk and boundary. As previously mentioned this only holds if the vertical variation is small so that the approximation is valid. However, this system is very similar to the standard Schnakenberg system as we have already seen that this system is capable of producing Turing patterns, it is natural to expect this system will as well. Collecting the relevant terms, we have

$$\frac{\partial \overline{Q}}{\partial t} = \gamma \left(a - \left(\frac{\eta}{\gamma} + 1 \right) \overline{Q} + \overline{Q}^2 \overline{R} \right) + \left(\frac{\partial^2}{\partial x^2} + \frac{\partial^2}{\partial y^2} \right) \overline{Q}, \tag{3.50}$$

$$\frac{\partial \overline{R}}{\partial t} = \gamma \left(b - \overline{Q}^2 \overline{R} \right) + D \left(\frac{\partial^2}{\partial x^2} + \frac{\partial^2}{\partial y^2} \right) \overline{R}. \tag{3.51}$$

Let us drop the $\overline{(\,\cdot\,)}$, and simplify slightly

$$\frac{\partial Q}{\partial t} = \gamma \left(a - \left(\frac{\eta}{\gamma} + 1 \right) Q + Q^2 R \right) + \nabla^2 Q, \tag{3.52}$$

$$\frac{\partial R}{\partial t} = \gamma \left(b - Q^2 R \right) + D \nabla^2 R. \tag{3.53}$$

By letting $\mu = \eta/\gamma$, then we can think of this as a perturbation of the original Schnakenberg system studied in Section 1.1,

$$\frac{\partial Q}{\partial t} = \gamma \left(a - (1+\mu) Q + Q^2 R \right) + \nabla^2 Q, \tag{3.54}$$

$$\frac{\partial R}{\partial t} = \gamma \left(b - Q^2 R \right) + D \nabla^2 R. \tag{3.55}$$

Performing a similar an analysis we assume that the system is at a chemical equilibrium with no spatial variation. Solving for the chemical equilibrium we have

$$0 = \gamma (a - (1+\mu) Q + Q^2 R), \tag{3.56}$$

$$0 = \gamma (b - Q^2 R). \tag{3.57}$$

Much like the Schnakenberg system in Equation (1.32), we find that $R = b/Q^2$. Substituting this into the remaining equation, we obtain the steady state for Q:

$$a - (1+\mu) Q + b = 0 \iff Q = \frac{a+b}{\mu+1}. \tag{3.58}$$

It follows that the reduced system has a unique fixed point given by

$$Q_{sc} = \frac{(a+b)}{1+\mu}, \qquad R_{sc} = \frac{b(1+\mu)^2}{(a+b)^2}. \tag{3.59}$$

From here, we can use our work in Section 1.1, and consider the linearization of the system around this equilibrium

$$\frac{\partial}{\partial t}\begin{bmatrix} Q(x,y) \\ R(x,y) \end{bmatrix} = \gamma \begin{bmatrix} f_Q & f_R \\ g_Q & g_R \end{bmatrix} + \nabla^2 \begin{bmatrix} Q(x,y) \\ DR(x,y) \end{bmatrix}. \tag{3.60}$$

where D is the diffusion. In this case, each term in the matrix is given by

$$\tag{3.61}$$

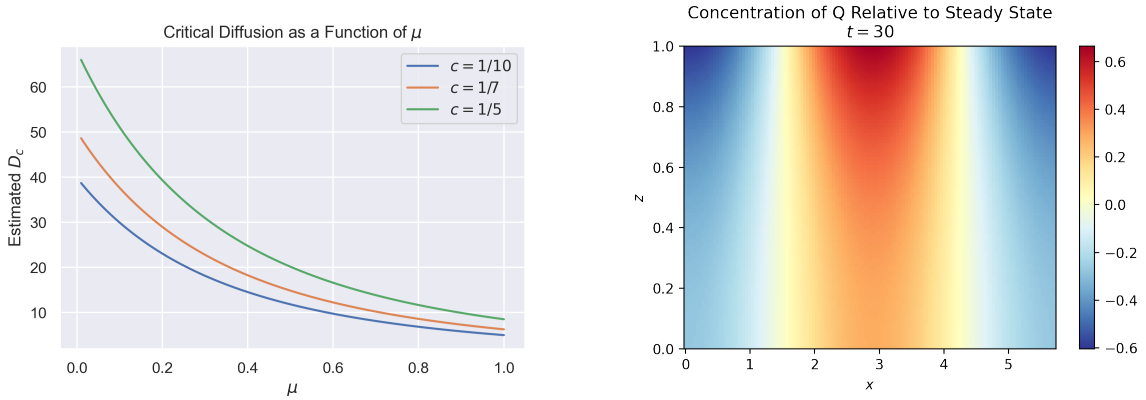
$$f_Q = -(1+\mu) + 2Q_{sc}R_{sc}. \quad f_R = Q_{sc}^2, \tag{3.62}$$

$$g_Q = -2Q_{sc}R_{sc}, \quad g_R = -Q_{sc}^2. \tag{3.63}$$

Referring to Equation (1.19) and Equation (1.21), we can compute both the critical mode and critical diffusion when they exist. We fix $b = 2$ and changing the ratio $a/b = c$ we plot the critical diffusion as a function of μ for $c = 1/10,\ 1/7,\ 1/5$ in Figure 3.3a. Comparing this with numerical results for the instabilities, we find that the critical diffusion in the limit $\mu \to 0$ is always a supercritical value, implying that the addition of decay has a destabilizing effect on the overall system. This is surprising since there is no immediate reason that the bulk decay should influence the behaviour of pattern formation at the boundary. In Section 3.4 we will see that the averaged equations overestimate the critical diffusion and will rely on a normal mode analysis performed later to more accurately study the critical diffusion and its behaviour relative to the other non-dimensionalized parameters. Instead, these equations will give us more insight into the pattern formation process before we look at the behaviour with flow. Since the averaged equations will can be used to estimate the resting amplitude, as well as explain analytically the emergence of long-wavelength oscillatory instabilities.

3.3.2 Amplitude Estimation

If the cross-sectional length scales are small, such as the case of a microfluidic channel then reaction dynamics will be well approximated by a one-dimensional model. Using the averaged equations, we can perform a weakly non-linear analysis of the Turing pattern formation process similar to Bozzini et al. [32] and Gambino et al. [13]. As a result, we will obtain some insight into how the patterns react to changes in the various key parameters of interest, as well as obtain analytical estimates for the vertically averaged resting amplitude. Bozzini et al. [32] and Gambino et al. [13] discuss how to extend their arguments to two dimensional pattern formation, but this is not done here.



(a) (b)

Figure 3.3: (a) Critical diffusion estimate as a function of $\mu = \eta/\gamma$ for various c with $b = 2$. (b) Simulation of Q at supercritical diffusion after sometime $(a, b, \eta, \gamma, D) = (0.2, 2.0, 1, 1, 6)$.

In the case where the bulk dynamics are well approximated by a two dimensional model, the vertically averaged dynamics reduce to a one-dimensional model,

$$\begin{bmatrix} Q_t \\ R_t \end{bmatrix} = \gamma \begin{bmatrix} a - (1+\mu)Q + Q^2 R \\ b - Q^2 R \end{bmatrix} + \frac{\partial^2}{\partial x^2} \begin{bmatrix} 1 & 0 \\ 0 & D \end{bmatrix} \begin{bmatrix} Q \\ R \end{bmatrix}. \tag{3.64}$$

Assuming that the Turing conditions in Equation (1.22) are satisfied so that pattern formation is expected and consider an expansion at long time in a small parameter $\epsilon^2 = (D - D_c)/D_c$,

$$\begin{aligned} D &= D_c + \epsilon D^1 + \epsilon^2 D^2 + \cdots \\ \begin{bmatrix} Q \\ R \end{bmatrix} &= \begin{bmatrix} q_0 + \epsilon q_1 + \epsilon^2 q_2 + \cdots \\ r_0 + \epsilon r_1 + \epsilon^2 r_2 + \cdots \end{bmatrix} = \mathbf{c}_0 + \epsilon \mathbf{c}_1 + \cdots \\ t &= \frac{T_1}{\epsilon} + \frac{T_2}{\epsilon} + \cdots \end{aligned} \tag{3.65}$$

Viewing the reaction terms in this lens we find that for Q, we have

$$\frac{\partial Q}{\partial t} = \frac{\partial Q}{\partial T_1}\frac{\partial T_1}{\partial t} + \frac{\partial Q}{\partial T_2}\frac{\partial T_2}{\partial t} + \cdots \tag{3.66}$$

and we obtain an identical equation for R. We can solve for $\frac{\partial T_n}{\partial t}$ by assuming that $\frac{\partial T_n}{\partial T_m} = 0$, so that

$$\frac{\partial t}{\partial T_n} = \frac{1}{\epsilon^m} \iff \epsilon^m = \frac{\partial T_n}{\partial t}. \tag{3.67}$$

Substituting the expansion up to third order we obtain the following:

Reaction for Q:

$$\begin{aligned}
&\mathrm{O}(1)\text{: } \gamma(a-(\mu+1)q_0+q_0^2r_0),\\
&\mathrm{O}(\epsilon)\text{: } \gamma(q_0^2r_1+2q_0q_1r_0-(1+\mu)q_1),\\
&\mathrm{O}(\epsilon^2)\text{: } \gamma(q_0^2r_2+2q_0q_1r_1+2q_0q_2r_0+q_1^2r_0-(1+\mu)q_2),\\
&\mathrm{O}(\epsilon^3)\text{: } \gamma(q_0^2r_3+2q_0q_1r_2+2q_0q_2r_1+2q_0q_3r_0+q_1^2r_1+2q_1q_2r_0-(1+\mu)q_3).
\end{aligned} \tag{3.68}$$

Reaction for R:

$$\begin{aligned}
&\mathrm{O}(1)\text{: } \gamma(a-q_0^2r_0),\\
&\mathrm{O}(\epsilon)\text{: } -\gamma(q_0^2r_1+2q_0q_1r_0),\\
&\mathrm{O}(\epsilon^2)\text{: } -\gamma(q_0^2r_2+2q_0q_1r_1+2q_0q_2r_0+q_1^2r_0),\\
&\mathrm{O}(\epsilon^3)\text{: } -\gamma(q_0^2r_3+2q_0q_1r_2+2q_0q_2r_1+2q_0q_3r_0+q_1^2r_1+2q_1q_2r_0).
\end{aligned} \tag{3.69}$$

Combined:

$$\begin{aligned}
&\mathrm{O}(1)\text{: } \gamma\begin{bmatrix}a-(1+\mu)q_0+q_0r_0\\ b-q_0r_0\end{bmatrix},\\
&\mathrm{O}(\epsilon)\text{: } \gamma\begin{bmatrix}2q_0r_0-(1+\mu) & q_0^2\\ -2q_0r_0 & -q_0^2\end{bmatrix}\begin{bmatrix}q_1\\ r_1\end{bmatrix},\\
&\mathrm{O}(\epsilon^2)\text{: } \gamma\begin{bmatrix}2q_0r_0-(1+\mu) & q_0^2\\ -2q_0r_0 & -q_0^2\end{bmatrix}\begin{bmatrix}q_2\\ r_2\end{bmatrix}+\gamma\begin{bmatrix}q_1^2r_0+2q_0q_1r_1\\ -q_1^2r_0-2q_0q_1r_1\end{bmatrix},\\
&\mathrm{O}(\epsilon^3)\text{: } \gamma\begin{bmatrix}2q_0r_0-(1+\mu) & q_0^2\\ -2q_0r_0 & -q_0^2\end{bmatrix}\begin{bmatrix}q_3\\ r_3\end{bmatrix}+\gamma\begin{bmatrix}2q_0r_1+2q_1r_0 & 2q_0q_1\\ -2q_0r_1-2u_1v_0 & -2q_0q_1\end{bmatrix}\begin{bmatrix}q_2\\ r_2\end{bmatrix}+\gamma\begin{bmatrix}q_1^2r_1\\ -q_1^2r_1\end{bmatrix}.
\end{aligned} \tag{3.70}$$

O(1) Problem:

$$0=\gamma(a-(1+\mu)q_0+q_0^2r_0)+\frac{\partial^2 q_0}{\partial x^2} \tag{3.71}$$

$$0=\gamma(b-q_0^2r_0)+D_c\frac{\partial^2 r_0}{\partial x^2} \tag{3.72}$$

We begin by assuming that q_0 and r_0 are constant in space, and can therefore eliminate the diffusion terms

$$\frac{\partial^2 q_0}{\partial x^2}=\frac{\partial^2 r_0}{\partial x^2}=0.$$

In doing so, we are assuming that there is a constant background concentration. This is reasonable, since we expect the constant mode to be stable with the formation of Turing patterns and at long time any transient portion should decay. As a result our equations are reduced to

$$0 = \gamma(a - (1+\mu)q_0 + q_0^2 r_0), \tag{3.73}$$
$$0 = \gamma(b - q_0^2 r_0), \tag{3.74}$$

which are solved by the steady state concentrations we discovered earlier

$$\mathbf{c}_0 = \begin{bmatrix} q_0 \\ r_0 \end{bmatrix} = \begin{bmatrix} \frac{a+b}{1+\mu} \\ \frac{b(\mu+1)^2}{(a+b)^2} \end{bmatrix} \tag{3.75}$$

As a result $\partial \mathbf{c}_0 / \partial T_n = 0$ for all n.

$\mathbf{O}(\epsilon)$ Problem:

$$\epsilon \frac{\partial \mathbf{c}_0}{\partial T_1} = \epsilon\gamma \begin{bmatrix} -(1+\mu) + 2q_0 r_0 & q_0^2 \\ -2q_0 r_0 & -q_0^2 \end{bmatrix} \begin{bmatrix} q_1 \\ r_1 \end{bmatrix} + \frac{\partial^2}{\partial x^2} \left(\epsilon \begin{bmatrix} 1 & 0 \\ 0 & D_c \end{bmatrix} \begin{bmatrix} q_1 \\ r_1 \end{bmatrix} + \epsilon \begin{bmatrix} 0 & 0 \\ 0 & D^1 \end{bmatrix} \begin{bmatrix} q_0 \\ r_0 \end{bmatrix} \right). \tag{3.76}$$

In the previous step we determined that q_0 and r_0 were constant so that this reduces to

$$\mathbf{0} = \gamma \begin{bmatrix} -(1+\mu) + 2q_0 r_0 & q_0^2 \\ -2q_0 r_0 & -q_0^2 \end{bmatrix} \begin{bmatrix} q_1 \\ r_1 \end{bmatrix} + \frac{\partial^2}{\partial x^2} \begin{bmatrix} 1 & 0 \\ 0 & D_c \end{bmatrix} \begin{bmatrix} q_1 \\ r_1 \end{bmatrix}. \tag{3.77}$$

For simplicity, we make the following substitutions

$$J = \gamma \begin{bmatrix} -(1+\mu) + 2q_0 r_0 & q_0^2 \\ -2q_0 r_0 & -q_0^2 \end{bmatrix} = \gamma \begin{bmatrix} f_q & f_r \\ g_q & g_r \end{bmatrix}, \quad \mathcal{D}^{(n)} = \begin{bmatrix} 0 & 0 \\ 0 & D^{(n)} \end{bmatrix}, \quad \mathcal{D}^c = \begin{bmatrix} 1 & 0 \\ 0 & D_c \end{bmatrix}, \tag{3.78}$$

so that the $O(\epsilon)$ problem can be written as

$$0 = J \begin{bmatrix} q_1 \\ r_1 \end{bmatrix} + \frac{\partial^2}{\partial x^2} \mathcal{D}^c \begin{bmatrix} q_1 \\ r_1 \end{bmatrix} = \left(J + \mathcal{D}^c \frac{\partial^2}{\partial x^2} \right) \begin{bmatrix} q_1 \\ r_1 \end{bmatrix}. \tag{3.79}$$

This equation forces

$$\begin{bmatrix} q_1 \\ r_1 \end{bmatrix} \in \ker(\mathcal{L}) = \ker \left(J + \mathcal{D}^c \frac{\partial^2}{\partial x^2} \right). \tag{3.80}$$

Since we are working with real amplitudes, our normal modes should be real-values. Consequently, we can assume that

$$\mathbf{c}_1 = \begin{bmatrix} q_1 \\ r_1 \end{bmatrix} = A(t)\mathbf{b}_1 \cos(k_c x), \qquad \mathbf{b}_1 = \begin{bmatrix} b_{11} \\ b_{12} \end{bmatrix}. \tag{3.81}$$

since the actual behaviour will only differ up to a phase shift. Substituting this into Equation (3.79), we obtain

$$\mathbf{0} = A(T)\cos(k_c x)\cdot\left(J - k_c^2\mathcal{D}^c\right)\mathbf{b}_1. \tag{3.82}$$

This can only be solved if $(J - k_c^2\mathcal{D}^c)$ is singular. However, k_c must correspond to a permissible mode and therefore the only valid values for k_c satisfy the equation

$$k_c = n_c\pi/L,\ n_c \in \mathbb{N} \tag{3.83}$$

This presents us with an additional problem. If D_c is the critical diffusion, then the critical wave number is given by

$$k_c^2 = \gamma\frac{D_c J_{11} + J_{22}}{2D_c}. \tag{3.84}$$

which may not take the form $(n_c\pi/L)^2$ for some $n_c \in \mathbb{Z}$. Therefore, we will assume that D_c is in fact the critical diffusion for the first permissible wavenumber, and call this k_c. This ensures that there exists some $\mathbf{b}_1 \neq \mathbf{0}$ such that $\mathcal{L}\mathbf{b}_1 = \mathbf{0}$. In particular, since

$$J - k_c^2\mathcal{D}^c = \begin{bmatrix}\gamma f_q - D_c^2 & \gamma f_r \\ \gamma g_q & \gamma g_r - D_c k_c^2\end{bmatrix}, \tag{3.85}$$

then $\mathbf{b}_1$ can be written up to scaling as

$$\mathbf{b}_1 = \begin{bmatrix}1 \\ \dfrac{k_c^2 - \gamma f_u}{\gamma f_v}\end{bmatrix}, \tag{3.86}$$

so that the first order solution is given by

$$\mathbf{c}_1 = A(T)\mathbf{b}_1\cos(k_c x). \tag{3.87}$$

$\mathbf{O}(\epsilon^2)$ Problem:

$$\frac{\partial\mathbf{c}_1}{\partial T_1} = \mathcal{L}\mathbf{c}_2 + \gamma\begin{bmatrix}2q_0q_1r_1 + q_1^2r_0 \\ -2q_0q_1r_1 - q_1^2r_0\end{bmatrix} + \frac{\partial^2}{\partial x^2}\begin{bmatrix}0 & 0 \\ 0 & D^{(1)}\end{bmatrix}\mathbf{c}_1, \tag{3.88}$$

or similar to Bozinni et al. [32]

$$\frac{\partial\mathbf{c}_1}{\partial T_1} + \gamma\begin{bmatrix}-2q_0q_1r_1 - q_1^2r_0 \\ 2q_0q_1r_1 + q_1^2r_0\end{bmatrix} - \frac{\partial^2}{\partial x^2}\begin{bmatrix}0 & 0 \\ 0 & D^{(1)}\end{bmatrix}\mathbf{c}_1 = \mathcal{L}\mathbf{c}_2. \tag{3.89}$$

From our previous discussion, we know that the solution of $\mathbf{c}_1$ will be a vector in the kernel of $\mathcal{L}$ described by Equation (3.87). In order to ensure that there is no resonance we must ensure that

$$\langle \mathcal{L}\mathbf{c}_2, \mathbf{c}_1 \rangle = 0. \tag{3.90}$$

In other words, we are requiring that $\mathbf{c}_2$ does not contain $\cos(k_c x)$ as a mode. This can be done by imposing $\partial \mathbf{c}_1 / \partial T_1 = 0$ and $\mathcal{D}^{(1)} = \mathbf{0}$. We note that this assumes that $\mathbf{c}_1$ does not change meaningfully the timescale of T_1, $(O(1/\epsilon))$.

With this assumption, Equation (3.89) reduces to

$$\mathcal{L}\mathbf{c}_2 = \gamma \begin{bmatrix} -2q_0 q_1 r_1 - q_1^2 r_0 \\ 2q_0 q_1 r_1 + q_1^2 r_0 \end{bmatrix}. \tag{3.91}$$

Substituting the $q_1 = b_{11} A(t)\cos(k_c x)$ and $r_1 = b_{12} A(t)\cos(k_c x)$, we can solve for $\mathbf{c}_2$. In particular, assuming that $\mathbf{c}_2$ takes the form $A(T)^2(\mathbf{b}_2 + \mathbf{b}_3 \cos(2k_c x))$. Then we will have

$$A(T)^2 \mathcal{L}\left(\mathbf{b}_2 + \mathbf{b}_3 \cos(2k_c x)\right) = \gamma A(T)^2 \begin{bmatrix} -2q_0 b_{11} b_{12} - b_{11}^2 r_0 \\ 2q_0 b_{11} b_{12} + b_{11}^2 r_0 \end{bmatrix} \cos(k_c x)^2. \tag{3.92}$$

Cancelling the amplitude and expanding the cosine squared term we have

$$\mathcal{L}\left(\mathbf{b}_2 + \mathbf{b}_3 \cos(2k_c x)\right) = \gamma \begin{bmatrix} -2q_0 b_{11} b_{12} - b_{11}^2 r_0 \\ 2q_0 b_{11} b_{12} + b_{11}^2 r_0 \end{bmatrix} \left(\frac{1}{2} + \frac{\cos(2k_c x)}{2}\right). \tag{3.93}$$

Then by separating the modes, this gives two equations,

$$\mathcal{L}\mathbf{b}_2 = \frac{\gamma}{2} \cdot \begin{bmatrix} -2q_0 b_{11} b_{12} - b_{11}^2 r_0 \\ 2q_0 b_{11} b_{12} + b_{11}^2 r_0 \end{bmatrix}, \tag{3.94}$$

$$\mathcal{L}\mathbf{b}_3 \cos(2k_c x) = \frac{\gamma}{2} \cdot \begin{bmatrix} -2q_0 b_{11} b_{12} - b_{11}^2 r_0 \\ 2q_0 b_{11} b_{12} + b_{11}^2 r_0 \end{bmatrix} \cos(2k_c x). \tag{3.95}$$

$$\tag{3.96}$$

Which upon expanding $\mathcal{L}$ gives the following two equations

$$J\mathbf{b}_2 = \frac{\gamma}{2} \cdot \begin{bmatrix} -2q_0 b_{11} b_{12} - b_{11}^2 r_0 \\ 2q_0 b_{11} b_{12} + b_{11}^2 r_0 \end{bmatrix}, \tag{3.97}$$

$$(J - 4k_c^2 \mathcal{D}^c)\mathbf{b}_3 = \frac{\gamma}{2} \cdot \begin{bmatrix} -2q_0 b_{11} b_{12} - b_{11}^2 v_0 \\ 2q_0 b_{11} b_{12} + b_{11}^2 v_0 \end{bmatrix}. \tag{3.98}$$

Since k_c was chosen as the critical mode for D_c and J is non-singular through the stability of the constant mode in the Turing conditions, we conclude that both equations can be solved for $\mathbf{b}_2$ and $\mathbf{b}_3$ yielding $\mathbf{c}_2$.

$\mathbf{O}(\epsilon^3)$ Problem:

Since the $O(\epsilon^3)$ problem is quite large, we will break this one into pieces. First, we note that from the reaction terms we obtain

$$\gamma \begin{bmatrix} 2q_0v_0 - 1 & q_0^2 \\ -2q_0v_0 & -q_0^2 \end{bmatrix} \begin{bmatrix} q_3 \\ r_3 \end{bmatrix} + \gamma \begin{bmatrix} 2q_0r_1 + 2q_1r_0 & 2q_0q_1 \\ -2q_0r_1 - 2q_1r_0 & -2q_0q_1 \end{bmatrix} \begin{bmatrix} q_2 \\ r_2 \end{bmatrix} + \gamma \begin{bmatrix} q_1^2r_1 \\ -q_1^2r_1 \end{bmatrix}. \tag{3.99}$$

On the left hand side we can collect the derivatives which result in order three terms

$$\frac{\partial \mathbf{c}_1}{\partial T_2} + \frac{\partial \mathbf{c}_2}{\partial T_1} m \tag{3.100}$$

and for the diffusion we will pick upm

$$\mathcal{D}^c \mathbf{c}_3 + \mathcal{D}^{(2)} \mathbf{c}_1. \tag{3.101}$$

Combining these three equations and solving for $\mathcal{L}\mathbf{c}_3$ we have,

$$\mathcal{L}\mathbf{c}_3 = \frac{\partial \mathbf{c}_1}{\partial T_2} + \gamma \begin{bmatrix} -2q_0r_1 - 2q_1r_0 & -2q_0q_1 \\ 2q_0r_1 + 2q_1r_0 & 2q_0q_1 \end{bmatrix} \mathbf{c}_2 + \gamma \begin{bmatrix} -q_1^2r_1 \\ q_1^2r_1 \end{bmatrix} - \frac{\partial^2}{\partial x^2} \mathcal{D}^{(2)} \mathbf{c}_1. \tag{3.102}$$

Substituting the known values for $\mathbf{c}_1$ and $\mathbf{c}_2$ gives

$$\begin{aligned} \mathcal{L}\mathbf{c}_3 = & \frac{\partial A}{\partial T_2} \cos(k_c x) \mathbf{b}_1 \\ & + \gamma A^3(T) \begin{bmatrix} -2q_0b_{12} - 2b_{11}r_0 & -2q_0b_{11} \\ 2q_0b_{12} + 2b_{11}r_0 & 2q_0b_{11} \end{bmatrix} (\mathbf{b}_2 \cos(k_c x) + \mathbf{b}_3 \cos(k_c x) \cos(2k_c x)) \\ & + \gamma A(T)^3 \begin{bmatrix} -b_{11}^2 b_{12} \\ b_{11}^2 b_{12} \end{bmatrix} \cos^3(k_c x) + k_c^2 A \cos(k_c x) \mathcal{D}^{(2)} \mathbf{b}_1. \end{aligned}$$

Finally by expanding the products of various modes into sums we obtain

$$\begin{aligned} \mathcal{L}\mathbf{c}_3 = & \frac{\partial A}{\partial T_2} \cos(k_c x) \mathbf{b}_1 \\ & + \gamma A^3(T) \begin{bmatrix} -2q_0b_{12} - 2b_{11}r_0 & -2q_0b_{11} \\ 2q_0b_{12} + 2b_{11}r_0 & 2q_0b_{11} \end{bmatrix} \left(\left(\mathbf{b}_2 + \frac{1}{2}\mathbf{b}_3 \right) \cos(k_c x) + \frac{1}{2}\mathbf{b}_3 \cos(3k_c x) \right) \\ & + \gamma A(T)^3 \begin{bmatrix} -b_{11}^2 b_{12} \\ b_{11}^2 b_{12} \end{bmatrix} \left(\frac{3}{4} \cos(k_c x) + \frac{1}{4} \cos(3k_c x) \right) + k_c^2 A \cos(k_c x) \mathcal{D}^{(2)} \mathbf{b}_1. \end{aligned}$$

Now we can attend to the issue of resonance. In particular, in order to ensure there is no resonance, we require that

$$\left\langle \mathbf{c}_3, \left(\frac{\partial A}{\partial T_2}\mathbf{b}_1 + AG_1 + \gamma A^3 G_2 \right) \cos(k_c x) \right\rangle = 0,$$

where

$$G_1 = \begin{bmatrix} 0 & 0 \\ 0 & k_c^2 D^{(2)} \end{bmatrix} \mathbf{b}_1, \tag{3.103}$$

$$G_2 = \begin{bmatrix} -2q_0 b_{12} - 2b_{11} r_0 & -2q_0 b_{11} \\ 2q_0 b_{12} + 2b_{11} r_0 & 2q_0 b_{11} \end{bmatrix} \left(\mathbf{b}_2 + \frac{1}{2}\mathbf{b}_3 \right) + \frac{3}{4} \begin{bmatrix} -b_{11}^2 b_{12} \\ b_{11}^2 b_{12} \end{bmatrix}. \tag{3.104}$$

For this, we can use the Fredholm solvability criterion [33, 34]. This requires that for all $\mathbf{c}_3$ with $\mathcal{L}^T \mathbf{c}_3 = 0$ it must be the case that

$$\left\langle \mathbf{c}_3, \left(\frac{\partial A}{\partial T_2}\mathbf{b}_1 + AG_1 + \gamma A^3 G_2 \right) \right\rangle = 0. \tag{3.105}$$

Then for the negation we need only show that there exists at least one $\mathbf{c}_3 \in \ker(\mathcal{L}^T)$ with

$$\frac{\partial A}{\partial T_2}\langle \mathbf{c}_3, \mathbf{b}_1 \rangle = -\langle \mathbf{c}_3, G_1 \rangle A - \gamma \langle \mathbf{c}_3, G_2 \rangle A^3, \tag{3.106}$$

having a nontrivial solution. This yields the cubic Stuart-Landau equation [35, 36, 37],

$$\begin{aligned} \frac{\partial A}{\partial T_2} &= -\frac{\langle \mathbf{c}_3, G_1 \rangle}{\langle \mathbf{c}_3, \mathbf{b}_1 \rangle} A - \gamma \frac{\langle \mathbf{c}_3, G_2 \rangle}{\langle \mathbf{c}_3, \mathbf{b}_1 \rangle} A^3, \\ &= \sigma A - L A^3, \end{aligned} \tag{3.107}$$

from which we can conclude that

$$A_\infty = \sqrt{\frac{\sigma}{L}}. \tag{3.108}$$

and an approximate longtime solution is given by

$$\begin{bmatrix} Q \\ R \end{bmatrix} = \mathbf{c}_0 + \epsilon A_\infty \mathbf{b}_1 \cos(k_c x) + \epsilon^2 A_\infty^2 \left(\mathbf{b}_2 + \mathbf{b}_3 \right) \cos(2k_c x) + O(\epsilon^3). \tag{3.109}$$

Gambino et al. [13] provides an additional analysis for an extended model where $L < 0$. This requires extending the perturbation to fifth order. However, since $L > 0$ for the reaction parameters considered we do not consider the extension here. From this work, we

can also make predictions about the time for the pattern to form, since the solutions to the cubic Stuart-Landau are know to be,

$$A(T)^2 = \frac{\sigma}{L + \left(\frac{\sigma}{A(0)^2} - L\right) e^{-\sigma T}}. \tag{3.110}$$

It follows that when $T \gg 1/\sigma$ we expect that $A(T) \approx \sqrt{\sigma/L}$. However, T is a very slow timescale on the order of $1/\epsilon^2$. Consequently, we expect pattern formation to be slow process requiring t on the order of $1/(\epsilon^2\sigma)$.

Since the amplitude estimates are derived from the averaged equations, their accuracy depends on the assumptions underpinning the averaged model. We recall from Equation (3.24) that $\gamma,\ \eta \sim O(1/d_Q)$. Therefore, in order for the assumption to be valid, we expect it to hold for small η and γ. In addition to this, η also describes the decay in the bulk and creates a vertical variation on its own. Recalling Equation (3.31) for the steady state of Q, we see that there is a non-linear relationship between γ and η, with η increasing the vertical variation and γ decreasing it. With these behaviours in mind, we focus our attention on scenarios where $\eta < \gamma \ll 1$, the pairings investigated are

$$(\gamma,\ \eta) \in \{(0.1, 0),\ (0.1, \gamma/100),\ (0.1, \gamma/10),\ (0.01, 0),\ (0.01, \gamma/100),\ (0.01, \gamma/10)\}. \tag{3.111}$$

Next we will need to determine a range of perturbations. In our setup of the perturbation problem we defined $\epsilon^2 = (D - D_c)/D_c$ implying that $D = (1 + \epsilon^2)D_c$. This gives a way of determining D which is agnostic of the actual reaction parameters. Therefore, we will step ϵ between 0.01 and 0.1 with step size 0.01. The results of these simulations are provided in Figure 3.4 and Figure 3.5.

As we might expect, the estimates are very good when γ is small and $\eta = 0$. However, in the most extreme case, which is when $\eta = \gamma/10$, the performance deteriorates dramatically, regardless of the value of γ considered. This can be explained in two ways. First, the vertical variation is much more significant when $\eta = \gamma/10$ violating one of our underlying assumptions for the lower dimensional model. However, the second source of error is due to the averaged equations underestimating the critical diffusion. Focusing on the cases in Figure 3.6 where $\eta = \gamma/100$, we we notice that the predicted amplitudes are smaller than their simulated results. This suggests that the perturbations may be larger than we estimated from the averaged equations.

Turning our attention to the rate of convergence, these are also good when $\eta = 0$. By looking at the ratio of $A_\infty/A(T)$ for the smallest perturbation, we predict that $A(T)$ should

be within 1% of A_∞ when $t \approx 3.3 \times 10^7$. However, for the $\eta = \gamma/100$, our analytical results predict this should occur when $t \approx 3.2 \times 10^7$. This differs much more significantly from our simulation results in Figure 3.7. If we take a moment to borrow from the next section, it can be explained by the reduced accuracy of the averaged equations. In this case, the normal mode analysis predicts a critical diffusion of $D_c = 38.699$. Comparing this to the averaged equations, which estimate $D_c = 38.701$, we find that the difference is on the order of ϵ^2 when $\epsilon = 0.01$. As a consequence, meaningful errors are to be expected. Despite these errors, the general trends are consistent with the analytical estimates for small η and γ and provide us with a means of making analytical predictions regarding pattern formation for boundary-bound reactions in various cases.

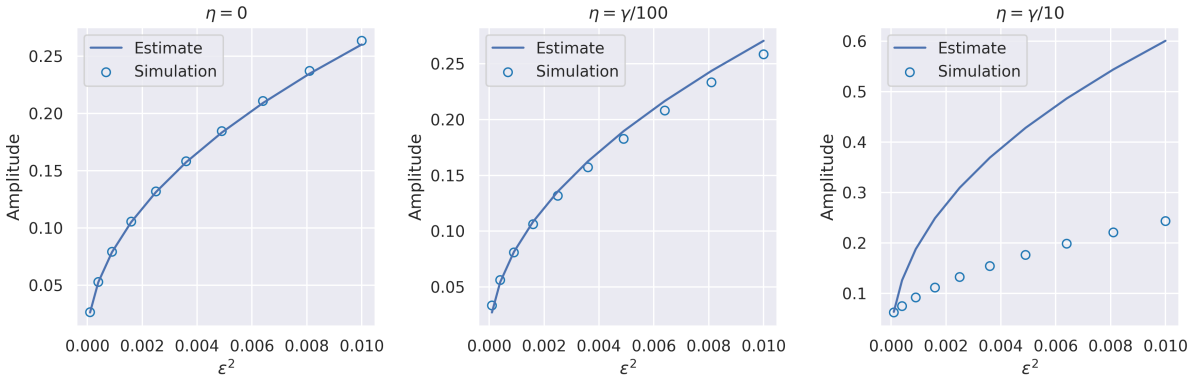


Figure 3.4: Resting simulation amplitude for $\overline{Q}$ vs. estimate for various η and perturbations with $\gamma = 0.01$

3.4 Normal Mode Analysis

We return our attention to Equation (3.19). We will perform a normal mode analysis on our model in the general case with flow so that we do not need to come back and perform it again in the next Chapter. Since we have already determined the steady state for the chemical reactions in Equation (3.31) the steady state pressure can be quickly calculated from

$$p(x, y, z) = \mathrm{Gr}\left(\delta^Q \int_0^1 Q(z)dz + \delta^R \frac{b}{Q(1)^2} z\right) \tag{3.112}$$

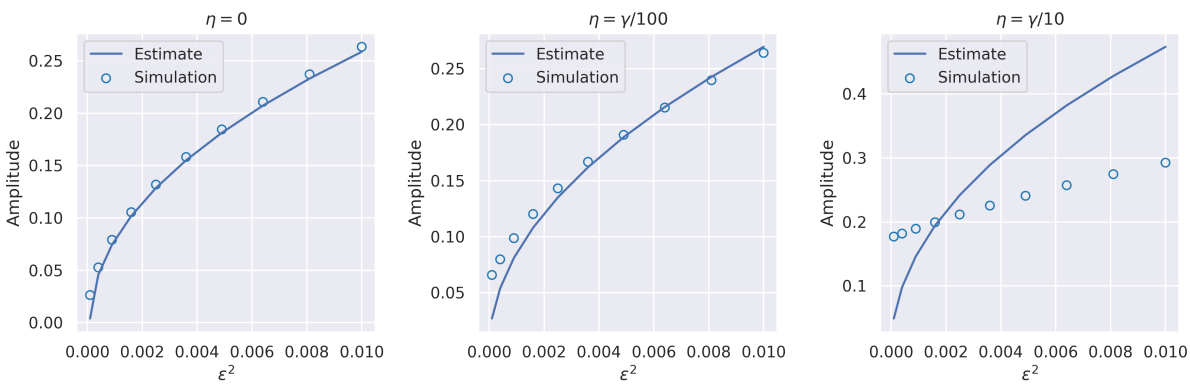


Figure 3.5: Resting simulation amplitude for $\overline{Q}$ vs. estimate for various η and perturbations with $\gamma = 0.1$

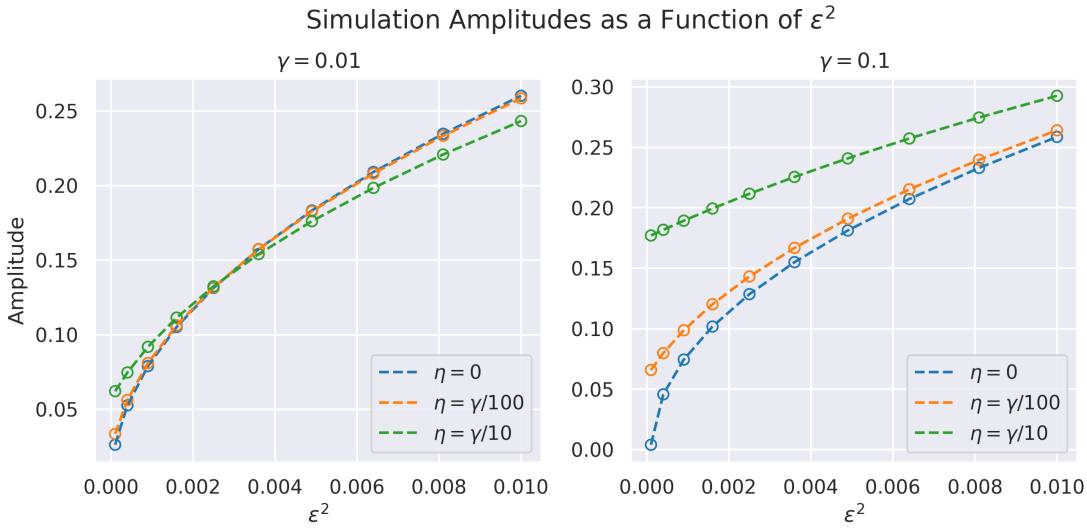


Figure 3.6: Resting simulation amplitudes for $\overline{Q}$ from Figure 3.4 and Figure 3.5.

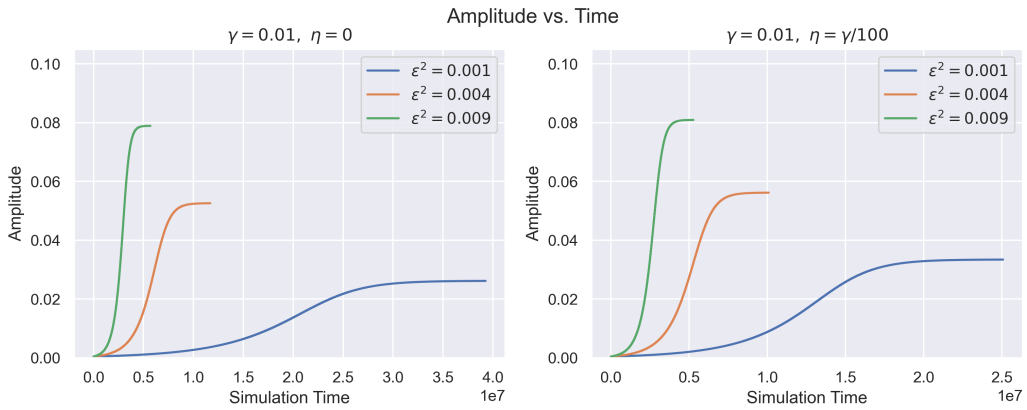


Figure 3.7: Emergence of Turing patterns as a function of time.

Now, consider a small perturbation of the functions described by

$$\begin{bmatrix} Q_0(x,y,z) + Q_1(x,y,z) \\ R_0(x,y,z) + R_1(x,y,z) \\ u_{1,x}(x,y,z) \\ u_{1,y}(x,y,z) \\ u_{1,z}(x,y,z) \\ p_0(x,y,z) + p_1(x,y,z) \end{bmatrix} \tag{3.113}$$

Substituting this into Equation (3.19) we solve for the evolution equations, discarding any products of the perturbation terms. This gives the following system of dynamical equations

$$\frac{\partial Q_1}{\partial t} = -\eta Q_1 + \nabla^2 Q_1 - u_{1,z}\frac{\partial Q_0}{\partial z} \tag{3.114}$$

$$\frac{\partial R_1}{\partial t} = D\nabla^2 R_1 - u_{1,z}\frac{\partial R_0}{\partial z} \tag{3.115}$$

$$\frac{\partial \mathbf{u}_1}{\partial t} = -\nabla p_1 + \mathrm{Sc}\nabla^2 \mathbf{u}_1 + \mathrm{Gr}(\delta^Q Q_1 + \delta^R R_1)\mathbf{e}_z \tag{3.116}$$

$$\nabla \cdot \mathbf{u}_1 = 0 \tag{3.117}$$

As we have done in both Section 1.2 and Chapter 2, we reduce the model to only consider the vertical velocity component and eliminate the pressure term. This allows us to remove the incompressibility condition from the equation set and rewrite Equation (3.116) as,

$$\frac{\partial}{\partial t}\nabla^2 u_{1,z} = \mathrm{Sc}\nabla^4 u_{1,z} + \mathrm{Gr}\nabla_H(\delta^Q Q_1 + \delta^R R_1). \tag{3.118}$$

We also obtain the following boundary conditions by repeating the steps in Chapter 2:

$$\left.\frac{\partial Q_1}{\partial z}\right|_{z=0} = 0, \qquad \left.\frac{\partial Q_1}{\partial z}\right|_{z=1} = \gamma(-Q_1 + 2Q_1Q_0R_0 + Q_0^2R_1), \tag{3.119}$$

$$\left.\frac{\partial R_1}{\partial z}\right|_{z=0} = 0, \qquad \left.\frac{\partial R_1}{\partial z}\right|_{z=1} = \gamma\frac{-2Q_1Q_0R_0 - Q_0^2R_1}{D}, \tag{3.120}$$

$$\left.u_{1,z}\right|_{z=0} = 0 = \left.u_{1,z}\right|_{z=1}, \tag{3.121}$$

$$\left.\frac{\partial u_{1,z}}{\partial z}\right|_{z=0} = 0 = \left.\frac{\partial u_{1,z}}{\partial z}\right|_{z=1}. \tag{3.122}$$

Now suppose that the perturbation takes the form of some vertical function times a horizontal normal mode

$$\begin{bmatrix} Q_1 \\ R_1 \\ u_{1,z} \end{bmatrix} = \begin{bmatrix} q(z) \\ r(z) \\ w(z) \end{bmatrix} e^{\lambda t + i(k_x x + k_y y)} \tag{3.123}$$

our goal is to determine conditions for when the mode is unstable.

After substituting the normal modes of Equation (3.123) into Equations (3.114 - 3.118), the governing equations for a fixed mode are given by

$$\begin{aligned} &\frac{d^2q}{dz^2} - (\lambda + \eta + k^2)q = w\frac{dQ_0}{dz}, \\ &\frac{d^2r}{dz^2} - \left(\frac{\lambda}{D} + k^2\right) r = 0, \\ &\mathrm{Sc}\left(\frac{d^2}{dz^2} - k^2\right)^2 w - \lambda\left(\frac{d^2}{dz^2} - k^2\right) w = k^2\mathrm{Gr}(\delta^Q q + \delta^R r), \end{aligned} \tag{3.124}$$

where $k = \sqrt{k_x^2 + k_y^2}$ and updated boundary conditions given by

$$\frac{dq}{dz}(0) = 0, \qquad \frac{dq}{dz}(1) = \gamma(-q(1) + 2q(1)Q_0(1)R_0(1) + r(1)Q_0^2(1)), \tag{3.125}$$

$$\frac{dr}{dz}(0) = 0, \qquad \frac{dr}{dz}(1) = \gamma\frac{-2q(1)Q_0(1)R_0(1) - r(1)Q_0^2(1)}{D}, \tag{3.126}$$

$$\left.w(z)\right|_{z=0,1} = 0, \qquad \left.\frac{dw}{dz}(z)\right|_{z=0,1} = 0. \tag{3.127}$$

For the remainder of the chapter we will continue our investigation of pattern formation without flow. We are interested in how the boundary-bound problem differs from the classical Schnakenberg problem. This will also serve as another opportunity to see how the results of Chapter 2 apply to this particular problem. Therefore, we will break the analysis into two major parts. First, we will look at the pattern formation properties of our system, and how the various non-dimensionalized values influence the patterns. Afterwards, we will investigate the appearance of chemical oscillations similar to those seen by Balazs et al. [1]. We extend their investigation to the Schnakenberg system, and to diffusion ratios not equal to one. Consequently, we observe a non-linear relationship between the bulk decay and the diffusion ratio for both pattern formation and the long-wavelength oscillatory mode. This makes it possible to identify where the two instabilities meet, and consequently identify a slow manifold of oscillatory Turing patterns. In our simulations using Dedalus [24] as discussed in Section 3.2, the oscillating pattern eventually decays to a stable pattern. However, in the search for oscillatory patterns with two reagents, we believe it may be possible by considering reactions on opposing boundaries and will show in Chapter 4 that oscillatory patterns can be made stable far from the critical Rayleigh number.

3.4.1 Pattern Formation

Eliminating the flow term, the stability of a single mode is governed by

$$\begin{aligned} \frac{d^2q}{dz^2} - (\lambda + \eta + k^2)q = 0, \\ \frac{d^2r}{dz^2} - \left(\frac{\lambda}{D} + k^2\right) r = 0, \end{aligned} \tag{3.128}$$

with the extra boundary conditions also removed

$$\begin{aligned} \frac{dq}{dz}(0) = 0, \qquad & \frac{dq}{dz}(1) = \gamma(-q(1) + 2q(1)Q_0(1)R_0(1) + r(1)Q_0^2(1)), \\ \frac{dr}{dz}(0) = 0, \qquad & \frac{dr}{dz}(1) = \gamma\frac{-2q(1)Q_0(1)R_0(1) - r(1)Q_0^2(1)}{D}. \end{aligned} \tag{3.129}$$

Focusing on the marginally stable mode the general solution is given by

$$q(z) = a_1 \cosh(\Gamma z), \quad \Gamma = \sqrt{\eta + k^2}, \tag{3.130}$$

$$r(z) = b_1 \cosh(kz). \tag{3.131}$$

Noting that our boundary conditions are linear in $q(z)$ and $r(z)$. After substitution, this again defines a homogeneous linear system of equations in a_1 and b_1 as we saw in Chapter 2. The solution of which exists if and only if the determinant of the system vanishes. The components of the corresponding matrix M are

$$M_{00} = \Gamma \sinh(\Gamma) - \gamma(2\cosh(\Gamma)Q_0(1)R_0(1) - \cosh(\Gamma)), \tag{3.132}$$
$$M_{01} = -\gamma \cosh(k)Q_0(1)^2, \tag{3.133}$$
$$M_{10} = \frac{2\gamma}{D}\cosh(\Gamma)Q_0(1)R_0(1), \tag{3.134}$$
$$M_{11} = \frac{\gamma}{D}\cosh(k)Q_0(1)^2 + k\sinh(k). \tag{3.135}$$

The minimum D and corresponding wavenumber k for which

$$\det(M) = M_{00}M_{11} - M_{01}M_{10} = 0 \tag{3.136}$$

defines the critical diffusion and mode. In this case we can solve directly for D as a function of k,

$$D = -\gamma \frac{Q_0(1)^2(\Gamma \sinh(\Gamma) + \cosh(\Gamma)\gamma)}{k\tanh(k)M_{00}}. \tag{3.137}$$

In order to determine the critical diffusion we minimize this, subject to $k = \sqrt{k_x^2 + k_y^2} > 0$.

Given our earlier discussions on the averaged estimate, the first question we seek to answer is how the averaged estimate and normal mode estimate compare. We plot the two estimates in Figure 3.10a for $\gamma = 1$ and various η. As we had mentioned previously, the normal mode estimate suggests that the critical diffusion is overestimated by the averaging method.

In Chapter 2 we also saw that there was a range of modes which could be unstable for a particular γ. This remains true once we have solved for the critical diffusion in Equation (3.137). Since the terms in the numerator are strictly positive, the sign of the critical diffusion is determined by terms in the denominator. The critical curves that define the sign changes are given by $k = 0$ and $M_{00} = 0$. However, the roots of M_{00} are slightly more complicated and require expanding $Q_0(1)$ and $R_0(1)$. Solving for γ we obtain

$$\gamma = \frac{2b\sqrt{\eta}\sinh(\sqrt{\eta})\cosh(\Gamma) - (a+b)\Gamma\sinh(\Gamma)\cosh(\sqrt{\eta})}{\cosh(\sqrt{\eta})\cosh(\Gamma)(a-b)}. \tag{3.138}$$

If γ is fixed, this yields a contour line defining boundaries in conjunction with $k = 0$ where the system can be made unstable through physical values of D, as shown in Figure 3.8.

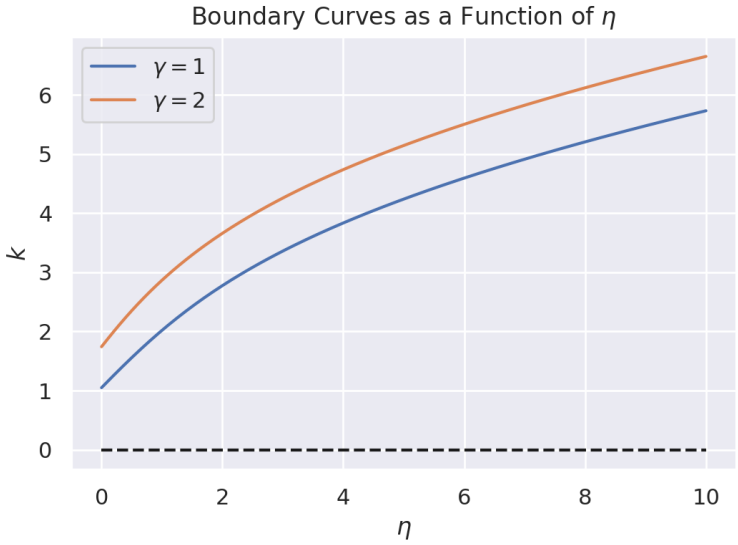


Figure 3.8: Bounding curves for the range of wavenumbers which have a positive critical diffusion given a particular γ.

Given the relationship between γ and η for the existence of instabilities, as well as the influence they have on the critical diffusion, we turn our attention to the critical mode. In Figure 3.9a, we plot the critical mode as a function of (γ, η). The results in Figure 3.9a indicate that there are now two ways to influence the critical diffusion. In the classical analysis, we saw that the critical mode k_c was proportional $\sqrt{\gamma}$ however now γ has a synonymous but different meaning and this is no longer the case. Instead, we observe what appears to be a linear relationship in γ and a sublinear one in η. The results are plotted in Figure 3.9. We conclude that not only does the decay term make the system more unstable to pattern formation but it also influences the pattern selection itself. In fact, the bulk decay term yields an eight-fold decrease in the critical diffusion when the non-dimensionalized bulk decay is one. However, as we have discussed this reduction can only go so far. As η grows, eventually a long-wavelength oscillatory instability becomes unstable overcoming the pattern formation process.

We can also study the behaviour of Equation (3.137) when $\eta = 0$ and in the large η limit. In this case the upper bound is given when $\eta = 0$ and corresponds to the classical critical diffusion we obtained in Chapter 1 for the Schnakenberg system. However, we can

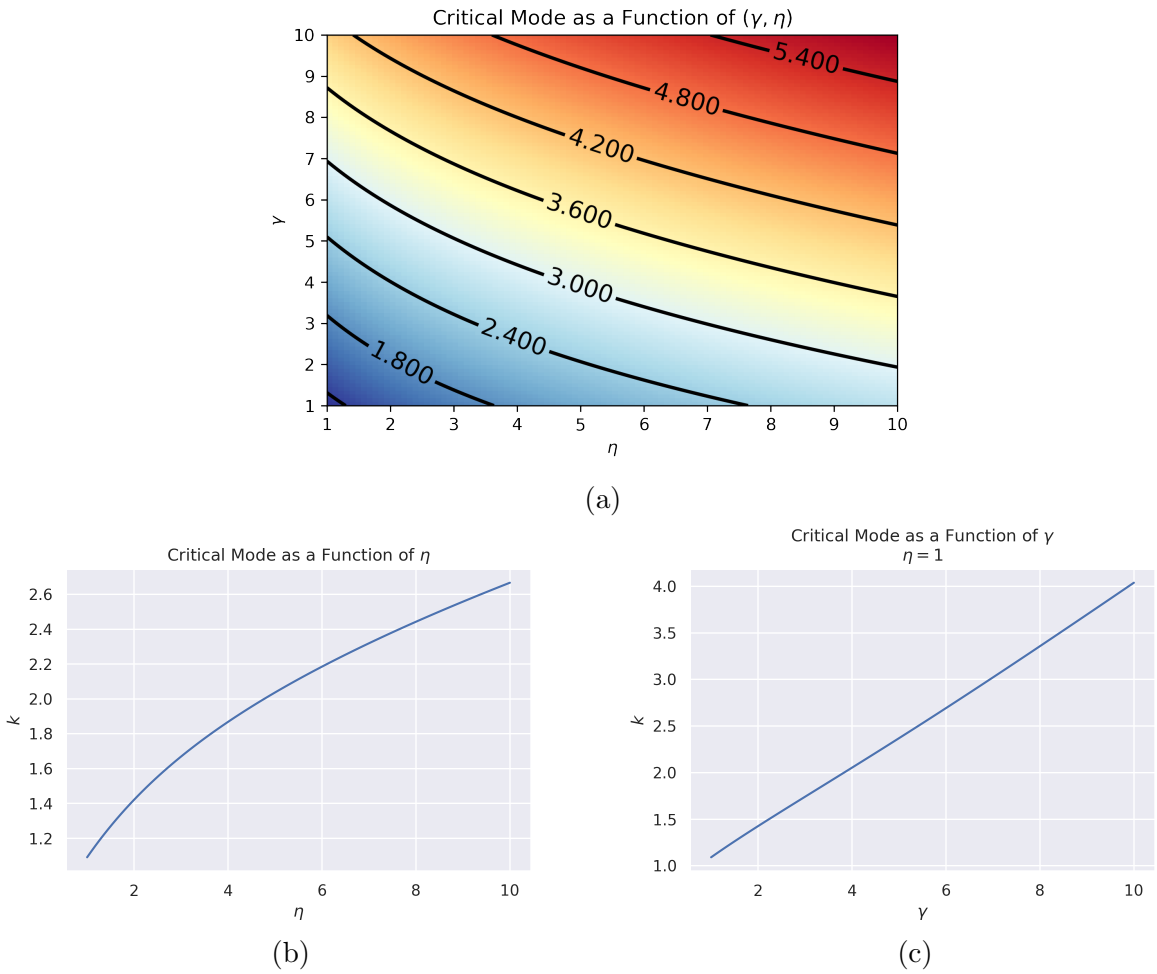


Figure 3.9: (a) Surface of most critical mode as a function of (γ, η), $(a, b) = (0.2, 2.0)$ (b) Critical mode for varied η and $\gamma = 1$. (c) Critical mode for varied γ and $\eta = 1$. Both figures used the shared parameters $(a, b) = (0.2, 2.0)$.

also estimate a lower bound by considering Equation (3.137) in the large η limit,

$$\lim_{\eta\to\infty} D = \lim_{\eta\to\infty} -\frac{\gamma\cosh(k)Q_0(1)^2(\Gamma\sinh(\Gamma)+\cosh(\Gamma)\gamma)}{k\sinh(k)M_{00}} \tag{3.139}$$

$$= \lim_{\eta\to\infty} -\frac{\gamma\cosh(k)Q_0(1)^2}{k\sinh(k)}\frac{(\Gamma\sinh(\Gamma)+\cosh(\Gamma)\gamma)}{\Gamma\sinh(\Gamma)-\gamma(2\cosh(\Gamma)Q_0(1)R_0(1)-\cosh(\Gamma))} \tag{3.140}$$

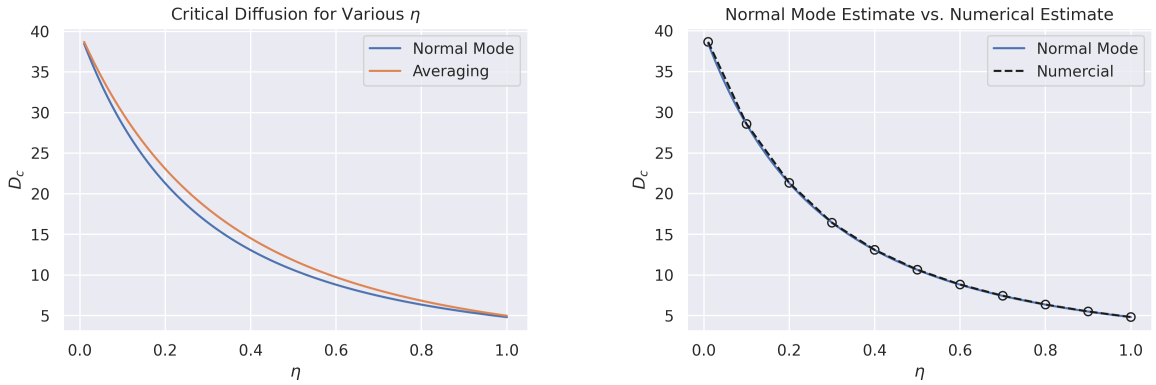
$$= \lim_{\eta\to\infty} -\frac{\gamma\cosh(k)Q_0(1)^2}{k\sinh(k)}\frac{1+\frac{\cosh(\Gamma)\gamma}{\Gamma\sinh(\Gamma)}}{1-\gamma(\frac{2\cosh(\Gamma)Q_0(1)R_0(1)}{\Gamma\sinh(\Gamma)}-\frac{\cosh(\Gamma)}{\Gamma\sinh(\Gamma)})}. \tag{3.141}$$

At this point we can calculate the limit by noting that $Q_0(1)^2 \to 0$ as $\eta \to \infty$ via Equation (3.31) and the second term in the product tends to 1, it follows that $\lim_{\eta\to\infty} D = 0$. This is not physically reasonable of course, but it does tell us that there exists some η for which $D = 1$. As we first discussed in Chapter 2 long-wavelength chemical oscillations begin to dominate as D approaches 1. In fact, we showed in Section 2.2.3 for $D = 1$, the long-wavelength instabilities are always the most unstable. Moreover, we also showed in Section 2.2.3 that the long-wavelength instability will always be the most unstable when $D = 1$ for boundary-bound reactions. Together this suggests that a long-wavelength oscillatory instability should also be searched for in this system. In Section 3.4.2 we will investigate the appearance of chemical oscillations as well as provide a method for finding when pattern formation and chemical oscillations are simultaneously marginally stable. Our numerical investigations suggest that this intersection always occurs when $D > 1$ implying that as η increases and the critical diffusion decreases, the oscillatory instability will become unstable before the critical diffusion is less than 1.

Before this however, we confirm the performance of the normal mode estimates against simulations by testing the critical diffusion and critical wavenumber using a bisection algorithm. The results of this are provided in Figure 3.10a. We have rarely seen numerical confirmation of critical estimates, and believe it is valuable to ensure that the analytical results are valid. For each update to the bisection algorithm, we simulate the proposed value until the system is stable. To determine when the system has stabilized we simulate until the rate of change in the amplitude relative to the current amplitude is on the order of 10^{-8} or until the amplitude is smaller than 10^{-8}. As a result, simulations for unstable diffusion coefficients near the critical value can take several hours to resolve. As a consequence, we only step the bisection algorithm 5 times for eleven different decay values.

To determine the initial values, we take a 10% window around the critical estimate, and test the proposed bounds. Should the proposed lower and upper bounds not bound the critical diffusion, we decrease/increase in steps of 10% until the lower bound is stable and

the upper bound is unstable. Once determined we begin the bisection algorithm, testing the average of the upper and lower bound for pattern formation. Depending on the specific result, we update the appropriate bound and repeat. In the event that no alterations needed to be made to the initial bounds, the final error of the bisection algorithm is at most $10\%/2^6$. In Table 3.1 we provide the results, as well as the maximum percent error obtained via the bisection algorithm. In all cases, the error is less than 1% suggesting that the normal mode estimates are exceedingly close to the simulations.



(a) (b)

Figure 3.10: (a) Normal mode estimate versus average estimate for critical diffusion for various η. (b) Normal mode estimate versus numerical estimate for critical diffusion for various η. Both figures used the shared parameters $(a, b, \gamma) = (0.2, 2.0, 1)$.

3.4.2 Chemical Oscillations

To motivate the search for chemical oscillations we can turn to Balazs et al. [1] who observed chemical oscillations for their system past a critical decay. Given the similarities between the two problems being considered, it is reasonable to suspect such instabilities also exist here. However, we can motivate this analytically by returning to the averaged equations. Recalling the Turing conditions we recovered in Chapter 1 and Equation (3.60), the Jacobian for the linearization without diffusion is given by

$$J = \begin{bmatrix} -(1+\mu) + 2Q_{sc}R_s & Q_{sc}^2 \\ -2Q_{sc}R_{sc} & -Q_{sc}^2 \end{bmatrix} \tag{3.142}$$

Decay	Diffusion Estimate	Bisection Algo.	Abs % Error
0.01	38.472	38.653	0.469%
0.1	28.514	28.558	0.156%
0.2	21.286	21.319	0.156%
0.3	16.445	16.419	0.156%
0.4	13.065	13.086	0.156%
0.5	10.624	10.641	0.156%
0.6	8.809	8.823	0.156%
0.7	7.428	7.439	0.156%
0.8	6.353	6.363	0.156%
0.9	5.022	5.511	0.156%
1.0	4.818	4.825	0.156%

Table 3.1: Comparison of normal mode and bisection algorithm critical diffusion estimates. Values are rounded to third decimal place.

and the eigenvalues are given by

$$\lambda_{\pm} = \frac{\mathrm{Tr}(J) \pm \sqrt{\mathrm{Tr}(J)^2 - 4\det(J)}}{2}. \tag{3.143}$$

A Hopf bifurcation occurs when $\mathrm{Tr}(J) = 0$ and $\det(J) > 0$ [38]. At this point the system admits a marginally stable oscillatory mode. However, by design, these parameters do not satisfy the conditions we found in Chapter 1 for the classical Turing problem. In particular, these conditions require that the trace is negative. However, by having the reactions occur at the boundary we will see that the introduction of the bulk decay term changes the behaviour of the system sufficiently to introduce an oscillatory instability as a function of η.

Applying the conditions for a Hopf bifurcation to Equation (3.142) and after substituting Equation (3.59), we have

$$\frac{2b(1+\mu)}{a+b} - \frac{(a+b)^2}{(1+\mu)^2} - (1+\mu) = 0 \quad \text{and,} \quad \frac{(a+b)^2}{(1+\mu)} > 0, \tag{3.144}$$

since we have assumed that $a, b, \mu > 0$ these conditions can be reduced to

$$b(1+\mu)^3 - a(1+\mu)^3 - (a+b)^3 = 0. \tag{3.145}$$

It follows that a Hopf bifurcation occurs when

$$\mu = \sqrt[3]{\frac{(a+b)^3}{b-a}} - 1 \iff \eta = \gamma\left(\sqrt[3]{\frac{(a+b)^3}{b-a}} - 1\right) \tag{3.146}$$

While the assumption that $\eta > 0$ restricts the range of a, b where the solutions are valid we can conclude that there exists a value of μ so that a Hopf bifurcation occurs in the averaged equations for a wide range of (a, b). In addition, when the term is positive this suggests that γ should have stabilizing effect on the critical parameter. Finally, while we have already discussed how the averaged equations are a poor estimate when η is large, we can infer that critical values of η for oscillatory behaviour should be common for the general problem.

With this in mind, we return to our normal mode analysis. The only necessary modification is to relax the assumption that λ is real and marginally stable. Instead, we assume that the λ lies on the imaginary axis. As we will see, these chemical oscillations are indeed possible for the mode $k = 0$. We are also able to find linearly unstable oscillatory patterns with $k \neq 0$. However, the numerical analysis done later suggests that these are more stable than the long-wavelength solution and never appear in our simulations. Returning to Equation (3.128), we recall that stability of a particular mode is given by solutions to

$$\frac{d^2q}{dz^2} - (\lambda + \eta + k^2)q = 0, \tag{3.147}$$

$$\frac{d^2r}{dz^2} - \left(\frac{\lambda}{D} + k^2\right)r = 0. \tag{3.148}$$

If $\lambda = i\omega$ then solutions take the form

$$q(z) = a_1 \cosh(\Omega_q z), \qquad \Omega_q = \sqrt{i\omega + \eta + k^2}, \tag{3.149}$$

$$r(z) = b_1 \cosh(\Omega_r z), \qquad \Omega_r = \sqrt{\frac{i\omega}{D} + k^2}. \tag{3.150}$$

As a result, we obtain a homogeneous linear system of equations much like before. In this case, the entries of the matrix are given by,

$$M_{00} = \Omega_q \sinh(\Omega_q) - \gamma(2\cosh(\Omega_q)Q_0(1)R_0(1) - \cosh(\Omega_q)), \tag{3.151}$$

$$M_{01} = -\gamma \cosh(\Omega_r)Q_0(1)^2, \tag{3.152}$$

$$M_{10} = \frac{2\gamma}{D}\cosh(\Omega_q)Q_0(1)R_0(1), \tag{3.153}$$

$$M_{11} = \frac{\gamma}{D}\cosh(\Omega_r)Q_0(1)^2 + \Omega_r \sinh(\Omega_r). \tag{3.154}$$

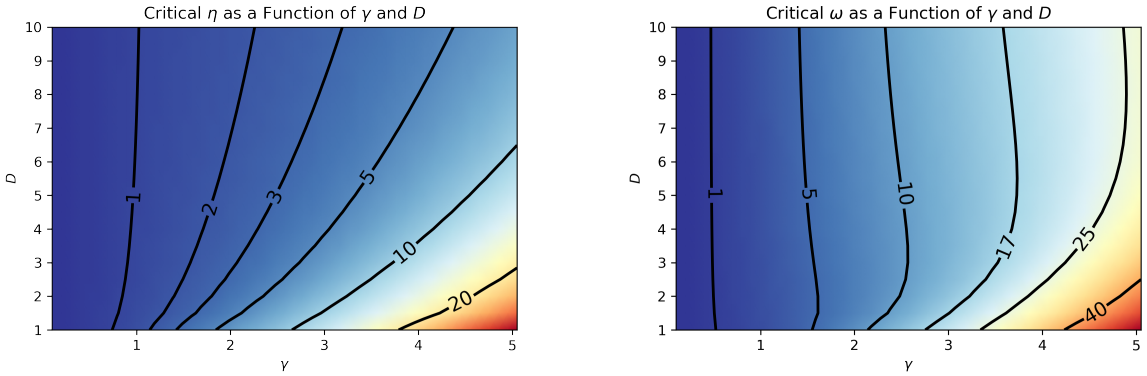
The system of equations has non-trivial solutions only if the determinant vanishes, therefore, we seek solutions to

$$\det(M) = M_{00}M_{11} - M_{01}M_{10} = 0. \tag{3.155}$$

If we restrict $\omega > 0$, the solutions to Equation (3.155) define unique critical values (η_c, ω_c) where the perturbations transition to being unstable. However, unlike in the previous section, we cannot determine D directly since there is now a non-linear dependence on D through Ω_r. Therefore we are left with solving for the roots of the equation with some sort of non-linear solver.

Since the equation is now complex-valued, we search for solutions which make the real and imaginary components of the determinant vanish. This gives us two degrees of freedom to optimize over and can easily be done with Scipy [39] using the root function. By default, this uses MINPAKs hybrd and hybrj routines. We did have some difficulty optimizing over the range of parameters considered. Rather than changing the optimization routine, we simply feed previous nearby solutions as initial guesses. To begin by verifying an initial point $(D,\ \gamma) = (1, 1)$ and then build a surface of estimates from there. In the event that the previous solution does not produce a good initial guess, we perturb the previous solution until the requested degree of convergence is obtained. The resulting critical values are provided in Figure 3.9. As a result, we are able to confirm numerically the stabilizing effect of γ discussed earlier.

To verify the correctness of our normal mode estimate, we consider 1% perturbations around the critical value and simulate until the oscillatory mode is stable. To determine when the oscillatory mode is stable, we integrate out the vertical and horizontal directions and store the value for a moving window of twenty units of time, comparing the change in amplitudes against the previous window. Using the same comparisons between the change in amplitude over the current amplitude as well as a cutoff at an amplitude of 10^{-8} as we did in Section 3.4 we are able to determine whether a proposed value is stable or unstable. However, in this case keep in memory a record of the current amplitude at each timestep, as well as perform the integration to calculate that amplitude. This increases our simulation time compared to the work done in Section 3.4. Therefore, rather than implementing the full-bisection algorithm, we test the critical decay by running simulations with a 1% perturbation above and below the estimated critical value. In all cases, we find that lower values converged to the steady state and the upper values resulted in steady oscillations in time. Consequently, we infer that that the critical values are within at least one 1% of the true value. We provide a table of values tested in Table 3.2



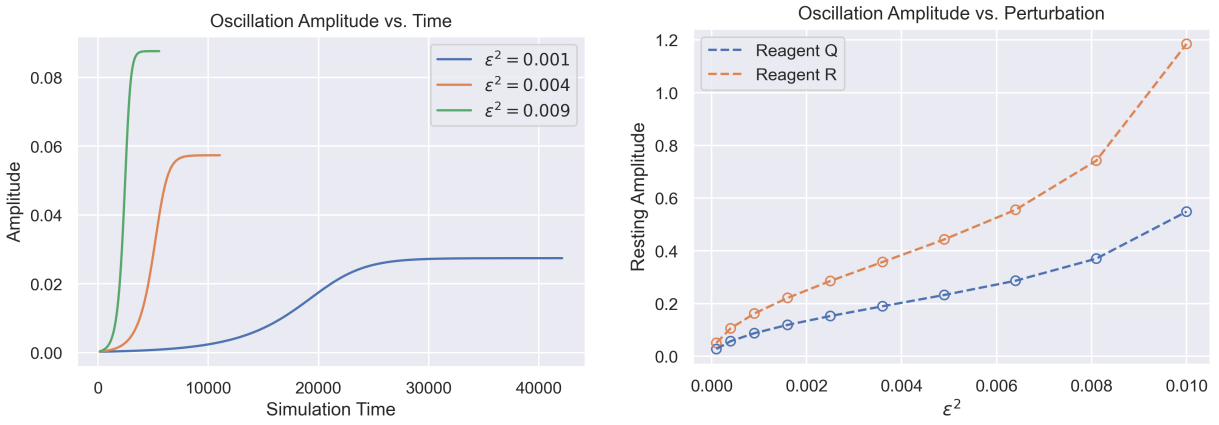
(a) (b)

Figure 3.11: (a) Contour plot of critical η determined by solving Equation (3.155) as a function of (γ, D). (b) Contour plot of critical ω as a function of (γ, D). Values were calculated from (3.155) with shared parameters $(a, b) = (0.2, 2.0)$

Gamma	Lower Value	Estimate	Upper Value
0.1	0.863	0.871	0.880
0.199	0.184	0.186	0.188
0.298	0.296	0.299	0.301
0.397	0.422	0.426	0.430
0.496	0.563	0.569	0.574
0.595	0.721	0.728	0.735
0.694	0.897	0.906	0.915
0.793	1.094	1.110	1.116
0.892	1.312	1.326	1.339
0.991	1.556	1.571	1.587

Table 3.2: Critical decays and tested values for a fixed $D = 1$ and various γ.

Finally, we can investigate their behaviour and compare it to pattern formation. In particular, we can at least ask the question of whether $A_{\text{osc}} \propto \sqrt{\eta_{ep}}$ and whether the timescales for convergence are comparable. This gives us some insight into which instability is generally more sensitive to its underlying parameter. What we find is that the oscillatory mode develops orders of magnitude faster than pattern formation. We also find that amplitudes of the oscillatory instability are much larger for similar sized perturbations and grow quite differently then the amplitudes for pattern formation. These are illustrated in Figure 3.12. In particular, we find that the growth rate of the amplitude with respect to the perturbation accelerates near the tail end of the perturbations considered. At its largest, the pattern formation for a similar-sized perturbation produces amplitudes around 0.3 while the oscillations are approximately four times larger in magnitude. This is likely connected to the development of a relaxation oscillator as the perturbation increases. We compare the smallest perturbation to the largest in Figure 3.13 where the relaxation can be seen. There we plot a window of time where the amplitude of the oscillations have ceased growing and we have reached a steady-state. This steady state differs from those we have discussed earlier since the concentrations now vary in time but has converged to a stable repeating pattern.



(a) (b)

Figure 3.12: (a) Amplitude development over time for oscillating chemical patterns for various perturbations. (b) Resting amplitude of oscillations at long time as a function of perturbation. Both figures used the parameters $(a, b, D, \gamma) = (0.2, 2.0, 1.0, 1.0)$, and $\eta = (1 + \epsilon^2)\eta_c$, where η_c is calculated from Equation (3.155) for the parameters of interest.

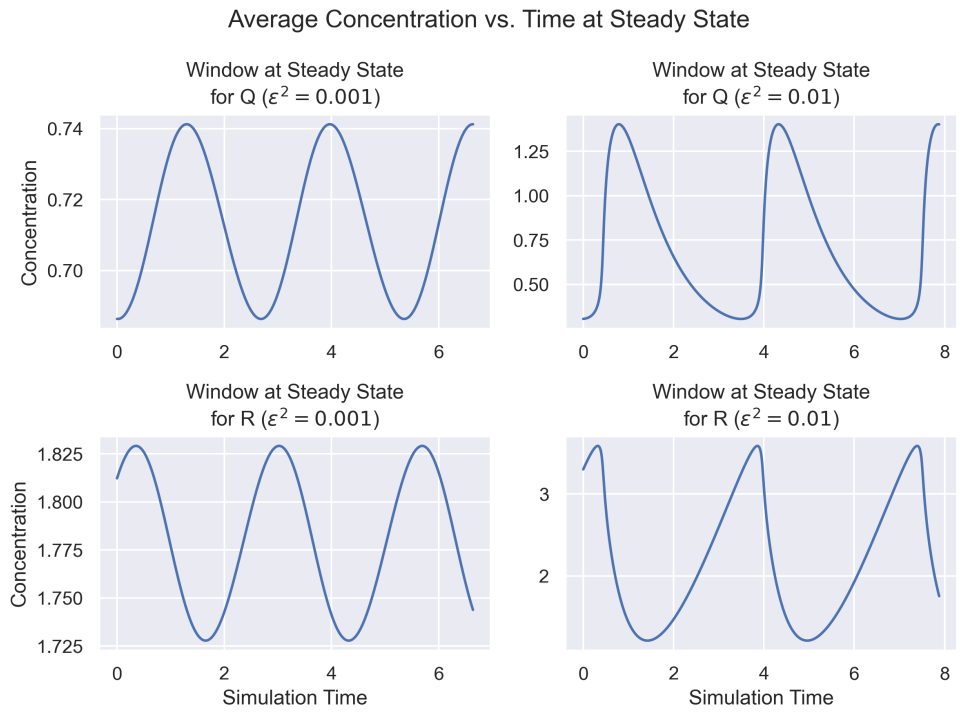
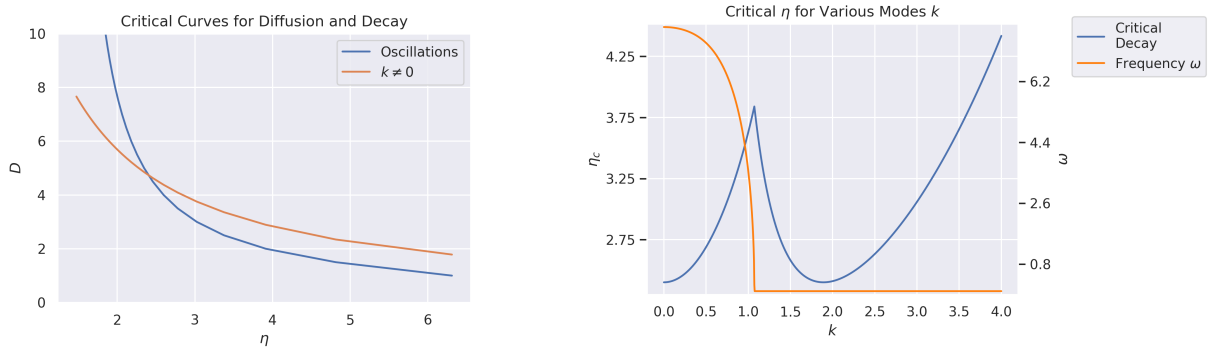


Figure 3.13: The average concentration versus time.

3.4.3 On Simultaneous Instabilities

As we have discussed previously, travelling waves and oscillating patterns are not possible for classical Turing patterns given the underlying assumptions. This is because the Turing conditions require that Equation (1.22) has a strictly positive determinant and strictly negative trace. As a consequence complex roots with a positive real component for Equation (1.15) are not possible. However, we have been able to make a long-wavelength oscillatory mode unstable through a mechanism other than diffusion. This suggests that it should be possible to create a slow manifold oscillating pattern. In particular, we would expect that if the linear growth rate for the Turing patterns, λ_{T}, and the linear growth rate for the oscillatory instability λ_{o} are approximately equal, $\lambda_{\mathrm{T}} \approx \lambda_{\mathrm{o}}$, then both instabilities should grow simultaneously from a perturbation. Further, if the growth rates are sufficiently small, then it should follow the linear stability analysis for sometime. In Figure 3.14, we see that the critical diffusion and critical decay for patterns and Turing patterns intersect at approximately $(\eta, D) \approx (2.40, 4.74)$. At this intersection, both the mode $k = 0$ and $k \approx 1.89$ are marginally stable. We plot the critical curves in Figure 3.14a and the critical η as a function of the critical modes in Figure 3.14b. It should be no surprise that the root-finding algorithm is able to simultaneously detect the oscillatory instability and the Turing instability when calculating the critical diffusion in Figure 3.14 since the Turing instability can be viewed as a special case of the oscillatory instability for short-wavelength patterns; it is simply the case where $\omega = 0$.



(a) (b)

Figure 3.14: (a) Critical curves for diffusion driven patterns and decay driven oscillations, $(a, b, \gamma) = (0.2, 2.0, 2.08)$. (b) Critical decay for various modes k with $(a, b, \gamma, D) \approx (0.2, 2.0, 2.08, 4.74)$.

In Figure 3.15 we simulate from a random perturbation near the intersection where

both λ_T and λ_o are unstable and approximately equal. Since our initial investigation of the two instabilities showed that the decay-driven oscillatory instability and the diffusion-driven patterning mechanism are slow in our non-dimensionalized timescale we expect the oscillating patterns to exist for some time. The simulation in Figure 3.16 captures the oscillatory patterns for forty units of time after a one-hundred units of warmup. At this time we find the oscillating patterns are still growing in magnitude. Unfortunately, after a sufficient amount of time the linear theory breaks down and the non-linear behaviour causes the oscillating pattern to decay to a fixed Turing pattern along the boundary.

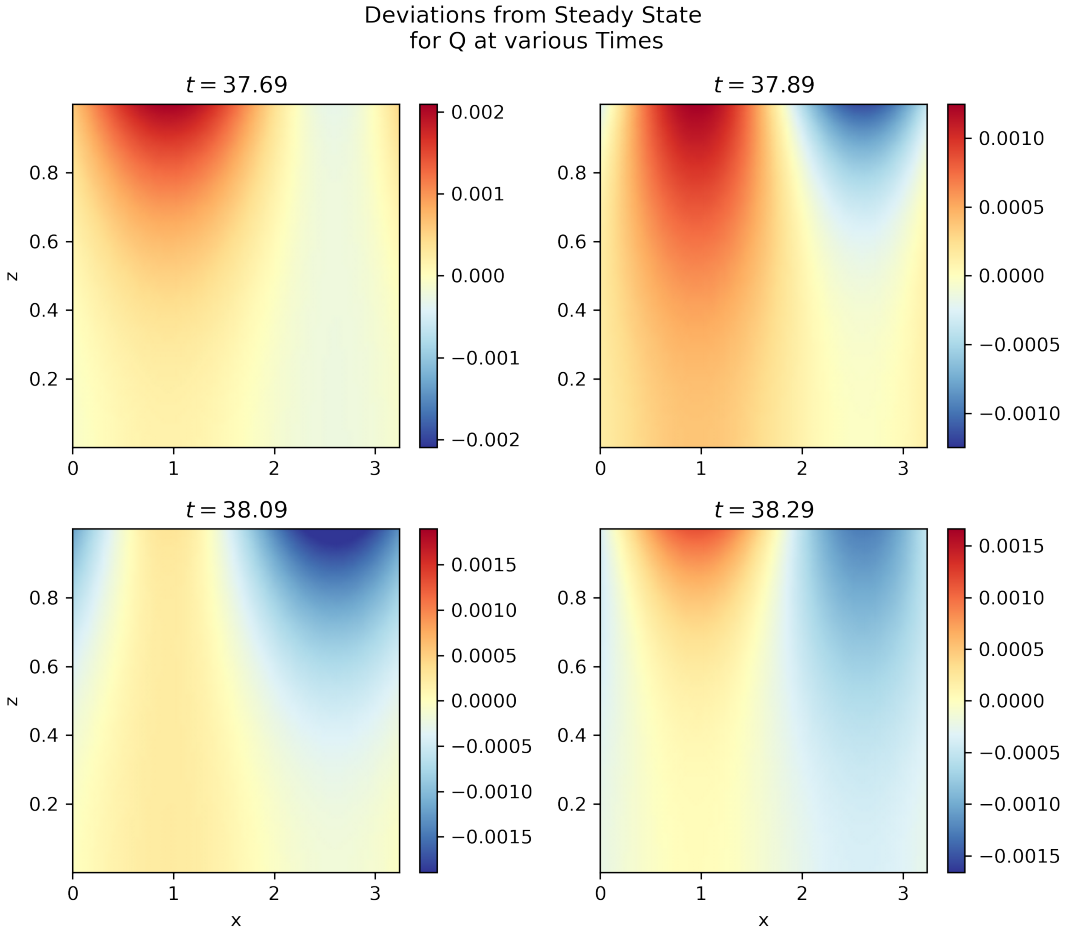


Figure 3.15: Snapshots of a simulation of oscillating patterns. This is simulated with a warm up of 100s and captured for 40s. In this case, we have selected $\lambda_t = 0.001 = \lambda_o$ and $\gamma = 2.08$.

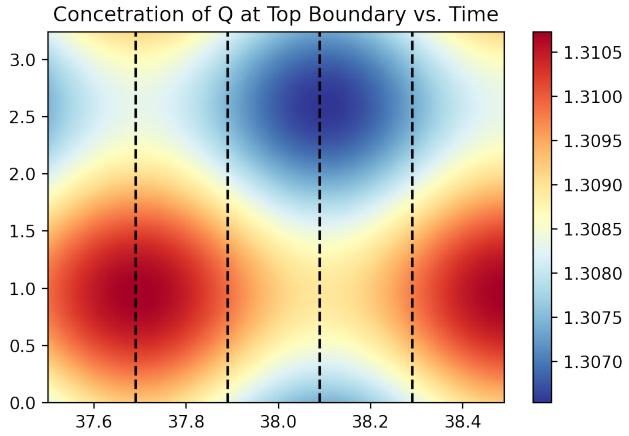


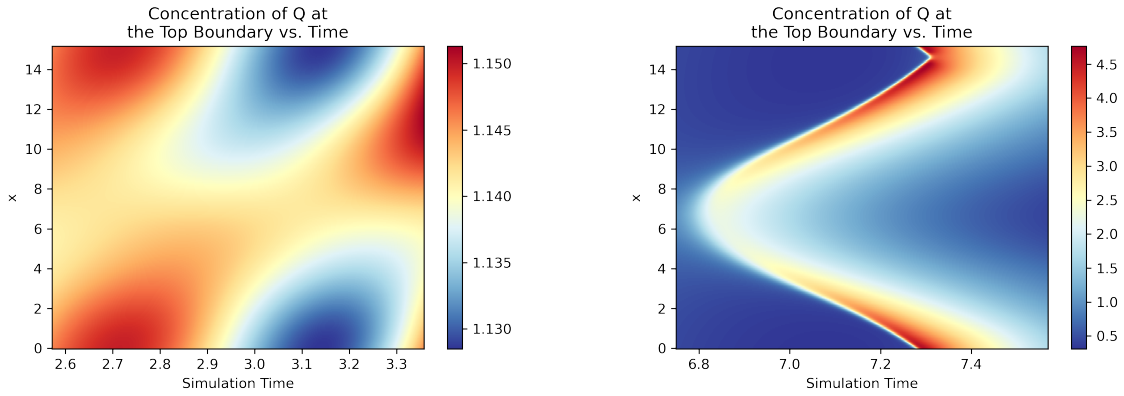
Figure 3.16: The top boundary of a simulation of oscillating patterns. This is simulated with a warm up of 100s and captured for 40s. In this case, we have selected $\lambda_t = 0.001 = \lambda_o$ and $\gamma = 2.08$. Horizontal marks indicate the snapshots plotted in Figure 3.15.

We can also predict more exotic behaviour, in particular, if the amplitudes of the patterns and oscillatory mode are sufficiently large that the non-linearities cannot be ignored. It follows that the first order approximation is no longer valid and we must extend to higher order. While the bulk equations remain the same, Equation (3.119) and Equation (3.120) are only valid at first order. The second order boundary equations are,

$$\frac{dQ_2}{dz}(1) = \gamma(Q_0^2 R_2 + 2Q_0 Q_1 R_1 + 2Q_0 Q_2 R_0 + Q_1^2 R_0 - Q_2), \tag{3.156}$$

$$\frac{dR_2}{dz}(1) = -\gamma(Q_0^2 R_2 + 2Q_0 Q_1 R_1 + 2Q_0 Q_2 R_0 + Q_1^2 R_0). \tag{3.157}$$

The products of Q_1 and R_1 lead to products of the long-wavelength oscillatory solution and the short-wavelength patterns as they develop. This suggests that at second-order, travelling waves are possible. As we see in Figure 3.17a and Figure 3.17b we observe this transitory phenomena when further from the critical parameter values. Moreover, as we would expect, the behaviour is localized to the boundary where the non-linear reaction occurs. One possible way to make the behaviour recurring is to combine the results from Chapter 2 where we could transition from a stable to unstable system by controlling fluxes at the bottom boundary. By designing a path through the various regions of stability we can stabilize the system again, winding up a spring before releasing it again.



(a) (b)

Figure 3.17: (a) A window of the observed transitory traveling waves along the boundary (b) A window of time capturing a transitory soliton along the boundary. Both figures were simulated with $\gamma = 2.08$, $\eta = 4.0$ and $D = 2.5$.

3.5 Summary

In this Chapter, we performed an in-depth analysis of the pattern formation properties of the Schnakenberg system when restricted to the boundary. Utilizing a vertically averaged equation we were able to find amplitude estimates for the patterns forming at the top boundary in the one-dimensional case. We found that the estimates performed well when the vertical variation was small, but that the estimates quickly broke down as the assumption became less valid. These results were illustrated in Figure 3.4 and Figure 3.5. We then performed a normal mode analysis and investigated the critical diffusion and decay numerically. We found that the averaged equations were outperformed by the normal mode estimates. By utilizing a bisection algorithm, we were able to verify their accuracy to at least 0.5%. Afterwards, we turned our attention to the critical mode where we studied it's relationship to η and γ. We found that that the relationship between k_c and γ changes in this case, no longer respecting the classical $k_c \propto \sqrt{\gamma}$ relation predicted in Chapter 1. Such differences are to be expected since these two γ's, while serving similar functions, have different non-dimensionalizations.

Returning to the averaged equations we were able to analytically motivate the existence of long-wavelength oscillatory instabilities whose critical parameter is η. We looked at its behaviour, and the frequency of oscillations as a function of the other parameters and also observed its transition from uniform oscillations to a relaxation oscillator as the

perturbations grew. We found that the behaviour with respect to the critical parameter differed greatly from the diffusion-driven pattern formation both in magnitude and in its rate of convergence.

We concluded by looking at more exotic behaviour when both the oscillatory mode and patterning are made unstable. Here, we were able to identify a slow manifold where oscillating patterns take place before eventually decaying. While we did not identify a region where oscillating patterns would be unstable and persist, a slow manifold can be sufficient for spatio-temporal patterning in biology.

We were also able to suggest a mechanism which may allow for transitory chemical signalling by controlling fluxes along the boundary. While we do not show it here, the model considered in Chapter 2 reduces to an identical perturbation up to the steady state reactions. As a result, we might expect a similar intersection of instabilities located where the blue and green regions intersect in Figure 2.4. Moreover, the exotic behaviour such as the soliton in Figure 3.17b is also likely reproducible. By changing the fluxes (a, b) between this intersection and the stable region, we are able to metaphorically wind up a spring before releasing it again, making it possible to repeat the transitory behaviour.

Chapter 4

Pattern Formation with Hydrodynamics

Now that we have discussed the situation without flow, we turn our attention to the system when the Rayleigh number is non-zero. The normal mode analysis we performed in Chapter 3 suggests that there should be a meaningful relationship between the chemical instability and the buoyancy-driven one. We also saw some hints of the relationship between chemical pattern formation at the boundary and the formation of convective cells in Figure 1.7b. However, research dealing with convection and pattern formation has generally dealt with bulk reaction-diffusion models. Either investigating pre-mixed reagents or assuming the concentrations are split between two fluids and the reaction occurs at interface. Examples of these fluid interface problems were studied by Rongy et al. [40] and Almarcha et al [41]. In their work, Rongy et al. looked at reaction fronts produced by $A + B \to C$ style reactions in the presence of buoyancy-driven convection, while, Almarcha et al. addressed a similar model but instead looked at how the reaction might destabilize otherwise stable density stratifications. Both Rongy et al. and Almarcha et al. investigate diffusion ratios which are not one, but not with the goal of studying steady pattern formation. The relationship between convection and bulk Turing instabilities was studied by Vasquez et al. [42]. In their research, they studied a classic bulk reaction-diffusion model capable of producing Turing patterns, buoyancy driven flows modeled by the Boussinesq approximation of the Navier-Stokes equations. In their work they showed how the convection influenced pattern selection, either coexisting, changing the pattern, or completely suppressing it. We suspect similar behaviour exists here, however, our research deals primarily with the two-dimensional problem. Since we lose a degree of freedom with boundary-bound pattern formation, our model only admits one-dimensional patterns at

the boundary. As a consequence, we can only produce a simple wave-like pattern. This pattern will either be enhanced or suppressed by the buoyancy-driven flows depending on its direction and how the reagents influence the density. Since there is no alternative style of pattern to choose from, we can only hypothesize about the impacts of domain geometry and convection on pattern formation in more general settings. However, it is reasonable to suspect it will mirror the commentary provided by Vasquez.

This enhancement or suppression of patterning through convection and pattern formation is reaffirmed by the work of Die Wald and Helmut [43] and further work by Vasquez [44]. Die Wald and Helmut showed conditions where convection stabilizes Turing patterns, while Vasquez showed that shear flow can induce patterning. In the material to follow, we will show that not only does convection enhance or suppress pattern formation, but the diffusion-driven pattern formation also changes the behaviour of the buoyancy-driven instability relative to the other parameters.

In Figure 4.1 we provide a simple diagram for the two-dimensional Rayleigh-Bénard style instability driven by chemical reagent density. Recalling that the Turing instability is caused by asymmetric diffusion rates, these influence the transport of the two chemical reagents along the boundary. If we simultaneously observe the formation of convective cells as part of a buoyancy-driven instability, this will also influence the transport along the boundary potentially aiding in pattern formation. Moreover, the patterning at the boundary caused by the diffusive instability can create pockets of high density and low density. These horizontal variations are nearly identical to that of the classical Rayleigh-Bénard problem and should promote the formation of convective cells. As a result, we would naturally expect that the Rayleigh-Bénard instability and the Turing instability can cooperate or interfere with each other depending on the direction of the buoyancy force and how the reagents influence the density of the fluid.

With this behaviour in mind, the chapter will be divided into two main parts. First, we will investigate how the diffusion-driven instabilities influence the buoyancy-driven ones. Investigating the critical Rayleigh number and critical mode with respect to the other parameters. Afterwards, we will turn our attention to how the flows influence the final resting pattern and change the oscillatory instability. While we will see that the formation of convective cells generally suppresses the oscillatory instability, we will observe stable oscillatory patterns when the parameters are far from their critical values, similar to Balazs et al. [1]

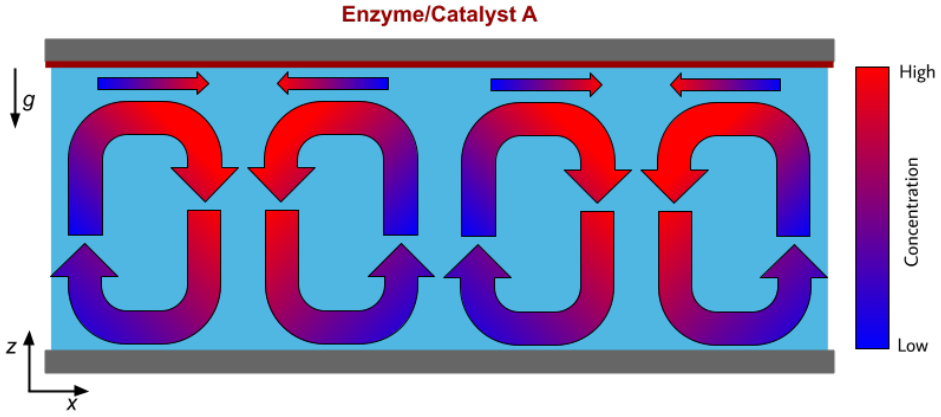


Figure 4.1: A simplified schematic for the behaviour at the onset of the instability where buoyancy driven flows are present.

4.1 Non-Zero Rayleigh Numbers

We recall Equation (3.124), which we derived during our normal mode analysis of Equation (3.19) in Chapter 3. By setting $\lambda = 0$ in Equation (3.124) we are considering a marginally stable mode with a fixed wavenumber k. To begin our analysis, we focus on Q driven flows. Recalling Equation (3.24) we defined $\beta^{\max} = \max\{|\beta^Q|, |\beta^R|$ if $\beta^{\max} = \beta^Q$ and $|\beta^R| \ll \beta^{\max}$ then $\delta^Q = 1$ and as a result, we can assume that $(\delta^Q, \delta^R) = (1, 0)$. We begin with this case since we are able solve for r in terms of q and therefore reduce the dimensionality of the problem. Considering the marginally stable problem with $\lambda = 0$, then with these assumptions in mind, Equation (3.124) reduces to

$$\begin{aligned} &\frac{d^2q}{dz^2} - (\eta + k^2)q = w\frac{dQ_0}{dz}, \\ &\frac{d^2r}{dz^2} - k^2 r = 0, \\ &\left(\frac{d^2}{dz^2} - k^2\right)^2 w = k^2 \mathrm{Ra} q. \end{aligned} \tag{4.1}$$

where Ra = Gr/Sc is the Rayleigh number. We reiterate the boundary conditions for Equation (3.124) below,

$$\frac{dq}{dz}(0) = 0, \qquad \frac{dq}{dz}(1) = \gamma(-q(1) + 2q(1)Q_0(1)R_0(1) + r(1)Q_0^2(1)), \tag{4.2}$$

$$\frac{dr}{dz}(0) = 0, \qquad \frac{dr}{dz}(1) = \gamma\frac{-2q(1)Q_0(1)R_0(1) - r(1)Q_0^2(1)}{D}, \tag{4.3}$$

$$w(0) = 0 = w(1), \tag{4.4}$$

$$\frac{dw}{dz}(0) = 0 = \frac{dw}{dz}(1). \tag{4.5}$$

Now that $r(z)$ is only coupled to the other equations through the boundary, we can calculate its solution in terms of the functions evaluated at the boundaries. In this case, the general solution is given by,

$$r(z) = A\cosh(kz) + B\sinh(kz). \tag{4.6}$$

Substituting this into the left end point, we immediately conclude that,

$$r(z) = A\cosh(kz). \tag{4.7}$$

Which can then be substituted into the right end point to obtain A,

$$kA\sinh(k) = -\frac{\gamma}{D}\left(2q(1)Q_0(1)R_0(1) + A\cosh(k)Q_0(1)^2\right), \tag{4.8}$$

$$A\left(Dk\sinh(k) + \gamma\cosh(k)Q_0^2\right) = -2\gamma q(1)Q_0(1)R_0(1), \tag{4.9}$$

$$A = -\frac{2\gamma q(1)Q_0(1)R_0(1)}{Dk\sinh(k) + \gamma\cosh(k)Q_0(1)^2}. \tag{4.10}$$

As a consequence, we can reduce Equation (4.1) to

$$\begin{aligned}\left(\frac{d^2}{dz^2} - (\eta + k^2)\right)q &= w\frac{dQ_0}{dz},\\ \left(\frac{d^4}{dz^4} - 2k^2\frac{d^2}{dz^2} + k^4\right)w &= k^2\mathrm{Ra}\cdot q,\end{aligned} \tag{4.11}$$

with

$$\begin{aligned}\left.\frac{dq}{dz}\right|_{z=0} &= 0,\\ \left.\frac{dq}{dz}\right|_{z=1} &= \gamma\left(-q(1) + 2q(1)Q_0(1)R_0(1) - \frac{2\gamma Q_0(1)^3R_0(1)\cosh(k)}{Dk\sinh(k) + \gamma\cosh(k)Q_0(1)^2}q(1)\right),\\ \left.w(z)\right|_{z=1,0} &= 0 = \left.\frac{dw}{dz}\right|_{z=1,0}.\end{aligned} \tag{4.12}$$

From Equation (4.11) we can determine $q(z)$ in terms of $w(z)$ and substitute it back to obtain a single governing equation in terms of $w(z)$,

$$\left(\frac{d^2}{dz^2} - (\eta + k^2)\right)\left(\frac{d^4}{dz^4} - 2k^2\frac{d^2}{dz^2} + k^4\right)w - k^2\mathrm{Ra}w\frac{dQ_0}{dz} = 0. \tag{4.13}$$

All that remains is expressing the boundary conditions in terms of $w(z)$. Starting with $q(z)$ at $z = 0$, we have

$$\frac{dq}{dz}(0) = 0, \tag{4.14}$$

$$\frac{d}{dz}\left(\frac{1}{k^2\mathrm{Ra}}\left(\frac{d^4w}{dz^4} - 2k^2\frac{\partial^2 w}{\partial z^2} + k^4 w\right)\right)\Bigg|_{z=0} = 0, \tag{4.15}$$

$$\left(\frac{d^5}{dz^5} - 2k^2\frac{d^3}{dz^3} + k^4\frac{d}{dz}\right)w\Bigg|_{z=0} = 0, \tag{4.16}$$

$$\frac{d^5w}{dz^5}(0) = 2k^2\frac{d^3w}{dz^3}(0). \tag{4.17}$$

Similarly, for the right end point we have,

$$\frac{d^5w}{dz^5}(1) - 2k^2\frac{d^3w}{dz^3}(1) = \gamma k^2\mathrm{Ra}(-q(1) + 2q(1)Q_0(1)R_0(1) + r(1)Q_0(1)^2) \tag{4.18}$$

substituting the known form for q and distributing the $k^2\mathrm{Ra}$, this can be re-expressed as,

$$\frac{d^5w}{dz^5}(1) - 2k^2\frac{d^3w}{dz^3}(1) = \gamma\left(\big(2Q_0(1)R_0(1) - 1\big)\left(\frac{d^4w}{dz^4}(1) - 2k^2\frac{d^2w}{dz^2}(1)\right) + k^2\mathrm{Ra}\cdot r(1)Q_0(1)^2\right) \tag{4.19}$$

which simplifies to

$$\left(\frac{d^5}{dz^5} - 2k^2\frac{d^3}{dz^3} - \gamma\big(2Q_0(1)R_0(1) - 1\big)\left(\frac{d^4}{dz^4} - 2k^2\frac{d^2}{dz^2}\right)\right)w\Bigg|_{z=1} = \gamma k^2\mathrm{Ra}Q_0(1)^2r(1). \tag{4.20}$$

and finally through Equation (4.10) we know the value of $r(1)$ at the top boundary.

Collecting everything together we obtain the following eigenvalue problem in Ra,

$$\left(\frac{d^2}{dz^2} - (\eta + k^2)\right)\left(\frac{d^2}{dz^2} - k^2\right)^2 w(z) - k^2\mathrm{Ra}\frac{dQ_0}{dz}(z)\cdot w(z) = 0 \tag{4.21}$$

with

$$\begin{aligned} w(0) = \frac{dw}{dz}(0) = 0 = \frac{dw}{dz}(1) = w(1), \\ \frac{d^5w}{dz^5}(0) = 2k^2\frac{d^3w}{dz^3}(0), \end{aligned} \tag{4.22}$$

and

$$\left(\frac{d^5}{dz^5} - 2k^2\frac{d^3}{dz^3} - \gamma\big(2Q_0(1)R_0(1) - 1\big)\left(\frac{d^4}{dz^4} - 2k^2\frac{d^2}{dz^2}\right)\right) w\Big|_{z=1} = \gamma k^2 \mathrm{Ra} Q_0(1)^2 r(1). \tag{4.23}$$

From here, we can implement a shooting algorithm solving for the critical Rayleigh number. Shooting algorithms are a useful method for solving boundary problems, which make guesses for the unknown initial conditions at the left/bottom endpoint and integrate the system of ODEs to the right/top endpoint in order to find a solution which satisfies the full set of boundary conditions. Classically, shooting methods do this by turning the problem into a root finding one. However, by introducing an additional trivial evolution equation, as shown in Stoer [16], these can be adapted to solve eigenvalue problems. For our problem in particular, we are interested in the critical Rayleigh number. Therefore, we add the evolution equation $d\mathrm{Ra}/dt = 0$ and consider its value as an additional initial condition.

By setting $x_i(z) = \frac{d^i w}{dz^i}(z)$ for $i = 0, 1, ..., 5$, we can rewrite Equation (4.21) as a non-linear system of first order differential equations. Adding the additional equation $\dot{\mathrm{Ra}} = 0$ we discussed above, we obtain

$$\begin{bmatrix} \dot{x}_0 \\ \dot{x}_1 \\ \dot{x}_2 \\ \dot{x}_3 \\ \dot{x}_4 \\ \dot{x}_5 \\ \dot{\mathrm{Ra}} \end{bmatrix} = \begin{bmatrix} 0 & 1 & 0 & 0 & 0 & 0 & 0 \\ 0 & 0 & 1 & 0 & 0 & 0 & 0 \\ 0 & 0 & 0 & 1 & 0 & 0 & 0 \\ 0 & 0 & 0 & 0 & 1 & 0 & 0 \\ 0 & 0 & 0 & 0 & 0 & 1 & 0 \\ (\eta + k^2)k^4 & 0 & -2k^2(\eta + k^2) - k^4 & 0 & \eta + 3k^2 & 0 & 0 \\ 0 & 0 & 0 & 0 & 0 & 0 & 0 \end{bmatrix} \begin{bmatrix} x_0 \\ x_1 \\ x_2 \\ x_3 \\ x_4 \\ x_5 \\ \mathrm{Ra} \end{bmatrix} + \begin{bmatrix} 0 \\ 0 \\ 0 \\ 0 \\ 0 \\ k^2 x_0 \mathrm{Ra}\frac{dQ_0}{dz} \\ 0 \end{bmatrix} \tag{4.24}$$

with

$$\begin{aligned} x_0(0) &= x_0(1) = 0, \\ x_1(0) &= x_1(1) = 0, \\ x_5(0) &= 2k^2 x_3(0), \\ x_5(1) &= 2k^2 x_3(1) + \gamma\big(2Q_0(1)R_0(1) - 1\big)\left(x_4(1) - 2k^2 x_2(1)\right), \\ &\quad + \gamma k^2 \mathrm{Ra} Q_0(1)^2 r(1). \end{aligned} \tag{4.25}$$

In order to construct the shooting method, we view the system as an initial value problem. This requires that we add $x_2(0)$, $x_3(0)$, $x_4(0)$ and the eigenvalue Ra as unknown initial values. If we obtain a solution to the eigenvalue problem, we would expect that after integrating the initial value problem to the right endpoint that it will satisfy the boundary conditions there. However, there are only three boundary conditions at the top boundary and we now have four unknowns. As consequence, we will need to introduce an additional equation. To do this, we note that if $||x_2||_2 = 0$, then $x_2(z)$ is trivial which implies that $x_0(z)$ and $x_1(z)$ are also trivial via $x_0(0) = x_1(0) = 0$. Since we seek a non-zero eigenfunction $x_0(z) = w(z)$, this case is degenerate. We conclude that if $w(z) \not\equiv 0$ then $||x_2||_2 \neq 0$. However, we will need a fixed value in order to add it to our root finding algorithm. For this, we note that if $w(z)$ satisfies Equation (4.21), as well as the boundary conditions in Equation (4.22) and Equation (4.23), then so does $cw(z)$ for any $c \in \mathbb{R}$. As a consequence, by choosing $||x_2||_2 = 1$ we are choosing a scaling c which has no effect on the solution.

With this in mind we can now describe the full root finding problem. Given some initial values

$$\mathbf{a} = (a_1,\ a_2,\ a_3, a_4)$$

the initial conditions are given by

$$\hat{\mathbf{x}}(0;\mathbf{a}) = \begin{bmatrix} \hat{x}_0(0;\mathbf{a}) \\ \hat{x}_1(0;\mathbf{a}) \\ \hat{x}_2(0;\mathbf{a}) \\ \hat{x}_3(0;\mathbf{a}) \\ \hat{x}_4(0;\mathbf{a}) \\ \hat{x}_5(0;\mathbf{a}) \\ \text{Ra} \end{bmatrix} = \begin{bmatrix} 0 \\ 0 \\ a_1 \\ a_2 \\ a_3 \\ 2k^2 a_2 \\ a_4 \end{bmatrix}. \tag{4.26}$$

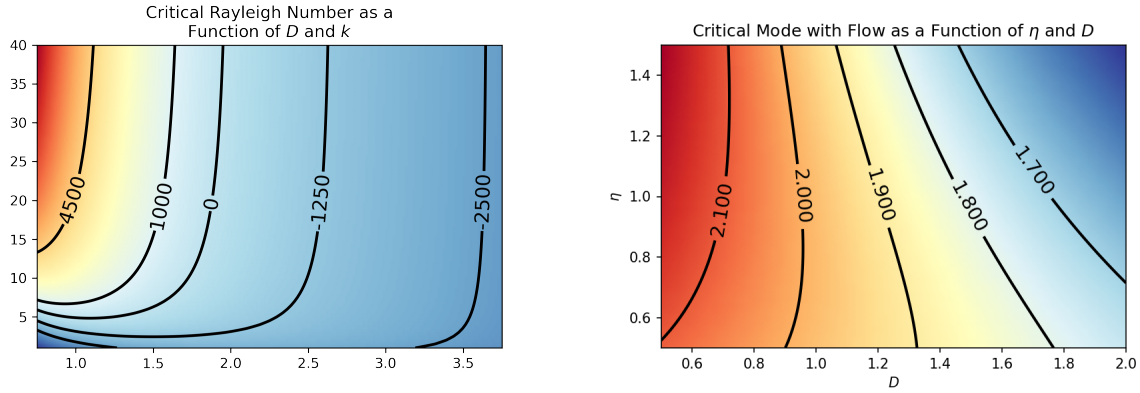
Integrating the initial value problem to $z = 1$, we obtain $\hat{\mathbf{x}}(1;\mathbf{a})$. Once a solution is obtained, we know that the initial values produce a solution which satisfies the full boundary conditions described in Equation (4.22) and Equation (4.23), as well as newly introduced condition on the norm of x_2. As a consequence, the function

$$\mathbf{G}(\mathbf{a}) = \begin{bmatrix} \hat{x}_0(1;\mathbf{a}) - x_0(1) \\ \hat{x}_1(1;\mathbf{a}) - x_0(1) \\ (\hat{x}_5(1;\mathbf{a}) - 2k^2\hat{x}_3(1;\mathbf{a})) - (x_5(1) - 2k^2 x_3(1)) \\ ||\hat{x}_2||_2 - 1 \end{bmatrix} \tag{4.27}$$

should vanish. As a result, Equation (4.27) defines our root finding problem. To integrate the system of ordinary differential equations we use SciPy's solve_ivp method with the

default RK45 method. We use a relative tolerance of 10^{-12} to ensure that we can calculate $||x_2||_2$ from the results. Finally, for the root finding algorithm, we use SciPy's root finder which uses the hybr method by default. We originally discussed the hybr method in Chapter 3.

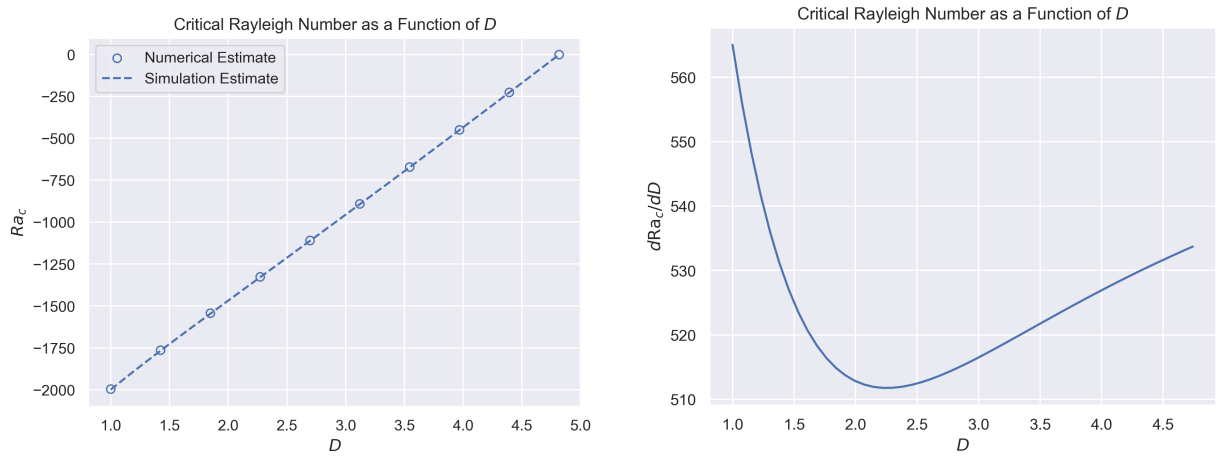
In testing, we found that the convergence of the root finding algorithm is sensitive to the initial guess. Therefore, as we did with the critical parameters for chemical oscillations in Chapter 3, we begin by solving for the critical Rayleigh number for a fixed parameter set. In this case we chose $\gamma = 1$, $\eta = 1$ and $D = 1$. After an estimate was obtained and verified, we used this singular solution to build a surface of estimates. A coarse (η, D, k) surface was resolved and was used as a jumping-off point when we need to optimize for an unknown set of parameters. The surface for $\eta = 1$ is provided in Figure 4.2a, as a function of both D and the wavenumber. We also provide some plots of the steady state in Figure 4.7 for supercritical Rayleigh numbers, superimposing both the flow field and the concentrations.



(a) (b)

Figure 4.2: (a) Critical Rayleigh number surface versus the diffusion ratio and wavenumber, $(\eta = 1,\ \gamma = 1)$. (b) Critical mode versus the diffusion ratio and decay, for $\gamma = 1$. Each Figure used $(a, b) = (0.2, 2.0)$

In Figure 4.2a, we can see that the critical diffusion corresponds to a critical Rayleigh number of zero and we confirm this in Figure 4.3a. In fact, as we continue to increase the diffusion ratio, the critical Rayleigh number becomes positive. This can be explained by viewing the critical diffusion for pattern formation as a subcase of the larger problem without flow, we simply set $\mathrm{Ra} = 0$. Consequently, when the diffusion grows past this critical value the pattern formation without flow is now unstable. As a result, by changing



(a) (b)

Figure 4.3: (a) Comparison of shooting method estimate versus a bisection algorithm detecting the formation of patterns. (b) Derivative of the Critical Rayleigh number as a function of the diffusion coefficient D. Parameters for both Figures where $(a, b, \eta, \gamma) = (0.2, 2.0, 1, 1)$

the sign of the Rayleigh number it becomes a stabilizing term and at the critical value, it is able to effectively suppress the pattern formation. In Figure 4.3 we provide the critical Rayleigh number as a function of D as well as its derivative.

To confirm our estimates, we implement a bisection algorithm similar to the one seen in Chapter 3. However, since the critical diffusion coincides with a critical Rayleigh number of zero we are unable to calculate a percent error. In its place, we calculate the absolute errors and provide the results in Table 4.1. Away from zero, the absolute errors are two orders of magnitude small than the estimates themselves. This suggests good performance in the normal mode estimates, however, we do slightly overestimate the critical Rayleigh number at the critical diffusion.

4.1.1 R Driven Flows

We originally set $\delta^R = 0$ for two reasons, first it aids the convergence of the numerical methods by reducing the dimensionality of the problem. In our original setup, we were able to solve for $r(z)$ since it was independent of the rest of the system except for the boundaries. In addition, the steady state profile for R is constant, and we may not initially

Diffusion	Estimate	Bisection Algo.	Abs Error
1	−1999.659	−1996.534	3.124
1.424	−1767.331	−1765.570	2.761
1.848	−1546.015	−1543.599	2.415
2.273	−1328.441	−1326.365	2.075
2.697	−1111.122	−1109.386	1.736
3.121	−892.542	−891.148	1.394
3.545	−672.156	−671.106	1.050
3.969	−449.864	−449.162	0.702
4.393	−225.758	−225.406	0.352
4.818	0	0.044	0.044

Table 4.1: Numerical estimate of critical Rayleigh number against bisection algorithm. Results are rounded to the third decimal place.

expect to produce an instability. However, if we return our attention to Figure 1.2 and Figure 4.1 there should be no difference between the scheme when Q drives the flow and the peaks/troughs of Q correspond to the high/low-density regions compared with when R drives the flow and the peaks/troughs of R correspond to low/high-density regions. Consequently, we might expect that in the case of R driven flow the critical Rayleigh number is positive.

To determine critical values in the case when R drives the flow instead of Q we constructed the general shooting problem without any simplifications and assume that $\beta^{\max} = |\beta^R|$ and $\delta^R = 1$. Much like before, we will also assume that $|\beta^Q| \ll \beta^{\max}$ so that we can assume that the contributions to the buoyancy force from Q are negligible and set $\delta^Q = 0$. We plot the critical Rayleigh number for $(\eta,\ \gamma) = (1.0, 1.0)$ in Figure 4.4. We also provide the results for Q driven flow adjacent to this for comparison. In both cases, we find that the critical diffusion results in a critical Rayleigh number of 0 and in Figure 4.5b we find that the critical curves cross when $D > D_c$.

As mentioned, this is initially surprising since the steady state for R is a constant but the non-linear interactions at the boundary and the gradient in Q are sufficient to produce a buoyancy-driven flow even if they do not directly drive the flow. This suggests that δ^R, depending on its sign and size can play an important role in determining the critical values for the pattern formation process.

To this end, we calculate the critical diffusion over the (δ^R, D) surface around the critical diffusion and with $|\delta^R| < \delta^Q = 1$. We note that by fixing $\delta^Q = 1$, we are assuming that

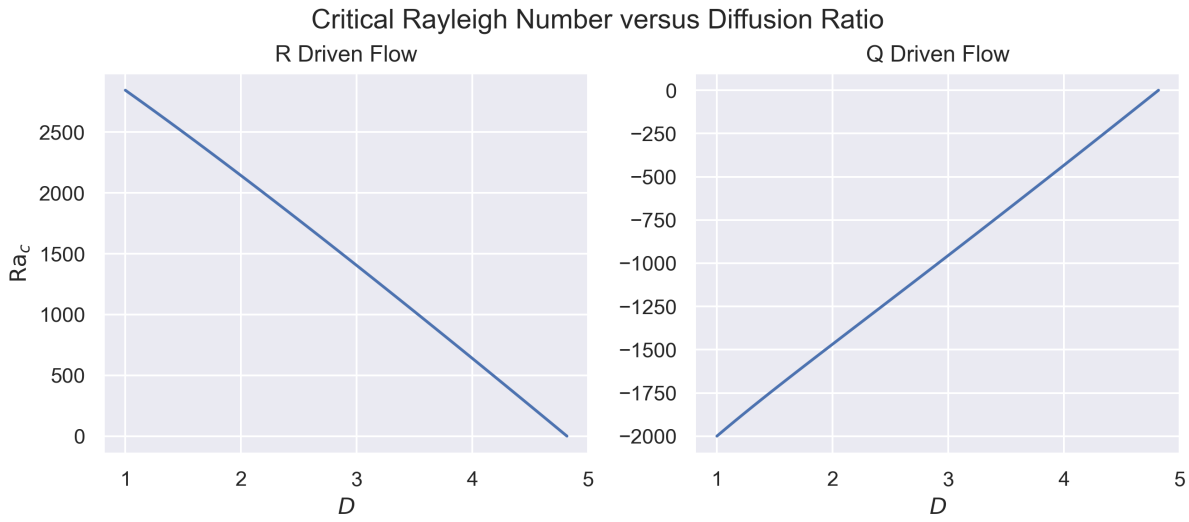
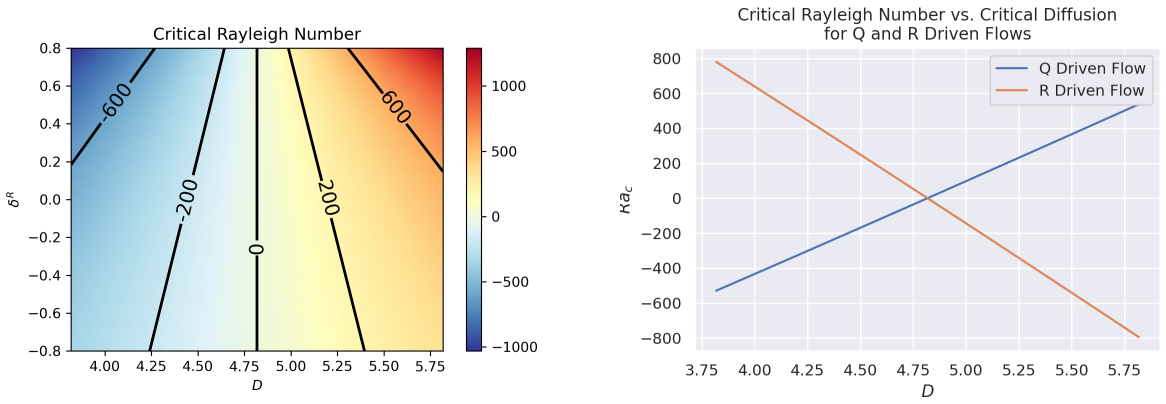


Figure 4.4: Comparison of critical Ra for Q and R driven flows as a function of the diffusion ratio, $(a, b, \eta, \gamma) = (0.2, 2.0, 1, 1)$

$\beta^{\max} = \delta^Q$. in Figure 4.5a. The contour marking $\mathrm{Ra} = 0$ is the region where the ratio of the densities Q and R should not matter since there is no flow. However, upon crossing this contour the stabilizing/destabilizing behaviour of δ^R changes. In particular, for $D < D_c$ we find that δ^R is a stabilizing term in our system, causing the critical Rayleigh number to decrease and after we transition across the critical diffusion, δ^R becomes a destabilizing term, causing the critical Rayleigh number to increase. A possible explanation is given in Figure 4.5b. After the two critical curves intersect, the Rayleigh number must be between the two regions for both R and Q driven flows to be unstable. As a result, flows which are primarily driven by R are already unstable at the critical Rayleigh number for Q driven flow. This would suggest that when we increase δ^R, we are allowing it to drive the dynamics more and consequently making the system more unstable.

4.1.2 Flows on Patterns

Having observed the effect of pattern formation on hydrodynamics, we can now look at how hydrodynamics influences the pattern formation process. There are two behaviours we would like to focus on. First, recalling Figure 1.2, the flows themselves are likely to deform the patterns compressing the peaks and expanding the troughs in the case of Q and vice versa for R. We can get an idea of how large this effect might be by looking at



(a) (b)

Figure 4.5: (a) Critical Rayleigh number on the (δ^R, D) surface, $\delta^Q = 1$. (b) Close up of critical Rayleigh number for Q and R driven flows at the transition. Shared parameters for the two Figures were $(a, b, \eta, \gamma) = (0.2, 2.0, 1, 1)$

buoyancy-driven patterns. In Figure 4.6 we plot the amplitude size as a function of the Rayleigh number when $(\eta, D) = (1, 1)$ and therefore the perturbations take place around $\mathrm{Ra}_c = -2000$. In order to be able to compare and contrast with the amplitude results in Chapter 3 we consider perturbations of the form $\mathrm{Ra} = (1 + \epsilon^2)\mathrm{Ra}_c$ where ϵ ranges between 0.01 and 0.1 in steps of 0.01. This is identical to how we studied the amplitudes previously and helps to relate their behaviour in a way that is independent of the actual critical values.

The primary point we would like to take away is that the amplitudes of the patterns produced by the buoyancy-driven flows are smaller than those created by the diffusion-driven instability for similar perturbations by an order of magnitude, see Figure 3.4 and 3.5 for reference. As a result, for the convection to have a meaningful impact on the pattern formation we will need much larger perturbations. We confirm this behaviour in Figure 4.7. Here we look at pattern formation when the critical Rayleigh number is zero. Simulating with a length of $2\pi/k_c$ to obtain a single peak and trough. Since there is only one peak and trough, we can compare the percentage of the upper boundary they occupy to get a sense of how the flows deform the patterns along the boundary.

We now turn our attention to oscillatory behaviour. In their original analysis, Balazs et al. [1] found that buoyancy-driven flow could enhance or suppress the oscillatory behaviour. This is quite natural in their design since the reagents produced on one side of the boundary are advected through the buoyancy-driven flows to the other side of the domain where the

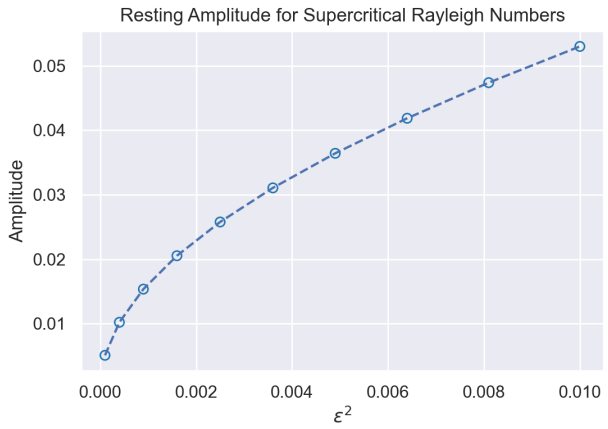
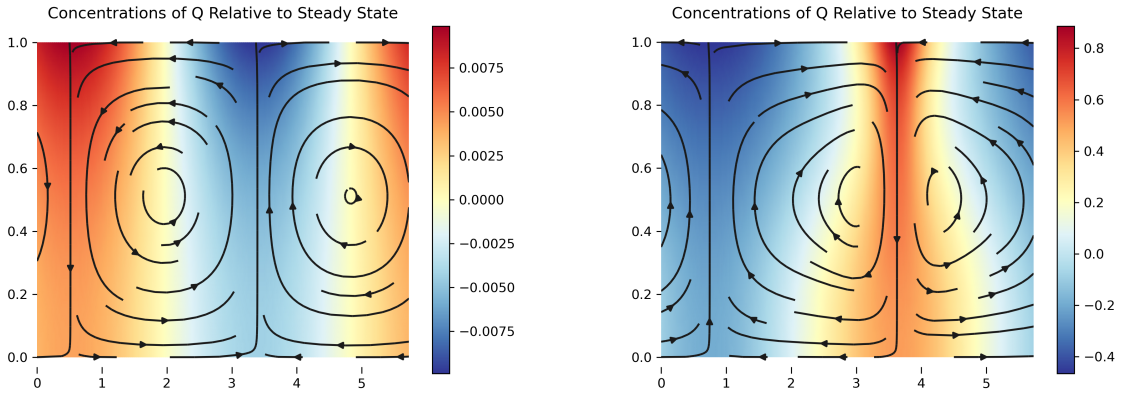


Figure 4.6: Amplitude of $\overline{Q}$ versus the pertubations in the critical Rayleigh number, $(\eta, \gamma, D) = (1, 1, 1)$.

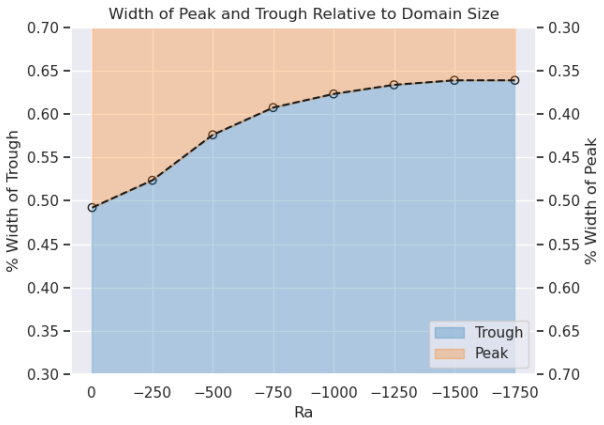
reagents are consumed. In our case, since no reaction occurs at the bottom boundary the advection carries reagents away from the boundary, influencing our ability to continue to carry out the reaction. Consequently, we find in Figure 4.8 that near the critical values supercritical Rayleigh numbers suppress the oscillatory instability. However, similar to Balazs et al. when the system is far from the critical values, it is able to create stable oscillating patterns along the upper boundary. This change in behaviour is likely caused by the supercritical Rayleigh number being able to effectively advect material back to the boundary before it decays.

4.2 Summary

In this chapter, we have looked at the relationship between Turing-style diffusion instabilities localized to the boundary and Rayleigh-Bénard style buoyancy instabilities. We have found that these two instabilities are deeply connected. In fact, when reduced to a normal mode analysis Turing instabilities at the boundary can be viewed as a subset of the larger model when Ra = 0. Consequently, we found that when the diffusion ratio between the two reagents is at the critical value for pattern formation, the critical Rayleigh number for buoyancy-driven instabilities is 0. This can be particularly interesting when we consider alternative geometries like the popular circular or spherical geometries meant to mimic embryos. This provides a possible mechanism for identifying orientation within the object since the pattern formation will be possible at the top of the domain and stable at the

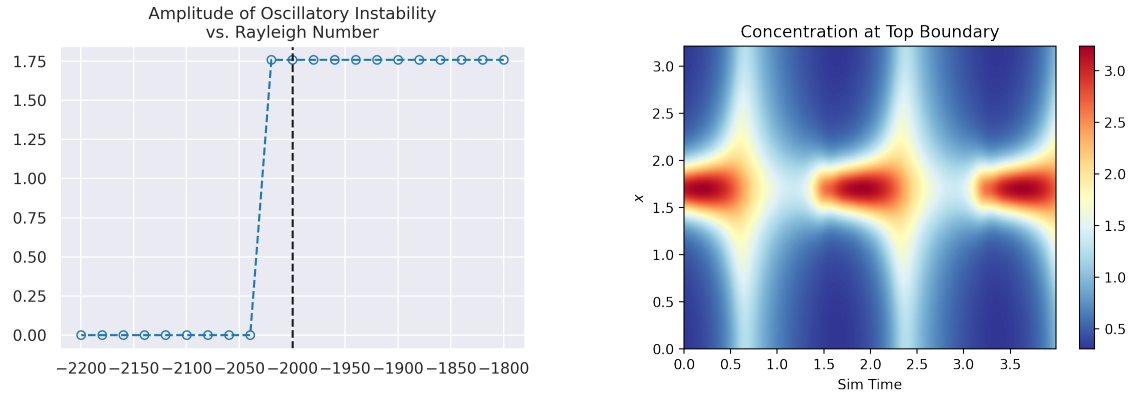


(a) (b)



(c)

Figure 4.7: (a) Concentration of Q at the steady state for $D \approx 4.78$ and $\mathrm{Ra} = -1$ (b) Concentration of Q at the steady state for $D \approx 4.78$ and $\mathrm{Ra} = -1$ (c) Comparison of the width of the peak and trough relative to the domain size as a function of Ra. Shared parameters across the Figures were $(a, b, \eta, \gamma) = (0.2, 2.0, 1, 1)$



(a) (b)

Figure 4.8: (a) Effect of the Rayleigh number on oscillations near their critical values. We have marked Ra_c and simulated with $(\eta, \gamma, D) = (1.612, 1, 1)$ (b) Concentration of Q relative to steady state at upper boundary, $(\eta, \gamma, D, \mathrm{Ra}) = (3, 1.8, 3, -2250)$ demonstrating how oscillations can appear when we are far from the critical values. Snapshot was captured after 200 units of simulation time.

bottom. However, the importance of the critical diffusion for buoyancy-driven flows was also identified in how it influenced the behaviour of other parameters. In our analysis, we allowed δ^R to vary, but the flow was primarily driven by Q since $|\delta^R| < 1$. Here, we found that as we crossed the critical diffusion, the parameter δ^R transitions from stabilizing the system to destabilizing it. This could be explained by looking at the critical Rayleigh numbers for R and Q driven flows respectively. In doing so, we found that both curves intersect and cross at the critical diffusion ratio. Consequently, R driven flow was unstable at the critical Rayleigh number for Q and vice versa. This helps to explain why the behaviour exists since by increasing δ^R we are allowing, the already unstable R driven flow to drive the dynamics more.

After having looked at how the buoyancy-driven instability and diffusion-driven instabilities were related, we turned our attention to the influence of flows on pattern formation. As a result, we noted that near the intersection the oscillatory instability and buoyancy-driven instabilities compete and the buoyancy-driven instability will suppress the oscillatory one. This isn't surprising given the differences between the model studied by Balazs et al. [1] and the one studied here. However, as we noted in Chapter 5, at high Rayleigh numbers there appears to be much more complicated dynamics worth investigating as the material is propagated more quickly throughout the domain. By considering parameters far

from critical, we found we could construct a stable oscillatory pattern along the boundary.

We also noted how pattern formation is changed by larger Rayleigh numbers. In particular, we confirmed predictions that could easily be made from Figure 1.2. We noted how the patterns should expand or contract along the top depending on the direction of the buoyancy force while projecting the opposite effect at the bottom boundary. While the large Rayleigh numbers required to make this effect meaningful can make the behaviour less relevant to biological applications, it allows us to distort chemical signals from one side of the boundary to the other. When combined with the example of controlling pattern formation in Chapter 2 we are able to control both the pattern formation and the appearance of convective cells.

Chapter 5

Conclusion

Throughout this thesis, we have dealt with pattern formation in boundary-bound reactions with and without flow. We began our investigation in Chapter 2 by studying the general problem for reaction networks consisting of two reagents and provided general results for the existence of pattern-forming instabilities. This is where we found the first significant differences between the classical bulk reaction-diffusion problem and boundary-bound reactions. In particular, we noted that for some classes of reactions there exist wavenumbers and linear growth rates that cannot be obtained with physical parameter values. An example this behaviour was demonstrated in section 2.2.4. There we could explicitly bound the range of wavenumbers for pattern formation brought about by a diffusive instability.

Consequently, since we were working with Fourier modes over a periodic interval, we conclude that the linear theory can only predict pattern formation for a finite number of modes. In the classical problem, this is not the case. There, for any fixed mode of interest, it is always possible to make the critical parameter sufficiently large it becomes unstable. Since we are limited in the range of wavenumbers that can be made unstable through boundary-bound reactions, this has consequences for biological morphogenesis, restricting the possible patterns that can form. To their credit, boundary-bound reactions have the benefit of reducing the critical diffusion ratio necessary for pattern formation. For example, in Chapter 3, the bulk decay term reduced the critical diffusion eight-fold. We also note that other authors studying active-membrane models have obtained pattern formation for a diffusion ratio of one. This suggests that boundary-bound reactions and active-membrane models present a description of chemical morphogenesis that can be easier to realize than bulk reaction-diffusion in nature.

We also studied the changes in the critical values and admissible modes for the Schnaken-

berg model restricted to one boundary. The critical mode appears to be linear in γ and sublinear in η. Consequently, not only does increasing η reduce the value of the critical diffusion, but it also increases the critical mode. Moreover, the introduction of η introduced a new kind of oscillatory instability that competes with pattern formation. This long-wavelength oscillatory instability was investigated, and we looked at its relationship to the rate of flux and the diffusion ratio. As a result, we found that not only does η make the system more sensitive to the diffusion parameter, but the diffusion parameter simultaneously makes the system more unstable to the long-wavelength oscillations. As a result, we were able to calculate the transition where the critical diffusion for pattern formation and critical decay for chemical oscillations meet. We studied the behaviour near this intersection, predicting and observing the formation of a slow manifold oscillating pattern. We also demonstrated more exotic transitory behaviour, such as travelling waves and solitons. Combined with the pattern control example, this would allow us to reset the system so that the transitory behaviour can be repeated.

With a good understanding of the pattern formation properties of our system without flow, we finally turned our attention to the system with flow. Here, we identified and explained several behaviours connecting boundary-bound pattern formation and the formation of convective cells. By viewing pattern formation without flow as a subcase of patterning with flow, we could explain why the critical Rayleigh number was zero at the critical diffusion for pattern formation without flow. As the diffusion ratio transitions from subcritical to supercritical, the system without flow goes from stable to unstable. Consequently, the critical Rayleigh number transitions from negative to positive. This is because we must reverse the buoyancy force in order to stabilize the now unstable system. This reinforces the results from Vasquez [42], and Die Wald and Helmut [43] where they showed how buoyancy forces can stabilize Turing pattern formation in the bulk.

Afterwards, we looked at two different problems: The first was to remove the assumption that the flow is driven by Q and instead consider R driven flows where δ^R was zero, and the second was to study flows driven by both Q and R. In the first, we noticed that while R does not have a vertical gradient, it can still produce buoyancy-driven instabilities through its non-linear relationship with Q. We motivated this by considering what happens when the Rayleigh number is positive. In this case, the buoyancy forces are flipped and the patterns produced at the upper boundary can imply the same density variations observed in the case of Q driven flow, but now through R.

Studying the behaviour of R driven flows with respect to the diffusion ratio we saw a similar transition in the critical Rayleigh number as the diffusion becomes supercritical. In this case, the critical Rayleigh number transitioned from positive to negative, and as a

result, the critical curves for Q and R driven flows cross each other. We concluded that R driven flow is unstable at the critical Rayleigh number for Q driven flow. Consequently, we were able to explain why δ^R transitioned from a stabilizing parameter to a destabilizing parameter when we considered Q driven flow with non-zero δ^R.

After investigating how the diffusion parameter influenced the hydrodynamics, we turned our attention to the effects of buoyancy-driven flow on pattern formation. We compared the magnitude of the patterns generated by the two instabilities, as well as the effects the flow has on the resting pattern. We found that when the flows were small, the patterns were relatively symmetric along the vertical direction. However, as the Rayleigh number was increased, this symmetry breaks down, and we find that we can project a different shaped pattern on the opposing boundary compared to the one that forms at the top boundary. We also looked at the oscillatory instability, noting in contrast to Balazs et al. it is damped out by the formation of convective cells. This was to be expected given the design of our system, where flows remove reagents from the reactive boundary. However, when the Rayleigh number was sufficiently supercritical, we were able to produce stable oscillating patterns on the upper boundary similar to those observed in their research. We suspect that this is because the flow is more effectively able to transport material back to the boundary at higher Rayleigh numbers and consequently produce interesting non-linear behaviour.

5.1 Future Research

Given our results in this thesis, it is natural to turn our attention to the next steps for continued research. In the next few sections, we will conclude the thesis by discussing potential future research avenues. One was originally introduced at the end of Chapter 3, where we discussed how it could be possible to make the travelling wave or soliton behaviour recurring. The second deals with extending our original insights in Chapter 4 to the example in Chapter 2 and some preliminary results are provided. Finally, we motivate the study of higher Rayleigh number flows first observed in Chapter 4.

5.1.1 Pattern Control at the Intersection

In Section 2.2.4, we assumed we had control of the fluxes along one boundary and used this to control the stability of the system. Given that the example considered there and

the system considered in Chapter 3 only differ in their steady state equations, it is natural to suspect that many of the behaviours we observed near the intersection of the long-wavelength and short-wavelength instabilities exist in this model as well. Therefore, it may be possible to reset the system so that the transitory behaviour originally observed in Chapter 3 can be reset. As a result, we can imagine jumping between stable and unstable systems so that the transitory behaviour repeats itself. In Figure 5.1 we provide an elliptical path through all three regions, with the contour for a critical diffusion of 10 marked as an example.

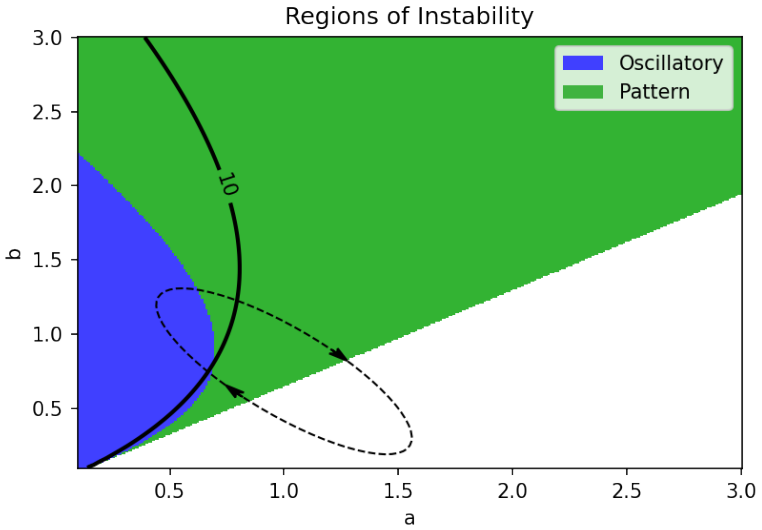


Figure 5.1: Pattern formation regions found in Section 2.2.4 with an elliptical path marked.

5.1.2 Extending the Pattern Control Problem

We recall the equations from Chapter 2, but now couple them to the Boussinesq approximation.

$$\begin{aligned}
\frac{\partial Q}{\partial t} &= -\eta Q + \nabla^2 Q + (\mathbf{u}\cdot\nabla)Q \\
\frac{\partial R}{\partial t} &= D\nabla^2 R + (\mathbf{u}\cdot\nabla)R \\
\frac{\partial \mathbf{u}}{\partial t} &= -(\mathbf{u}\cdot\nabla)\mathbf{u} - \frac{1}{\rho_0}\nabla p + \nu\nabla^2\mathbf{u} + g(\beta^Q Q + \beta^R R)\mathbf{e}_z \\
\nabla\cdot\mathbf{u} &= 0
\end{aligned} \tag{5.1}$$

with

$$\frac{\partial Q}{\partial z}(0) = -\gamma a \qquad \frac{\partial Q}{\partial z}(1) = \gamma(-Q + Q^2 R) \tag{5.2}$$

$$D\frac{\partial R}{\partial z}(0) = -\gamma b \quad D\frac{\partial R}{\partial z}(1) = -\gamma Q^2 R \tag{5.3}$$

$$\mathbf{u}(0) = 0 \qquad \mathbf{u}(1) = 0 \tag{5.4}$$

We already determined the steady state concentrations in the case without flow. In this case, both Q and R have a non-trivial gradient.

$$Q_0(x, y, z) = \gamma \frac{a\Gamma \cosh(\Gamma(z-1)) + b\Gamma \cosh(\Gamma z) - a\gamma \sinh(\Gamma(z-1))}{\Gamma^2 \sinh(\Gamma) + \gamma\Gamma(\cosh(\Gamma))} \tag{5.5}$$

$$R_0(x, y, z) = b\left[\left(\frac{\Gamma \sinh(\Gamma) + \gamma \cosh(\Gamma)}{\gamma(a + b\cosh(\Gamma))}\right)^2 - \frac{\gamma}{D}(z-1)\right] \tag{5.6}$$

Linearising around the steady state and performing the same reductions we have seen throughout this thesis, we obtain the following eigenvalue problem which governs the stability of a particular mode

$$\begin{aligned}
&\frac{\partial^2 q}{\partial z^2} - (\lambda + \eta + k^2)q = w\frac{\partial Q_0}{\partial z} \\
&\frac{\partial^2 r}{\partial z^2} - \left(\frac{\lambda}{D} + k^2\right) r = \frac{w}{D}\frac{\partial R_0}{\partial z} \\
&\mathrm{Sc}\left(\frac{d^2}{dz^2} - k^2\right)^2 w - \lambda\left(\frac{\partial^2}{\partial z^2} - k^2\right) w = k^2 \mathrm{Gr}(q + \delta r)
\end{aligned} \tag{5.7}$$

and boundary conditions

$$\left.\frac{\partial q}{\partial z}\right|_{z=0} = 0, \qquad \left.\frac{\partial q}{\partial z}\right|_{z=1} = \gamma(-q(1) + 2q(1)Q_0(1)R_0(1) + r(1)Q_0^2(1)) \tag{5.8}$$

$$\left.\frac{\partial r}{\partial z}\right|_{z=0} = 0, \qquad \left.\frac{\partial r}{\partial z}\right|_{z=1} = \gamma\frac{-2q(1)Q_0(1)R_0(1) - r(1)Q_0^2(1)}{D} \tag{5.9}$$

$$\left. w \right|_{z=0,1} = 0 \tag{5.10}$$

$$\left.\frac{dw}{dz}\right|_{z=0,1} = 0 \tag{5.11}$$

Which is nearly identical to the Schnakenberg model we investigated in Chapter 4. As a result, it is easy to adapt the shooting methods we already implemented in the previous Chapter to this problem. The primary differences between this problem and the original are the steady states and the addition of a second non-trivial advection term in $r(z)$. As a result of this second gradient, we find that Q driven flow now admits a positive and negative critical Rayleigh number. We suspect this is an extension of what we saw in Chapter 4. There we observed R driven flows despite R having a trivial gradient. We hypothesized that this was because of the non-linear interactions between Q and R. Since they both have gradients in the example considered here, this appears to extend and allows us to define two critical regions for two different kinds of buoyancy-driven instabilities.

Interestingly, only one of these curves tends towards zero as the critical diffusion is reached. This suggests that the diffusive instability selects for a particular kind of pattern that is impossible when the alternative buoyancy-driven instability is at play. As a result, the self-generated flows will either suppress or enhance the Turing-style patterns, which is in line with the discussion by Vasquez [42].

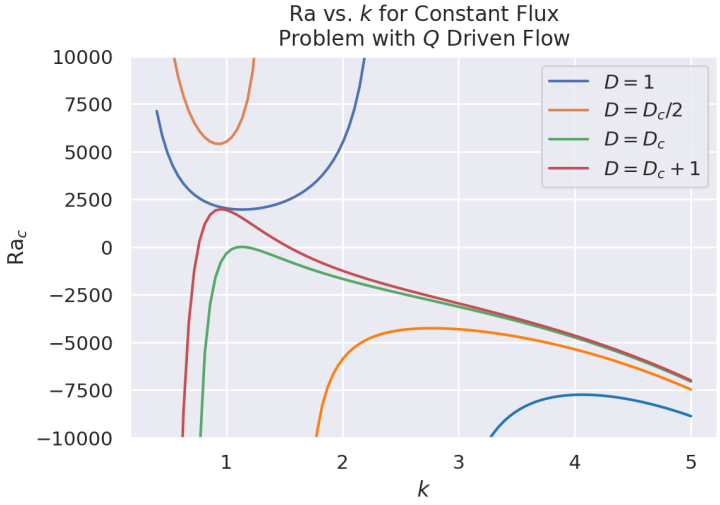


Figure 5.2: Q driven flow for the example in Chapter 2 with $(a, b, \eta, \gamma) = (0.2, 2.0, 1, 1)$.

The next step would be to clarify these behaviours and investigate the relationship between Q driven flow and R driven flow. It may be possible to recover analytical results by applying the discussion on flow in Chapter 2 to the case where both Q and R have no bulk decay. In addition, we can now control the critical Rayleigh number through the constant fluxes (a, b). In particular, if we travel through the regions in Figure 5.1, we

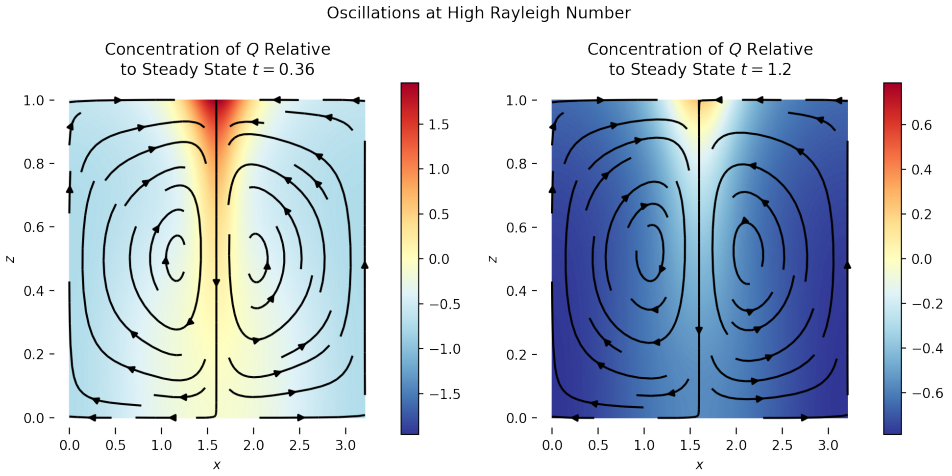


Figure 5.3: Approximate peak and trough of stable oscillatory patterns with flow for Q after 200 units of simulation time, $(\eta, \gamma, D, \mathrm{Ra}) = (3, 1.8, 3, -2250)$.

know that when the Turing instability is super-critical, we will form convective cells, which presents a simple mechanism for controlling the buoyancy-driven instabilities.

5.1.3 Large Rayleigh Numbers

In Chapter 4 we investigated various interactions between chemical instabilities and hydrodynamics for boundary-bound reactions. We showed how the diffusion-driven instability could influence the behaviour of the buoyancy-driven one and investigated how the buoyancy-driven instability influences the final pattern. In Figure 4.7c we saw how the pattern is distorted by the flow field. We also saw how the buoyancy-driven flow could be used to suppress oscillations or produce stable oscillating patterns. This result was provided in Figure 4.8. Since the oscillatory behaviour reappeared when the Rayleigh number was far from critical, it highlights the importance of studying the high Rayleigh number regime. We suspect this will reveal much more exotic behaviour as the boundary and bulk components influence each other. We provide a snapshot of the expansion and contraction of the stable oscillations obtained in Chapter 4 in Figure 5.3 as motivation.

References

[1] O. Shklyaev, V. Yashin, S. Stupp, and A. Balazs. Enhancement of chemical oscillations by self-generated convective flows. *Communications Physics*, 3(1):70, 2020.

[2] J. Schnakenberg. Simple chemical reaction systems with limit cycle behaviour. *Journal of theoretical biology*, 81(3):389–400, 1979.

[3] E. Sel'kov. Self-oscillations in glycolysis 1. a simple kinetic model. *European Journal of Biochemistry*, 4(1):79–86, 1968.

[4] D. Scalise and R. Schulman. Designing modular reaction-diffusion programs for complex pattern formation. *TECHNOLOGY*, 02(01):55–66, 2014.

[5] J. Murray. *Mathematical Biology II*. Springer New York, 3rd edition, 2003.

[6] P. Kundu and I. Cohen. *Fluid Mechanics*. Academic Press, 2nd edition, 2002.

[7] S. Chandrasekhar. *Hydrodynamic and hydromagnetic stability*. Courier Corporation, 1st edition, 2013.

[8] A. Turing. The chemical basis of morphogenesis. *Philosophical Transactions of the Royal Society of London. Series B, Biological Sciences*, 237(641):37–72, 1952.

[9] S. Kondo, M. Watanabe, and S. Miyazawa. Studies of Turing pattern formation in zebrafish skin. *Philosophical Transactions of the Royal Society A: Mathematical, Physical and Engineering Sciences*, 379(2213):20200274, 2021.

[10] L. Krause, A. Gaffney, K. Maini, and V. Klika. Modern perspectives on near-equilibrium analysis of Turing systems. *Philosophical Transactions of the Royal Society A: Mathematical, Physical and Engineering Sciences*, 379(2213):20200268, 2021.

[11] P. Liu, J. Shi, Y. Wang, and X. Feng. Bifurcation analysis of reaction–diffusion Schnakenberg model. *Journal of Mathematical Chemistry*, 51(8):2001–2019, 2013.

[12] C. Konow, M. Dolnik, and I. R. Epstein. Insights from chemical systems into Turing-type morphogenesis. *Philosophical Transactions of the Royal Society A: Mathematical, Physical and Engineering Sciences*, 379(2213):20200269, 2021.

[13] G. Gambino, M. C. Lombardo, S. Lupo, and M. Sammartino. Super-critical and sub-critical bifurcations in a reaction-diffusion schnakenberg model with linear cross-diffusion. *Ricerche di Matematica*, 65(2):449–467, 2016.

[14] H. Bénard. Les tourbillons cellulaires dans une nappe liquide. - Méthodes optiques d'observation et d'enregistrement. *J. Phys. Theor. Appl.*, 10(1):254–266, 1901.

[15] J. Rayleigh. On convection currents in a horizontal layer of fluid, when the higher temperature is on the under side. *The London, Edinburgh, and Dublin Philosophical Magazine and Journal of Science*, 32(192):529–546, 1916.

[16] R. Bulirsch and J. Stoer. *Introduction to numerical analysis*, volume 3. Springer, 2nd edition, 2002.

[17] H. Levine and W. Rappel. Membrane-bound turing patterns. *Phys. Rev. E*, 72:061912, Dec 2005.

[18] D. Gomez, S. Iyaniwura, F. Paquin-Lefebvre, and M. J. Ward. Pattern forming systems coupling linear bulk diffusion to dynamically active membranes or cells. *Philosophical Transactions of the Royal Society A: Mathematical, Physical and Engineering Sciences*, 379(2213):20200276, 2021.

[19] A. Madzvamuse, A. Chung, and C. Venkataraman. Stability analysis and simulations of coupled bulk-surface reaction–diffusion systems. *Proceedings of the Royal Society A: Mathematical, Physical and Engineering Sciences*, 471(2175):20140546, 2015.

[20] D. Gomez, M. Ward, and J. Wei. The linear stability of symmetric spike patterns for a bulk-membrane coupled Gierer–Meinhardt model. *SIAM Journal on Applied Dynamical Systems*, 18(2):729–768, 2019.

[21] C. McTaggart and B. Straughan. Chemical surface reactions and nonlinear stability by the method of energy. *SIAM Journal on Mathematical Analysis*, 17(2):342–351, 1986.

[22] J. Bdzil and H. Frisch. Chemical Instabilities. II. Chemical surface reactions and hydrodynamic instability. *The Physics of Fluids*, 14(3):475–482, 1971.

[23] T. Shores. *Applied linear algebra and matrix analysis*, volume 2541. Springer, 1st edition, 2007.

[24] K. Burns, G. Vasil, J. Oishi, D. Lecoanet, and B. Brown. Dedalus: A flexible framework for numerical simulations with spectral methods. *Physical Review Research*, 2(2):023068, 2020.

[25] J. Boyd. *Chebyshev and Fourier Spectral Methods*. Springer Berlin, Heidelberg, 1st edition, 2000.

[26] C. Lanczos. Trigonometric interpolation of empirical and analytical functions. *Journal of Mathematics and Physics*, 17(1-4):123–199, 1938.

[27] C. Clenshaw. The numerical solution of linear differential equations in chebyshev series. *Mathematical Proceedings of the Cambridge Philosophical Society*, 53(1):134–149, 1957.

[28] S. Ruuth. *Implicit-explicit methods for time-dependent PDE's*. PhD thesis, University of British Columbia, 1993.

[29] S. Ruuth. Implicit-explicit methods for reaction-diffusion problems in pattern formation. *Journal of Mathematical Biology*, 34(2):148–176, Jan 1995.

[30] D. Wang and S. Ruuth. Variable step-size implicit-explicit linear multistep methods for time-dependent partial differential equations. *Journal of Computational Mathematics*, 26(6):838–855, 2008.

[31] D. Wang. Variable step-size implicit-explicit linear multistep methods for time-dependent pdes. Master's thesis, Simon Fraser University, Burnaby, Canada, 2005.

[32] B. Bozzini, G. Gambino, D. Lacitignola, S. Lupo, M. Sammartino, and I. Sgura. Weakly nonlinear analysis of turing patterns in a morphochemical model for metal growth. *Computers & Mathematics with Applications*, 70(8):1948–1969, 2015.

[33] I. Fredholm. Sur une classe d'équations fonctionnelles. *Acta Mathematica*, 27:365 – 390, 1903.

[34] A. Ramm. A simple proof of the Fredholm alternative and a characterization of the Fredholm operators. *arXiv Mathematics e-prints*, page math/0011133, 2000.

[35] J. Stuart. On the non-linear mechanics of wave disturbances in stable and unstable parallel flows part 1. the basic behaviour in plane poiseuille flow. *Journal of Fluid Mechanics*, 9(3):353–370, 1960.

[36] J. Watson. On the non-linear mechanics of wave disturbances in stable and unstable parallel flows part 2. the development of a solution for plane Poiseuille flow and for plane Couette flow. *Journal of Fluid Mechanics*, 9(3):371–389, 1960.

[37] E. Palm. On the tendency towards hexagonal cells in steady convection. *Journal of Fluid Mechanics*, 8(2):183–192, 1960.

[38] J. Guckenheimer and P. Holmes. *Nonlinear oscillations, dynamical systems, and bifurcations of vector fields*, volume 42. Springer Science & Business Media, 1st edition, 2013.

[39] J. Eric, O. Travis, and P. Pearu. SciPy: Open source scientific tools for Python, 2001–.

[40] L. Rongy, P. Trevelyan, and A. De Wit. Dynamics of $A + B \rightarrow C$ reaction fronts in the presence of buoyancy-driven convection. *Physical review letters*, 101(8):084503, 2008.

[41] C. Almarcha, P. M. J. Trevelyan, P. Grosfils, and A. De Wit. Chemically driven hydrodynamic instabilities. *Phys. Rev. Lett.*, 104:044501, 2010.

[42] Desiderio A. Vasquez, Joseph W. Wilder, and Boyd F. Edwards. Convective Turing patterns. *Phys. Rev. Lett.*, 71:1538–1541, 1993.

[43] M. Diewald and H. Brand. Chemically driven convection can stabilize Turing patterns. *Phys. Rev. E*, 51:R5200–R5203, 1995.

[44] D. Vasquez. Chemical instability induced by a shear flow. *Phys. Rev. Lett.*, 93:104501, 2004.

[45] E. Spiegel and G. Veronis. On the Boussinesq approximation for a compressible fluid. *apj*, 131:442, March 1960.

[46] A. Meurer, C. Smith, M. Paprocki, O. Čertík, S. Kirpichev, M. Rocklin, A. Kumar, S. Ivanov, J. Moore, S. Singh, T. Rathnayake, S. Vig, B. Granger, R. Muller, F. Bonazzi, H. Gupta, S. Vats, F. Johansson, F. Pedregosa, M. Curry, A. Terrel, Š. Roučka, A. Saboo, I. Fernando, S. Kulal, R. Cimrman, and A. Scopatz. Sympy: symbolic computing in python. *PeerJ Computer Science*, 3:e103, 2017.

[47] J. More, B. Garbow, and K. Hillstrom. User guide for MINPACK-1. [in FORTRAN]. Technical report, August 1980.

[48] A Doelman. Pattern formation in reaction-diffusion systems — an explicit approach. pages 129–182.

[49] S. Lam, A. Pitrou, and S. Seibert. Numba: A LLVM-Based Python JIT Compiler. In *Proceedings of the Second Workshop on the LLVM Compiler Infrastructure in HPC*, LLVM '15, New York, NY, USA, 2015. Association for Computing Machinery.

[50] A. De Wit, K. Eckert, and S. Kalliadasis. Introduction to the focus issue: chemo-hydrodynamic patterns and instabilities. *Chaos: An Interdisciplinary Journal of Nonlinear Science*, 22(3):037101, 2012.

[51] M. Budroni and A. De Wit. Dissipative structures: From reaction-diffusion to chemo-hydrodynamic patterns. *Chaos: An Interdisciplinary Journal of Nonlinear Science*, 27(10):104617, 2017.

[52] J. Wei. On single interior spike solutions of the Gierer–Meinhardt system: uniqueness and spectrum estimates. *European Journal of Applied Mathematics*, 10(4):353–378, 1999.

[53] A. Gierer and H. Meinhardt. A theory of biological pattern formation. *Kybernetik*, 12(1):30–39, December 1972.

[54] E. Routh. *A Treatise on the Stability of a Given State of Motion: Particularly Steady Motion*. Macmillan and Company, 1877.

[55] A. Hurwitz. Ueber die bedingungen, unter welchen eine gleichung nur wurzeln mit negativen reellen theilen besitzt. *Mathematische Annalen*, 46(2):273–284, 1895.